Finite Element Methods for Advection - Diffusion - Absorption and Fluid Flow Problems

Article-based Doctoral Thesis

Albert Puigferrat Pérez

Supervisors:
Eugenio Oñate Ibáñez de Navarra
Ignasi de-Pouplana Sardà

PhD in Civil Engineering
Universitat Politècnica de Catalunya

June 2021

TEXIS v.1.0.

Abstract

The objective of the thesis is to develop a numerical tool to describe how the concentration of one or more substances distributed in a fluid environment changes under the effect of three transport processes: advection, diffusion and absorption. For that purpose, it is essential to know the interaction of the transported substance with the fluid medium.

The thesis aims to develop stabilized numerical methods for solving the transport and fluid flow equations in a coupled manner for greater accuracy, efficiency and speed when predicting the motion of the transported substances in the fluid. Emphasis is put in the transport of substances in fluids at high Péclet numbers.

The practical motivation of the work is predicting the transport of a pollutant in air in urban environments.

The thesis document summarizes the research published in three papers published in JCR journals of high impact. The author of the thesis is also the first author in the three papers. The papers are attached to the document in the corresponding chapters.

The description of the thesis developments has been organized as follows. First, we present the research carried out in the thesis for the development of a generalized stabilized Finite Increment Calculus-Finite Element Method (FIC–FEM) formulation for solving the multidimensional transient advection-diffusion-absorption equation. The starting point of the developments are the governing equations for the multidimensional steady advection-diffusion-absorption and the unidimensional transient advection-diffusion-absorption problems obtained via the FIC procedure. The good behaviour of the new FIC–FEM formulation is shown in several examples of application. This work was published in the first of the three papers mentioned.

In the following chapter we present an innovative numerical method for solving transport problems with high values of advection and / or absorption. A Lagrangian approach based on the updated version of the classical Particle Finite Element Method (PFEM) has been developed to calculate the advection of substances in fluids, while a Eulerian strategy based on the stabilized FIC–FEM formulation is adopted to compute diffusion and absorption effects. The new semi-Lagrangian approach has been validated in its application of a series of academic examples of transport of substances for different values of the Péclet and Damköhler numbers.

Finally, we derive a procedure for coupling the fluid and transport equations to model the distribution of a pollutant in a street canyon. In our case, we have considered black carbon (BC) as the pollutant. The evolution of the fluid flow is calculated with a standard stabilized finite element method using the Quasi-Static Variational Multiscale (QS-VMS) technique. For the temperature and pollutant transport we use the semi-Lagrangian procedure developed in the thesis.

Several examples of application have been solved to illustrate the accuracy and practicability of the proposed numerical tool for predicting the transport of a pollutant in air in urban environments. One of the examples are presented in the third paper, while another academic one is presented in the appendix of this document.

Resumen

El objetivo de la tesis es desarrollar una herramienta numérica para describir cómo cambia la concentración de una o más sustancias distribuidas en un medio fluido bajo el efecto de tres procesos de transporte: advección, difusión y absorción. Para ello, es fundamental conocer la interacción de la sustancia transportada con el medio fluido.

La tesis pretende extender métodos numéricos estabilizados para resolver las ecuaciones de transporte y flujo de fluidos de manera acoplada para una mayor precisión, eficiencia y velocidad a la hora de predecir el movimiento de las sustancias transportadas en el fluido. Se hace hincapié en el transporte de sustancias en fluidos con números de Péclet elevados.

La motivación práctica del trabajo es predecir el transporte de un contaminante en el aire en entornos urbanos.

El documento de tesis resume la investigación publicada en tres artículos publicados en revistas de alto impacto del JCR en los cuales el autor de la tesis también es el primer autor. Los trabajos se adjuntan al documento en los capítulos correspondientes.

La descripción de los desarrollos de tesis se ha organizado de la siguiente manera. En primer lugar, presentamos la investigación realizada en la tesis para el desarrollo de una formulación generalizada estabilizada de cálculo de incrementos finitos - método de elementos finitos (FIC–FEM) para resolver la ecuación transitoria multidimensional advección-difusión-absorción. El punto de partida son las ecuaciones que gobiernan los problemas multidimensionales estacionarios de advección-difusión-absorción y los problemas de advección-difusión-absorción unidimensionales transitorios obtenidos mediante el procedimiento FIC. El buen comportamiento de la nueva formulación FIC–FEM

se muestra en varios ejemplos de aplicación. Este trabajo fue publicado en el primero de los tres artículos mencionados.

En el siguiente capítulo presentamos un método numérico innovador para resolver problemas de transporte con altos valores de advección y / o absorción. Se ha desarrollado un enfoque lagrangiano basado en la versión actualizada del método clásico de elementos finitos de partículas (PFEM) para calcular la advección de sustancias en fluidos, mientras que se adopta una estrategia euleriana basada en la formulación estabilizada FIC–FEM para calcular los efectos de difusión y absorción. El nuevo enfoque semilagrangiano ha sido validado mediante su aplicación en una serie de ejemplos académicos de transporte de sustancias para diferentes valores de los números de Péclet y Damköhler.

Finalmente, derivamos un procedimiento para acoplar las ecuaciones de fluido y transporte para modelar la distribución de un contaminante en una calle. En nuestro caso, hemos considerado el carbono negro (BC) como contaminante. La evolución del flujo de fluido se calcula con un método estándar de elementos finitos estabilizados utilizando la técnica Quasi-Static Variational Multiscale (QS-VMS). Para la temperatura y el transporte de contaminantes utilizamos el procedimiento semilagrangiano desarrollado en la tesis.

Se han resuelto varios ejemplos de aplicación para ilustrar la precisión y viabilidad de la herramienta numérica propuesta para predecir el transporte de un contaminante en el aire en entornos urbanos. Uno de los ejemplos se presenta en el tercer artículo, mientras que otro académico se presenta en el apéndice de este documento.

"Todos los hombres desean por naturaleza saber."
Aristóteles, *Metafísica*, I, 1, 980a 21

A la meva familia.

Acknowledgements

There is no doubt that the completion of this doctoral thesis has been one of the most important milestones in my life so far. There is no doubt, either, that I would not have achieved it without many people who have been walking with me throughout these years. I will try to at least mention as many as I can.

I would like to express my deepest appreciation to my two supervisors, Eugenio Oñate and Ignasi de-Pouplana. I thank them for giving me the opportunity to do this job and to hang on to the end with me, even when the road got tough. Their prompt response to any question is undoubtedly a virtue. Without their support it is clear that this thesis would not have been possible.

I also want to thank the CIMNE colleagues who have been solving doubts that may have arisen and who have brightened my journey. Among them I include: Ferran A., Alejandro C., Guillermo C., Miguel-Ángel C., Kike E., Roberto F., Joaquín G., Salva L., Mercè L., Miguel M., Cecilia S., Francisco Z. and Rubén Z.. I am grateful to Fulvio for providing me with the data for the last paper and I want to acknowledge the support of the *Agencia de Gestió d'Ajuts Universitaris i de Recerca* (AGAUR) for the funding.

I cannot finish without mentioning the meals at CIMNE that have always ended up extending more than they should, with: Marc A., Chloe B., Javi G., Laura M., Javier M., Miguel P. and Maria R.. Outside of CIMNE, I want to thank the friends who have always been there: Marc A., Pere C., Marc G., Oriol H., Èric R., Marc T., Pau T., David Z., the ones that made the quarantine a little bit less boring and Judith, who I met thanks to the quarantine.

And last, but not least, thanks to my family for their constant support specially during the days it seems that the thesis is not going anywhere, just by being there it has been more than enough to get through.

Contents

Chapter 1

Introduction

1.1 Motivation of the thesis

Outdoor air pollution is linked to an estimated 4.2 million premature deaths worldwide every year [32]. Over 80% of people living in urban areas are exposed to levels of pollution above the limits established by the World Health Organization [101].

The increasing concern to improve sustainability and air quality in urban areas has made numerical prediction increasingly important for helping take decisions on how to build and design cities. Mathematical modeling and numerical simulation of the dispersion of pollutants in the atmosphere are fundamental tools for supporting an adequate management of air quality in urban areas. Such numerical tool provides the necessary information to be able to carry out actions that reduce the impact of pollution on pedestrians. Also, it can be used to assess the suitability of new urban development projects to fit pollution standards.

Traffic emissions are one of the most important sources of pollution in cities where streets are narrow and the configuration of the buildings create the so-called "street canyons" in which pollutants accumulate. The accurate prediction of the transport of these pollutants is basic for the design of solutions to minimize the exposure of citizens to traffic pollution.

Pollutants come mainly from the exhaust pipes of the vehicles moving on the street and are dispersed through air by means of advection, diffusion and absorption. There are

different factors to consider in predicting these effects. First, the temperature of the facades of buildings and the street cause thermal effects that affect the wind speed field [102]. Secondly, the importance of thermal effects versus the diffusivity induced by air turbulence must be studied. The wind speed and its direction plays an important role in the dispersion of a pollutant in air. Finally, the mathematical and computational models and the numerical parameters chosen are a key factor when simulating these air transport processes.

The numerical prediction of the distribution of a pollutant in a street canyon is an important and complex environmental problem, as well as an architectural one. The construction of more efficient cities in terms of environmental pollution has architectural difficulties in the sense that the requirements for these constructions can be difficult to meet. The transport of pollutant particles in air has been studied by several authors [14, 42, 50, 90]. Finite Element Methods (FEM) have been used mainly for air pollution simulations at a microscale range (i.e. for street canyons) [14, 42, 50, 90]. In these kind of problems, microscale – that is the street scale – processes dominate the numerical solution [59].

The equations that govern the dynamics of a substance transported by a fluid cannot be solved by analytical methods for practical cases and, hence, numerical methods are needed to find useful solutions. One of the main problems with using these tools is the fact that many of them only work for a specific range of situations and parameters. In this thesis we have aimed to develop an accurate tool, as general as possible, that is capable of carrying out simulations for pollution transport in fluids, for a wide range of the physical parameters, without introducing instabilities.

Improvements in current mathematical modeling and computational capabilities allow addressing the solution of complex coupled fluid flow-transport problems,incorporating different physical phenomena into the governing equations.

The numerical modelling of the transport of substances in fluids has several applications of practical interest. Among these we note:

- Study of the environmental impact of a pollutant in air in a metropolitan area in order to identify the main contributors to existing air pollution problems, manage existing focus of emissions or forecasting pollution episodes.
- Study of environmental pollution, be it the quality of air or of water in rivers and

aquifers.

- Study of the dispersion of dissolved substances in estuaries and coastal seas.

The above applications are examples of the several possibilities of the numerical methods developed in the thesis.

1.2 Objectives

The main objective of the thesis is to develop an accurate and robust numerical tool to describe how the concentration of one or more substances distributed in a fluid environment changes under the effect of three transport processes: advection, diffusion and absorption. To this end, the thesis has successfully addressed the following goals:

- Improvement of an existing stabilized finite element method (FEM) based on the Finite Increment Calculus procedure (hereafter called the FIC–FEM technique) for solving the advection-diffusion-absorption equations in two-dimensional (2D) and 3D stationary cases.
- Generalization of the stabilized FIC–FEM procedure to 2D and 3D transient advection-diffusion-absorption problems. For this purpose, we have developed and validated with existing numerical solutions two different numerical strategies:
  - A transient Eulerian formulation based on the stabilized FIC–FEM technique.
  - A transient semi-Lagrangian formulation combining a stabilized FIC–FEM procedure and an innovative particle-based method (PFEM2).
- Development of the necessary numerical tools for the coupled solution of the advection-diffusion-absorption equations with the Navier-Stokes equations for an incompressible fluid. The goal has been the combined resolution of thermal fluid flows and the transport of substances in the fluid.
- Application of the stabilized numerical methods developed in the thesis to practical problems of transport of pollution substances in air in order to show the practical capabilities of the methods.

1.3 State of the art

The solution of advection-diffusion-absorption problems with numerical methods has been a challenge for researchers in this field. It is well known that in solving advection dominated situations the numerical solutions suffer from inherent negative diffusions when a centered finite difference discretization of the convective terms (or a Galerkin FEM) is used [33, 74, 106]. This lack of stability can be partially overcome with a refinement of the mesh/grid used for the computations. Unfortunately, this approach is not viable for practical 3D problems due to the simulation cost that it introduces.

It is also known that the numerical solutions of the advection-diffusion-absorption problem with the Galerkin FEM tend to show global, Gibbs and dispersive oscillations [22, 106]. The stationary solution with the FEM exhibits spurious global oscillations for the convection dominant case. Local Gibbs oscillations are also displayed along the characteristic layers for 2D/3D convective problems. For the case of dominant absorption, on the other hand, Gibbs oscillations can be found near the Dirichlet conditions and in regions where the source term is not distributed regularly. In addition, the solution of the transient problem can show dispersive oscillations when the initial solution and / or the source term are irregularly distributed.

Considerable effort has been invested in recent years to derive stabilized FEM that overcome the above-mentioned misbehaviours in order to accurately solve advection-diffusion-absorption problems. Among these we highlight Artificial Diffusion [33, 74, 106], Taylor-Galerkin [22],Streamline-Upwind Petrov-Galerkin (SUPG) [7, 34, 37], Characteristic Galerkin (CG) [23, 52], Galerkin Least Squares (GLS) [36], Bubble Functions [5, 6], Variational Multiscale (VMS) [30, 35, 76] and Finite Increment Calculus (FIC) [61, 65–67, 69, 73] procedures.

The developments in this thesis are focused on extensions of the FIC–FEM procedure developed in recent years by one of the thesis supervisors and his research team [67–70]. The FIC–FEM procedure allows to reinterpret and derive most stabilized numerical methods using physical arguments. The FIC–FEM approach has also proved to be efficient in the finite element solution of steady-state and transient advection-diffusion-absorption and fluid flow problems [61, 65–70, 73].

In the last decades, various authors have investigated ways of solving transient problems

for advection-dominant (i.e. high-Péclet numbers) problems. For instance, Sevilla et al. [83] studied the influence of the number of integration points in the accuracy of the computation, using high-order curved stabilized FEM and proved that they were one order of magnitude more accurate than classical isoparametric FEM.

However, these numerical techniques, which can all be seen as the addition of artificial diffusion terms to the discretized form of the governing equations, tend to spoil the accuracy of the numerical solution in highly advective cases where the physical diffusion plays almost no role. This difficulty needs to be faced, as problems involving high-Péclet numbers (Pe) are common in many practical situations, namely the study of environmental pollution [8], the simulation of microfluidic channels [92] or some electrohydrodynamics phenomena [87], among others. Idelsohn et al. [38] have recently developed a method which gets rid of these numerical instabilities calculating several scales although it can be too costly with large domains.

Lagrangian, Eulerian-Lagrangian and other combined formulations

Numerical methods based on fully Lagrangian formulations have been developed for high-Péclet flows. For instance, in [79] good results for the convection-diffusion equations coupled to the incompressible flow equations were obtained using two Lagrangian methods. Although Lagrangian methods are less time consuming than Eulerian ones, they can only transport a substance along a single trajectory per particle. Lagrangian methods are used primarily for long-range calculations and they require the addition of a large number of particles over the analysis domain for higher accuracy in diffusive and absorptive problems.

A third option that exploits the benefits of a combined Eulerian-Lagrangian procedure has been studied to solve the advection-diffusion equation [9, 10, 58]. Many of these studies have proved that a splitting of the numerical solution into a Eulerian and a Lagrangian one can overcome the problem of the excessive numerical diffusion observed in stabilized Eulerian methods for high Péclet numbers. The Eulerian-Lagrangian splitting can accurately solve the advective part of the transport equation using a Lagrangian method and then calculate the diffusion (or diffusion-absorption) problem via a Eulerian numerical technique.

Several numerical techniques have been developed within the context of combined methods, such as the Eulerian-Lagrangian method mentioned in the previous lines. For instance, a combination of the Backward Method of Characteristics with various Eulerian methods such as finite differences or the FEM was studied in [3]. Good results were obtained for high Courant numbers, but no clear conclusion was reached on stability and convergence. Cady [9] used a Modified Method of Characteristics together with finite differences and the Galerkin method but found accuracy problems.

In the following years, the problem of global mass conservation due to time integration was addressed. In 1998, Healy and Russell [31] proposed the finite volume Eulerian-Lagrangian localized method with a forward tracking of the characteristics that lead to better results in comparison with previous methods. The performance of four Eulerian-Lagrangian solvers that relied on different interpolators was studied in [80], where it was found that a taut spline interpolator yielded accurate solutions for high-Péclet numbers. This approach, based on a forward tracking algorithm, proved to be more efficient than other methods such as the Petrov-Galerkin technique, for this kind of problems. The accuracy of the Petrov-Galerkin method was improved with the FIC–FEM approach in [68, 70, 77]. Other combined schemes based on Eulerian-Lagrangian localized adjoint methods have been proposed to solve the advection-reaction equations with different tracking algorithms such as the Euler and Runge-Kutta [94].

In the early 2000's, Young et al. studied several Eulerian-Lagrangian methods such as the Eulerian-Lagrangian Boundary Element Method [104], which provided the solution for low numerical diffusion and the Eulerian-Lagrangian method of fundamental solutions [103], which is a mesh-free method that combines the simplicity of a Eulerian solution on a fixed cloud of points and the computational power of the Lagrangian method. More recently, Wang et al. have studied a Eulerian-Lagrangian Discontinuous Galerkin Method [95, 97] and a Modified Method of Characteristics with an adjusted advection procedure [96] for the transient advection-diffusion equations. In 2012, Al-Lawatia [1] developed a mass conservative Eulerian-Lagrangian control volume scheme for solving the same equations in two dimensions (2D), based on the Eulerian-Lagrangian localized adjoint method [31]. In [60], a method for the solution of the advection-diffusion-absorption equations was presented. In 2019, a high-order parallel Eulerian-Lagrangian algorithm for advection-diffusion problems on unstructured meshes was proposed [88]. In 2020, another combined numerical technique based on an explicit, discontinuous spectral element method (DSEM) discretization of the Eulerian equations was developed [57].

In the thesis we have used this bakckground knowledge for deriving a new Eulerian-Lagrangian procedure for solving the advection-diffusion-absorption of a scalar field (either the temperature of a pollution field) and for coupling this numerical technique with the solution of the Navier-Stokes equations for an incompressible thermal flow. As previously mentioned, the practical goal of the work is the accurate modelling and simulation of the transport of pollution substances in air.

The importance of accurately predicting air pollution transport

The increasing awareness recently seen in many cities around the world to reduce greenhouse emissions and, therefore, improve their air quality has made numerical prediction methods take on more and more relevance when designing and building these areas. FEM methods have been used mainly for air pollution simulations at a microscale range (i.e. for street canyons) [14, 43, 51, 90].

Both Lagrangian and Eulerian methods (instead of Gaussian models) have been used for these smaller scale simulations. The Micro Scale Air Pollution Model (MISCAM) [24], for instance, is a Eulerian model used to study dispersion of pollutants in dense urban areas. GEOS-Chem is another Eulerian model which can be used to solve mixing of chemical components in the atmosphere on a regional scale [4]. Yet another Eulerian modelling system is the WRF-Chem which takes into account chemical reactions, turbulence, emissions and the meteorological data at urban and regional scales [27]. The Community Multi-scale Air Quality (CMAQ) is another Eulerian model used for air quality simulations at small and large space scales [98]. Although these models work for different space scales, most of them focus on larger domains than the microscale. Two examples of Lagrangian methods are the NAME and the FLEXPART models, used for smoke tracking and epidemic evolution predictions [81, 85].

Various mathematical models have been used in the past to study air quality in urban areas and can be classified in three main family models: Gaussian, Lagrangian and Eulerian dispersion models. Gaussian parametrical models are based on the well known analytical solution for the Gaussian plume distribution [54] and they provide reliable results at the mesoscale. Gaussian models include AERMOD [16], CTDM [75] and ADMS [11–13], among others. AERMOD is a steady-state dispersion model developed by the US Environmental Protection Agency (EPA) and is generally used to simulate

plumes in the mesoscale. The EPA also developed the Complex Terrain Dispersion Model (CTDM), which is able to get rid of the simulation cost of the mesoscale wind computation. ADMS is a British atmospheric dispersion modeling system which can take into account different locations (urban, coastal or mountain areas) and is able to calculate the interaction of several plumes in an urban area accounting for chemical processes. Since Gaussian plume models are not based on the fluid mechanics equations, they do not provide accurate results for more complex problems [89]. Also, they provide poor results in situations in which the Péclet number is low i.e. diffusive dominant [47] and they cannot account for chemical reactions [53]. As the geometry gets more complex at the microscale range, other models based on the numerical solution of the fluid flow equations at the street level have appeared.

Lagrangian and Eulerian methods are generally used for smaller scale numerical simulations. Eulerian methods aim to solve the fluid transport equations in a fixed reference frame. The Micro Scale Air Pollution Model (MISCAM) [24], for instance, is an Eulerian model used to study dispersion of pollutants in dense urban areas. GEOS-Chem is an Eulerian model which can be used to solve mixing of chemical components in the atmosphere at a regional scale [4]. Another Eulerian modeling system is the WRF-Chem, which takes into account chemical reactions, turbulence, emissions and the meteorological data at urban and regional scales [28]. The Comunity Multi-scale Air Quality (CMAQ) is yet another model used to predict air quality simulations at urban and regional scales [99]. Although these models work on various scales, most of them focus on larger domains than the microscale. Lagrangian methods, on the other hand, transport a property using single point particles, which simplifies and reduces numerical diffusion in advection-dominant processes, many times at the expense of increasing the computational cost. They are used primarily for long-range calculations. Two examples of Lagrangian methods are the NAME and the FLEXPART models, used in smoke tracking and epidemic situations [82, 86].

A more extensive classification of dispersion models can be found in [93].

In the thesis we have developed a new Eulerian-Lagrangian numerical procedure for tracking the transport of substances in air. The resulting method does not require adding stabilization terms for dealing with high advective effects while providing stable and accurate numerical solutions for transport problems at high Péclet and Damköhler numbers.

Kratos framework

The software implementation of the formulation has been done by the author of the thesis in Kratos Multiphysics [21, 44], which is an Open-Source framework for building parallel multi-disciplinary simulation software. Modularity, extensibility and High Performance Computing (HPC) are some of its main objectives. Kratos has BSD licence and is written in C++ with extensive Python interface.

Kratos provides a core which defines the common framework (databases, linear algebra, solvers, etc.) and several applications which work like plug-ins that can be extended in diverse fields.

The implementations of this thesis have given as a result the "FluidTransport Application".

The main features of the numerical approach to be developed in the thesis are outlined in the next section.

1.4 Organization

The thesis is organized as follows.

In Chapter 2 we present the stabilized FIC–FEM formulation for the multidimensional advection-diffusion-absorption transient equation. The new formulation is validated through various transient advection-diffusion-absorption problems.

In Chapter 3 we present the numerical method developed in the thesis for solving advection-diffusion-absorption problems with high advection and/or absorption values to overcome the numerical diffusivity of those cases. Several examples are shown to assess the robustness and accuracy of the new numerical procedure.

In Chapter 4 we present a procedure for coupling the fluid and transport equations to model the distribution of a pollutant in a street in Barcelona. This represents a practical application of the semi-Lagrangian method presented in the second article coupled with fluid equations.

Finally, Chapter 5 summarizes the most relevant conclusions of this work, pointing out

the main achievements of the thesis. In the end, the future lines of work are outlined.

In Appendix A we present an application of the numerical formulation developed in the thesis to validate it through an academic example. This study has been made in parallel with the third paper, presented in Chapter 4.

Chapter 2

FIC–FEM formulation for the multidimensional transient advection-diffusion-absorption equation

2.1 Article data

Title: FIC–FEM formulation for the multidimensional transient advection-diffusion-absorption equation.

Authors: A. Puigferrat, I. de-Pouplana and E. Oñate

Journal: Computer Methods in Applied Mechanics and Engineering 365 (2020) 112984

Received: 2 October 2019 / Accepted: 1 March 2020 / Available online: 21 March 2020

DOI: 10.1016/j.cma.2020.112984

2.2 Introduction

The numerical solution to the advection, diffusion and absorption problem is prone to exhibit global, Gibbs and dispersive oscillations, which require the application of specific stabilization techniques to control instabilities. The local Gibbs oscillations appear along

the characteristic layers in advection-dominated problems. For absorption-dominated cases, Gibbs oscillations can be found near the Dirichlet boundaries and in regions where the distributed source term is nonregular. Also, the solution of the transient problem may exhibit dispersive oscillations when the initial solution and/or the distributed source term are nonregular [70].

Various techniques for solving these problems can be found in literature, such as the Petrov-Galerkin method [7, 34, 37, 41, 52], the Galerkin Least Squares (GLS) method [25, 36], the Variational Multiscale (VMS) method [35] or the characteristic split procedure [105, 106].

In this paper we have chosen the Finite Increment Calculus (FIC) stabilization technique which has been widely used to solve problems involving quasi and fully incompressible fluids and solids with the FEM [15, 61–64, 71, 72]. The FIC technique is based on expressing the equations of balance of mass and momentum in a space/time domain of finite size and retaining higher-order terms in the Taylor series expansion used for expressing the change in the transported variables within the balance domain. In addition to the standard terms of infinitesimal theory, the FIC form of the balance equations contains derivatives of the classical differential equations multiplied by characteristic distances in space and/or time [61–64, 71, 72].

Therefore, the objective of this part of the thesis is the improvement of an existing stabilized finite element method (FEM) based on Finite Increment Calculus for solving the advection-diffusion-absorption equations in two-dimensional (2D) and 3D stationary cases and the generalization and extension of the stabilized FIC–FEM procedure to 2D and 3D transient advection-diffusion-absorption problems. These objectives have been successfully achieved. Details of the mathematical and numerical models developed are given in the paper attached to this chapter.

The content of the paper has been organized as follows. In the first section we formulate the FIC form of the equations governing multidimensional transient convection-diffusion-absorption problems. The finite element discretization is then presented. The stabilization parameters are obtained as an extension of the expression for the stationary case [68]. The accuracy of the multidimensional transient FIC-FEM formulation is finally verified in the solution of a number of 2D transient advection-diffusion-absorption problems using uniform meshes of 3-noded triangles and 4-noded quadrilateral elements.

First we solve a transient advection-diffusion-absorption problem to show the capabilities of the method and validate the results, then three validation problems that result in a steady state are run. After these examples, a purely convective problem with no concentration loss is solved with an explicit scheme and, finally, the advection-diffusion of a concentration drop is calculated in the last example.

2.3 Scientific contribution

This chapter of the compendium presents a novel stabilized FIC–FEM formulation for the multidimensional transient advection-diffusion-absorption equation.

The stabilized variational expression has the standard residual form typical of the FIC–FEM procedure. The stabilized terms introduced by the FIC approach depend on a characteristic element length and two stabilization parameters whose expression is obtained as an extension of the transient 1D form presented in [68] and the multidimensional steady-state forms presented in [70].

A shock capturing term is introduced to account for the Gibbs oscillations across internal/boundary layers. The good behavior of the FIC–FEM formulation has been verified for transient advection-diffusion-absorption problems with numerical solutions evolving to a steady-state, as well as to two fully transient problems.

The results obtained in this part of the thesis are a very first step towards the final objective of the thesis. More specifically, the outcomes of this research have been the starting point for the developments in following chapters.

Available online at www.sciencedirect.com
ScienceDirect
Comput. Methods Appl. Mech. Engrg. 365 (2020) 112984
Computer methods in applied mechanics and engineering
www.elsevier.com/locate/cma

FIC–FEM formulation for the multidimensional transient advection–diffusion–absorption equation

Albert Puigferrat[a], Ignasi de-Pouplana[a,b], Eugenio Oñate[a,b,*]

[a] *Centre Internacional de Metodes Numerics a l'Enginyeria (CIMNE), Barcelona, Spain*
[b] *Universitat Politècnica de Catalunya (UPC), Barcelona, Spain*

Received 2 October 2019; received in revised form 28 February 2020; accepted 1 March 2020
Available online 21 March 2020

Abstract

In this paper we present a stabilized FIC–FEM formulation for the multidimensional transient advection–diffusion–absorption equation. The starting point is the non-local form of the governing equations for the multidimensional transient advection–diffusion–absorption problems obtained via the Finite Increment Calculus (FIC) procedure. The FIC governing equations have a residual form that introduces a characteristic length vector that depends on streamline, absorption and shock capturing stabilization parameters, as well as on a characteristic element size that ensures a stabilized numerical solution using a standard Galerkin FEM. The value of the stabilization parameters is obtained as an extension of the steady-state form. The accuracy of the FIC–FEM formulation is verified in the solution of several transient advection–diffusion–absorption problems using regular meshes of 3-noded triangles and 4-noded quadrilaterals.
© 2020 Elsevier B.V. All rights reserved.

Keywords: Advection–diffusion–absorption; Transient solution; Multidimensional; Finite element method; Finite increment calculus; FIC

1. Introduction

The numerical solution of the advection–diffusion–absorption equation by the Galerkin FEM can exhibit oscillations due to a number of reasons. For the stationary convection-dominated case global oscillations in the analysis can be found, as well as local Gibbs oscillations along the characteristic layers for 2D and 3D problems. Gibbs oscillations near the Dirichlet boundaries and in regions where the source term has an irregular distribution can also appear for stationary absorption-dominated problems. For transient problems dispersive oscillations can appear when the initial solution and/or the distributed source term are non regular [1,2].

A number of numerical procedures has been derived in recent decades aiming to overcome the above limitations of Galerkin FEM for solving advection–diffusion–absorption problems. The goal in all cases has been to obtain "stabilized" numerical solution that is free of spurious oscillations and has a physical meaning. Among the many procedures we can mention the family of streamline-upward Petrov–Galerkin (SUPG) methods. The original SUPG methods for advection–diffusion problems [3–7] where enhanced with the addition of non linear shock-capturing terms aiming to control the Gibbs oscillations across internal/boundary layers for advection–diffusion problems

* Corresponding author at: Universitat Politècnica de Catalunya (UPC), Barcelona, Spain.
E-mail address: onate@cimne.upc.edu (E. Oñate).

https://doi.org/10.1016/j.cma.2020.112984
0045-7825/© 2020 Elsevier B.V. All rights reserved.

[8–16]. Other families of stabilized methods for this type of problems were based on Galerkin Least Squares (GLS) [17], Variational Multiscale (VMS) [18] and Characteristic split procedures [2,19]. Many of these methods are reviewed in [20].

Control over the dispersive oscillations for transient advection–diffusion problems via SUPG methods and space–time FEM were reported in [21] and [22], respectively.

Extensions of the SUPG method for advection–diffusion–reaction problems were reported in [23–25]. Other stabilization techniques for these problems were based in the GLS method [26,27], the addition of internal bubbles [28–33] and on variations of VMS procedures [34–38]. A review of some of these methods is presented in [39].

Oñate et al. [40,41] derived a non linear stabilization procedure for the steady state advection–diffusion–absorption problem using a single stabilization parameter via a Finite Increment Calculus (FIC) approach. Oñate and Felippa [42] used the variational FIC method for obtaining exact nodal solutions for 1D diffusion–reaction problems (including Helmholtz problems) using also a single linear stabilization parameter.

The homogeneous steady advection–diffusion–reaction equation has typically two fundamental solutions. This has led the way to the derivation of linear stabilized methods that provide nodally exact solutions in 1D using *two stabilization parameters* via internal bubbles [31], SUPG [27] and VMS [37] procedures.

A particular class of two-parameter stabilized models for 1D and multidimensional steady and transient advection–diffusion production problems using the FIC approach and the FEM was presented by Nadukandi, Oñate and García-Espinosa [43,44].

Starting from a different perspective, but still within the FIC framework, Oñate, Miquel and Nadukandi [45] presented a FIC–FEM formulation for the 1D steady-state and transient advection–diffusion–absorption equations using two linear stabilization parameters. The FIC–FEM formulation yielded exact nodal solution for 1D steady-state problems using regular meshes of 2-noded linear elements. Very accurate results were also obtained in [45] for 1D stationary problems solved with irregular meshes, as well as for 1D transient problems. The FIC–FEM formulation presented in [45] was extended by the same authors in [46] to multidimensional steady-state advection–diffusion–absorption problems. Good results were obtained for the problems analyzed using linear 3-noded triangles and bilinear 4-noded quadrilaterals.

In this work we extend to the multidimensional transient case the 1D FIC–FEM formulation presented in [46]. The lay-out of the paper is the following. In the next section we formulate the FIC form of the equations governing multidimensional transient convection–diffusion–absorption problems. The finite element discretization is then presented. The stabilization parameters are obtained as an extension of the expression for the stationary case [45]. The accuracy of the multidimensional transient FIC–FEM formulation is verified in the solution of a number of 2D transient advection–diffusion–absorption problems using uniform meshes of 3-noded triangles and 4-noded quadrilateral elements. Accurate solutions are obtained in all cases.

2. The multidimensional transient advection–diffusion–reaction problem

2.1. Governing equations

Transport balance

The transport balance equation in a domain of area/volume Ω can be expressed as

$$r_t = 0 \quad \text{in } \Omega \tag{1a}$$

with

$$r_t := \rho c \left(\frac{\partial \phi}{\partial t} + \mathbf{v}^T \boldsymbol{\nabla} \phi \right) - \boldsymbol{\nabla}^T \mathbf{D} \boldsymbol{\nabla} \phi + s\phi - Q \tag{1b}$$

For 3D problems,

$$\mathbf{v} = [v_1 \ , \ v_2 \ , \ v_3]^T \quad , \quad \mathbf{D} = \begin{bmatrix} k_1 & 0 & 0 \\ 0 & k_2 & 0 \\ 0 & 0 & k_3 \end{bmatrix} \quad , \quad \boldsymbol{\nabla} = \left[\frac{\partial}{\partial x_1} \ , \ \frac{\partial}{\partial x_2} \ , \ \frac{\partial}{\partial x_3} \right]^T \tag{2}$$

In Eqs. (1a)–(1b) ϕ is the transported variable (i.e., the temperature in a heat transfer problem or the concentration in a mass transfer problem), v_i is the ith component of the velocity vector $\mathbf{v}$; ρ, c and k_i are the density, the specific

flux parameter and the conductivity of the material along the ith global direction, respectively and s is the reaction parameter. In the following, and unless otherwise specified, we will assume that the velocity field is solenoidal and that the problem parameters (ρ, c, k, s) are constant over the analysis domain Ω.

Boundary conditions

$$\phi - \phi^p = 0 \quad \text{on } \Gamma_\phi \tag{3}$$

$$r_\Gamma = 0 \quad \text{on } \Gamma_q \tag{4}$$

with

$$r_\Gamma := -q_n + q_n^p \tag{5}$$

where

$$q_n = \mathbf{q}^T \mathbf{n} \quad , \quad \mathbf{q} = -\mathbf{D}\nabla\phi \tag{6}$$

In Eqs. (3)–(6) ϕ^p and q^p are the prescribed values of the transported variable and the outgoing diffusive flux at the Dirichlet and Neumann boundaries Γ_ϕ and Γ_q, respectively, with $\Gamma_\phi \cup \Gamma_q = \Gamma$, Γ being the total boundary of the domain and $\mathbf{n}$ is the unit vector normal to the boundary.

The definition of the problem is completed with the *initial conditions*

$$\phi(\mathbf{x}, t_0) = \phi_0(\mathbf{x}) \tag{7}$$

where $\phi_0(\mathbf{x})$ is the value of the transported variable at time $t = t_0$.

In this work we will consider cases for which $s \geq 0$ only. This includes the following particular problems:

(i) Advection–diffusion–absorption ($|\mathbf{v}| \neq 0$, $K \neq 0$, $s > 0$).
(ii) Advection–diffusion ($|\mathbf{v}| \neq 0$, $K \neq 0$, $s = 0$).
(iii) Diffusion–absorption ($|\mathbf{v}| = 0$, $K \neq 0$, $s > 0$).
(iv) Advection–absorption ($|\mathbf{v}| \neq 0$, $K = 0$, $s > 0$).

In the above K is the average diffusion given by $K = \left[\frac{1}{n_d}\sum_{i=1}^{n_d}(k_i)^2\right]^{1/2}$, where n_d is the number of space dimensions (i.e. $n_d = 2$ for 2D problems).

2.2. Finite increment calculus (FIC) expressions

The governing equations (1a) and (1b) and the boundary conditions (3)–(6) are expressed using the FIC theory as [41].

Transport balance

$$r_t - \underline{\frac{1}{2}\mathbf{h}^T \nabla r_t} = 0 \qquad \text{in } \Omega \tag{8}$$

with $\mathbf{h} = [h_1, h_2, h_3]^T$ in 3D.

Boundary conditions

$$\phi - \phi^p = 0 \quad \text{on } \Gamma_\phi \tag{9a}$$

$$r_\Gamma + \underline{\frac{1}{2}h_n r_t} = 0 \quad \text{on } \Gamma_q \quad , \quad \text{with } h_n = \mathbf{h}^T \mathbf{n} \tag{9b}$$

Eqs. (8) and (9b) are obtained by expressing the balance of fluxes in an arbitrary prismatic space domain of size $h_1 \times h_2 \times h_3$ within the global problem domain and at the Neumann boundary, respectively. The distances h_i

are termed *characteristic lengths* of the FIC method. The variations of the transported variable within the balance domain are approximated by Taylor series expansions retaining one order higher terms than in the infinitesimal theory [47]. This higher order expansions lead to the underlined terms in Eqs. (8) and (9). These terms lead naturally to stabilized numerical schemes.

Note that as the characteristic length vector $\mathbf{h}$ tends to zero the FIC governing equations gradually recover the standard infinitesimal form, giving in the limit (for $\mathbf{h} = \mathbf{0}$) $r_t = 0$ in Ω and $r_\Gamma = 0 \quad$ on Γ_q.

The stability and accuracy of the numerical solution depends on the components of the characteristic length vector $\mathbf{h}$. At the discretization level the length of $\mathbf{h}$ is usually expressed as a proportion of a typical grid dimension [47].

The FIC equations are the starting point for deriving different stabilized numerical methods. Combining the FIC equations with the Galerkin FEM leads to the so-called FIC–FEM procedure that has been successfully applied to the solution of many problems in convective transport, fluid and solid mechanics such as advection–diffusion [16, 47–49], diffusion–absorption and Helmholtz [42], advection–diffusion–absorption [40,41], advection–diffusion–reaction [45], incompressible fluid flow [50–54], fluid–structure-interaction [55–57], particle–laden flows and standard and incompressible solid mechanics [58–60]. The FIC approach has also been applied to the solution of a variety of problems in mechanics using the meshless finite point method [61–64].

3. Definition of the characteristic length vector

The characteristic length vector $\mathbf{h}$ is designed so that the expression for all the stabilization matrices and vectors reduces to those given for the 1D case as reported in [45].

With this objective in mind the following expression for the characteristic length vector has been chosen in this work

$$\mathbf{h} = \mathbf{h}_v + \mathbf{h}_r + \mathbf{h}_{sc} \tag{10}$$

The characteristic length vectors in the r.h.s. of Eq. (10) are defined as follows.

Streamline characteristic length vector, $\mathbf{h}_v$

In Eq. (10) $\mathbf{h}_v$ is a length vector along the velocity direction defined as

$$\mathbf{h}_v = \alpha_v l_v \frac{\mathbf{v}}{|\mathbf{v}|} = \alpha_v l_v \hat{\mathbf{v}} \tag{11}$$

where α_v is a streamline stabilization parameter, l_v is a characteristic element dimension and $\hat{\mathbf{v}}$ is a unit velocity vector.

Absorption characteristic length vector, $\mathbf{h}_r$

In Eq. (10) $\mathbf{h}_r$ is a characteristic length vector induced by absorption effects and defined as

$$\mathbf{h}_r = \mathbf{H}_r \nabla\phi \qquad \text{with} \quad \mathbf{H}_r = \frac{2sgn(r_t)}{r_s}\left[\mathbf{D}_s + \alpha_r D \hat{\mathbf{v}}\hat{\mathbf{v}}^T\right] \tag{12a}$$

where α_r is an absorption stabilization parameter, $D = \hat{\mathbf{v}}^T \mathbf{D} \hat{\mathbf{v}}$ and r_s is the space residual defined as

$$r_s := r_t - \rho c \frac{\partial \phi}{\partial t} \tag{12b}$$

Matrix $\mathbf{D}_s$ in Eq. (12a) is defined for different element types as follows.

3-noded triangles and 4-noded tetrahedra

$$\mathbf{D}_s = \frac{s}{(n+1)} \sum_{i=1}^{n} \mathbf{l}_i \mathbf{l}_i^T \tag{13}$$

where $\mathbf{l}_i$ is the vector joining the baricenter of the element and the ith node, and n is the number of nodes of the element.

The diffusion introduced by matrix $\mathbf{D}_s$ takes care of the instabilities induced by the irregularity of the triangular mesh near boundaries that develop parabolic layers [46].

Any other element $\mathbf{D}_s = [0]$

Shock capturing characteristic length vector $\mathbf{h}_{sc}$

In Eq. (10) $\mathbf{h}_{sc}$ is a shock-capturing characteristic length vector in the direction of the gradient of the solution. This vector accounts for the Gibbs oscillations across characteristic internal/boundary layers in the numerical solution for advection–diffusion problems. It is defined as

$$\mathbf{h}_{sc} = h_{sc}\widehat{\nabla\phi} \tag{14a}$$

where $\widehat{\nabla\phi} = \frac{\nabla\phi}{|\nabla\phi|}$ is the unit gradient vector, and

$$h_{sc} = (1-\beta^2)\left[l_{sc}sgn(r_s) - \frac{2|\nabla\phi|}{r_s}(\mathbf{D}+\mathbf{D}_s) : (\mathbf{I}-\hat{\mathbf{v}}\hat{\mathbf{v}}^T)\right] \tag{14b}$$

In Eq. (14b) β is a non linear parameter that depends on the angle θ between the velocity vector and the gradient vector. It is defined as

$$\beta = \begin{cases} 1 & \text{if} \quad \theta < \theta_c \\ \hat{\mathbf{v}}^T\widehat{\nabla\phi} & \text{if} \quad \theta \geq \theta_c \end{cases} \tag{14c}$$

where θ_c is a critical angle. In this work we have taken $\theta_c = 20°$.

The parameter β controls the amount of shock-capturing nonlinear diffusion active at any point of the domain [46]. When the gradient vector is parallel to the velocity vector then $\beta = 1$, h_{sc} vanishes and the linear stabilization terms suffice to diminish spurious numerical oscillations about the layers. The term $1-\beta^2$ in Eq. (14b) gradually increases the magnitude of the shock-capturing term from zero, when the gradient vector is aligned to velocity vector, to a maximum value when the layer gradient is orthogonal to the velocity.

The shock capturing term is neglected in fully transient problems in which the transported variable has space gradients that move in time within the analysis domain. Examples are the convection of a temperature plateau (Section 7.5) or the advection–diffusion of a concentration field (Section 7.6). Introducing shock capturing effects in these cases leads to an excessive and unrealistic numerical diffusion.

4. FIC-FEM formulation for the multidimensional transient advection–diffusion–absorption problem

4.1. Weighted residual form of the FIC equations

The weighted residual form of the FIC governing equations (8) and (9) is written as

$$\int_\Omega W(r_t - \frac{1}{2}\mathbf{h}^T\nabla r_t)d\Omega + \int_{\Gamma_q} W(-q_n + q_n^p + \frac{1}{2}h_n r_t)d\Gamma = 0 \tag{15}$$

where W are arbitrary weighting functions.

Integrating by parts the FIC term in the first integral of (15) gives

$$\int_\Omega \left(W + \frac{1}{2}(\nabla^T W)\mathbf{h}\right) r_t d\Omega + \oint_{\Gamma_q} W(-q_n + q_n^p)d\Gamma = 0 \tag{16}$$

Note that the FIC term has vanished from the boundary integral, as it is usual in the FIC–FEM approach [47,65].

Let us substitute the expression for the characteristic vector $\mathbf{h}$ of Eq. (10) into Eq. (16). This gives (using Eqs. (11), (12a) and (14a))

$$\int_\Omega \left[W r_t + \frac{1}{2}(\nabla^T W)\left(\alpha_v l_v \hat{\mathbf{v}} + \mathbf{H}_r\nabla\phi + h_{sc}\frac{\nabla\phi}{|\nabla\phi|}\right) r_t\right] d\Omega + \oint_{\Gamma_q} W(-q_n + q_n^p)d\Gamma = 0 \tag{17}$$

The final step is the integration by parts of the diffusive term in the expression of r_t in the first term of the first integral of Eq. (17). This gives, after replacing the definition of $\mathbf{H}_r$ in Eq. (17) and grouping some terms, the following expression for the weak variational form of the FIC governing equations

$$\begin{aligned} &\int_\Omega \left[\rho c\bar{W}\frac{\partial\phi}{\partial t} + \rho c W\mathbf{v}^T\nabla\phi + (\nabla^T W)\mathbf{D}_T\nabla\phi + W s\phi + \frac{1}{2}(\nabla^T W)\mathbf{h}_v s\phi\right] d\Omega + \\ &\int_\Omega \frac{1}{2}(\nabla^T W)\mathbf{h}\left[-\nabla^T(\mathbf{D}\nabla\phi) - Q\right] d\Omega - \int_\Omega W Q d\Omega + \oint_{\Gamma_q} W q_n^p d\Gamma = 0 \end{aligned} \tag{18}$$

The space weighting function $\bar{W}$ in Eq. (18) is given by

$$\bar{W} = W + \frac{1}{2}\mathbf{h}_v^T \boldsymbol{\nabla} W \tag{19}$$

The expression of the total diffusivity matrix $\mathbf{D}_T$ in Eq. (18) is

$$\boxed{\mathbf{D}_T = \mathbf{D} + \alpha_v \mathbf{D}_v + \mathbf{D}_s + \alpha_r D \hat{\mathbf{v}}\hat{\mathbf{v}}^T + \mathbf{D}_{sc}\mathbf{I}} \tag{20}$$

where $\mathbf{D}$ and $\mathbf{D}_s$ are defined in Eqs. (2) and (13), respectively, $\mathbf{I}$ is the unit matrix and

$$\mathbf{D}_v = \frac{l_v}{2}\hat{\mathbf{v}}\mathbf{v}^T \tag{21a}$$

$$\mathbf{D}_{sc} = \left(\frac{1}{2} l_{s_c} \frac{|r_t|}{|\boldsymbol{\nabla}\phi|} - (\mathbf{D} + \mathbf{D}_s) : (\mathbf{I} - \hat{\mathbf{v}}\hat{\mathbf{v}}^T)\right)(1 - \beta^2) \tag{21b}$$

4.2. FIC-FEM Equations

We interpolate the transported variable ϕ in the standard FEM fashion over a mesh of elements with n nodes [2,66] as

$$\phi \simeq \hat{\phi} = \sum_{i=1}^{n} N_i \phi_i \tag{22}$$

where N_i denotes the usual shape function associated to the nodal global point i, ϕ_i is the value of ϕ at the nodal global point i (hereafter denoted as nodal variables) and n denotes the number of points of the mesh.

Introducing Eq. (22) into the FIC variational form (18) and using a Galerkin approach ($W_i = N_i$) gives the final system of discretized equations as

$$\mathbf{M}\dot{\boldsymbol{\phi}} + [\mathbf{K} + \mathbf{C} + \mathbf{S}]\boldsymbol{\phi} = \mathbf{f} \tag{23}$$

where $\boldsymbol{\phi} = [\phi_1, \phi_2, \ldots, \phi_N]^T$ is the vector of nodal unknowns, with N being total number of nodes in the mesh.

The rest of matrices and vector $\mathbf{f}$ in Eq. (23) are obtained in the standard FEM fashion by assembling the element contribution given by

$$\mathbf{M}^e_{ij} = \int_{\Omega^e} \rho c N_i N_j d\Omega + \int_{\Omega^e} \rho c \frac{1}{2}(\boldsymbol{\nabla}^T N_i)\mathbf{h}_v N_j d\Omega \tag{24}$$

$$\mathbf{K}^e_{ij} = \int_{\Omega^e} (\boldsymbol{\nabla}^T N_i)\mathbf{D}_T \boldsymbol{\nabla} N_j d\Omega - \int_{\Omega^e} \frac{1}{2}(\boldsymbol{\nabla}^T N_i)\mathbf{h}\boldsymbol{\nabla}^T(\mathbf{D}\boldsymbol{\nabla} N_j) d\Omega \tag{25}$$

$$\mathbf{C}^e_{ij} = \int_{\Omega^e} \rho c N_i \mathbf{v}^T \boldsymbol{\nabla} N_j d\Omega \tag{26}$$

$$\mathbf{S}^e_{ij} = \int_{\Omega^e} s N_i N_j d\Omega + \int_{\Omega^e} \frac{1}{2}(\boldsymbol{\nabla}^T N_i)\mathbf{h}_v s N_j d\Omega \tag{27}$$

$$\mathbf{f}^e_i = \int_{\Omega^e} \left(N_i + \frac{1}{2}(\boldsymbol{\nabla}^T N_i)\mathbf{h}\right) Q d\Omega - \oint_{\Gamma^e_q} N_i q^p_n d\Gamma \tag{28}$$

We note that the second integral in Eq. (25) vanishes for linear finite element approximations, such as those used in this work.

Good results have been obtained for the solution of the problems presented in this paper using a lumped form of matrix $\mathbf{M}$. An exception is the problem of the evolution of a concentration field presented in Section 7.6 for which using the consistent form of matrix $\mathbf{M}$ given in Eq. (24) was essential to reduce excessive diffusion.

5. Transient solution scheme

5.1. Implicit time integration scheme

We discretize in time the system of Eq. (23) using a Generalized Trapezoidal rule [66,67]. The solution for the nodal values at a time instant is found using an incremental iterative strategy as

$${}^{i}\mathbf{H}^n \Delta\boldsymbol{\phi} = -{}^{i}\mathbf{r}^n_t \tag{29}$$

$$ {}^{i}\mathbf{H}^{n} = \frac{1}{\theta \Delta t}\mathbf{M} + {}^{i}\mathbf{K}^{n} + \mathbf{C} + \mathbf{S} \tag{30} $$

$$ {}^{i}\mathbf{r}_{t}^{n} := \mathbf{M}\dot{\boldsymbol{\phi}} + [{}^{i}\mathbf{K}^{n} + \mathbf{C} + \mathbf{S}]{}^{i}\boldsymbol{\phi}^{n+\theta} - {}^{i}\mathbf{f}^{n} \tag{31} $$

where $\Delta\boldsymbol{\phi}$ is the increment of the nodal variables, θ is a non dimensional time parameter with $0 \leq \theta \leq 1$. A value of $\theta > 0.5$ is required for the integration scheme to be unconditionally stable [2,66,67], $(\cdot)^n$ denotes values at time $t = t_n$ and ${}^{i}(\cdot)$ denotes values at the ith iteration.

In Eq. (31) we define $\dot{\boldsymbol{\phi}} = \frac{\boldsymbol{\phi}^{n+\theta} - \boldsymbol{\phi}^{n}}{\theta \Delta t}$.

From the value of $\Delta\boldsymbol{\phi}$ obtained from solving Eq. (29) we compute the value of $\boldsymbol{\phi}^{n+\theta}$ at the $i+1$ iteration as

$$ {}^{i+1}\boldsymbol{\phi}^{n+\theta} = {}^{i}\boldsymbol{\phi}^{n+\theta} + \Delta\boldsymbol{\phi} \tag{32} $$

The iterative solution at t_{n+1}, ${}^{i+1}\boldsymbol{\phi}^{n+1}$, is obtained as

$$ {}^{i+1}\boldsymbol{\phi}^{n+1} = \frac{1}{\theta}{}^{i+1}\boldsymbol{\phi}^{n+\theta} + \left(1 - \frac{1}{\theta}\right)\boldsymbol{\phi}^{n} \tag{33} $$

The non-linearity in the expression of matrix $\mathbf{H}$ in Eq. (30) is due to the dependence of the shock-capturing term in matrix $\mathbf{K}$ via matrix $\mathbf{D}_{sc}$ (see Eq. (21b)).

The iterations proceed until convergence is achieved for both the unknown ϕ and the residual measured in a L_2 norm. In the transient problems solved in this work, convergence within each time step was typically achieved in 2–3 iterations.

5.2. Explicit time integration scheme

If we rewrite the residual in Eq. (31) choosing $\theta = 0$ and defining now $\dot{\boldsymbol{\phi}}$ as $\frac{\boldsymbol{\phi}^{n+1} - \boldsymbol{\phi}^{n}}{\Delta t}$ leads to the following explicit solution scheme

$$ \boldsymbol{\phi}^{n+1} = \boldsymbol{\phi}^{n} + \Delta t \mathbf{M}_{d}^{-1}\left[\mathbf{f}^{n} - (\mathbf{K}^{n} + \mathbf{C} - \mathbf{S})\boldsymbol{\phi}^{n}\right] \tag{34} $$

where $\mathbf{M}_d$ denotes the lumped diagonal form of matrix $\mathbf{M}$.

In the expression of $\mathbf{K}$ of Eq. (34) the shock-capturing terms are taken as constant within a time step.

6. Computation of the stabilization parameters

6.1. General expression of the stabilization parameters

The optimal value of the stabilization parameters α_v and α_r giving nodally exact solutions is quite difficult in the transient case due to the multiple forms that the solution can take as it evolves in time. We present a procedure for computing a quasi-optimal value of α_v and α_r that has proved to yield accurate results for transient advection–diffusion–absorption problems evolving towards a steady state solution, as well as for solutions involving the pure advection of a discontinuous function. The method is an extension of the approach proposed and successfully tested for 1D transient problems in [45].

The transient equation (1b) can be written as follows

$$ \rho c \mathbf{v}^{T}\boldsymbol{\nabla}\phi - \boldsymbol{\nabla}^{T}(\mathbf{D}\boldsymbol{\nabla}\phi) + \bar{s}\phi - Q = 0 \tag{35} $$

where

$$ \bar{s} = s + s_t \quad \text{with } s_t = \rho c \frac{\dot{\phi}}{\phi} \tag{36} $$

Eq. (35) defines a pseudo-stationary problem in which a non linear reaction term has been introduced.

The non linear reaction term s_t can be approximated as

$$ s_t = \frac{\rho c}{\theta \Delta t} f(\kappa) \tag{37} $$

with

$$ f(\kappa) \geq 0 \quad \text{and} \quad \kappa = \frac{\phi^{n+\theta} - \phi^{n}}{\phi^{n+\theta}} \tag{38} $$

The value of s_t in Eq. (37) has been limited in this work to a ten percent of the value of the actual absorption parameter s. s_t has been taken as zero for advective–diffusive problems.

From Eq. (36) we can define an equivalent Damköhler number $\bar{\sigma}$ as

$$\bar{\sigma} = \sigma + \sigma_t \quad \text{with} \quad \sigma_t = \frac{\rho c}{\theta C} f(\kappa) \tag{39}$$

where σ is the Damköhler number defined in Eq. (44) and $C = \frac{v \Delta t}{l^e}$ is the element Courant number where l^e is the characteristic element length. For 1D problems l^e is taken as the element length. For 2D problems we have chosen $l^e = \sqrt{2\Omega^e}$ where Ω^e is the area of the element.

The following definition for $f(\kappa)$ has been chosen in the examples solved in this work

$$f(\kappa) = \frac{2}{\tanh 1} \tanh \left(\delta \frac{\left| \phi^n - \phi^{n-1} \right|_\infty^e}{\left| \phi^n + \phi^{n-1} \right|_\infty^e} \right) \tag{40}$$

where $|a|_\infty^e$ denotes the maximum value of a within an element and δ is a positive number that controls the slope of the function $\tanh(\cdot)$ that ranges from zero to one.

Function $f(\kappa)$ has been designed so that $f(\kappa) = 0$ (and $\sigma_t = 0$) for a steady-state problem (or in zones where $\dot{\phi} = 0$), and $f(\kappa) = \frac{2}{\tanh 1}$ (and $\sigma_t = \frac{2}{\theta C}$) for cases when $\phi(x,t)$ suddenly changes from a zero value to a finite value at a node.

Good results were obtained in the transient problems solved using Eq. (40) with $\delta = 1$. The optimal choice of δ in terms of the nature of the transient solution is a matter that deserves further research.

We highlight that for the explicit time integration scheme we have used $\theta = 1$ in the definition of s_t and σ_t.

The stabilization parameters α_v and α_r in Eqs. (11) and (12a) for the transient convection–diffusion-radiation problem are defined as follows

$$\alpha_v = \begin{cases} \dfrac{2}{\bar{\sigma}} \left(1 - \dfrac{\bar{\sigma} \tanh \gamma}{\xi - 1} \right) & , \quad \bar{\sigma} \geq 2^{-12} \\ \dfrac{\bar{\sigma}}{3} + \bar{\alpha}_v \left(1 - \dfrac{\bar{\sigma}}{\gamma} \right) & , \quad \bar{\sigma} < 2^{-12} \end{cases} \tag{41}$$

with

$$\bar{\alpha}_v = \coth \gamma - \frac{1}{\gamma} \tag{42}$$

and

$$\alpha_r = \gamma \left[\frac{\sigma}{\varphi} \left(\frac{\xi - 1 + \varphi}{\xi - 1} \right) - \alpha_v \right] - 1 - \frac{1}{D} \hat{\mathbf{v}}^T \mathbf{D}_s \hat{\mathbf{v}} \tag{43}$$

In the above expressions

$$\begin{aligned} &\xi = \frac{\cosh \lambda}{\cosh \gamma} \quad \text{with} \quad \lambda = \left(\gamma^2 + w \right)^{1/2} \\ &\gamma = \frac{\rho c |\mathbf{v}| l_v}{2D} \quad , \quad w = \frac{\rho c s (l_v)^2}{D} \quad , \quad \sigma = \frac{s l_v}{|\mathbf{v}|} = \frac{w}{2\gamma} \end{aligned} \tag{44}$$

The expressions of α_v and α_r in Eqs. (41) and (43) are an extension of the values for the steady-state problem presented in [46].

In Eq. (43) φ is a constant such that $2 \leq \varphi \leq 3$. The "exact" expression of α_r for 1D problems requires choosing $\varphi = 3$ [46]. In our computations for 2D problems we have obtained good results using $\varphi = 2$.

The characteristic length l_v is defined as the size of the element in the direction of the velocity $\mathbf{v}$. Representing the element's edge joining nodes a and b with the vector $\mathbf{l}_{ab}$, l_v is computed as

$$l_v = \max_{\text{edges}} \left\{ \mathbf{v}^T \mathbf{l}_{ab} \right\} \tag{45}$$

The characteristic length l_{sc} is generally defined as

$$l_{sc} = \sqrt{2\Omega^e} \tag{46}$$

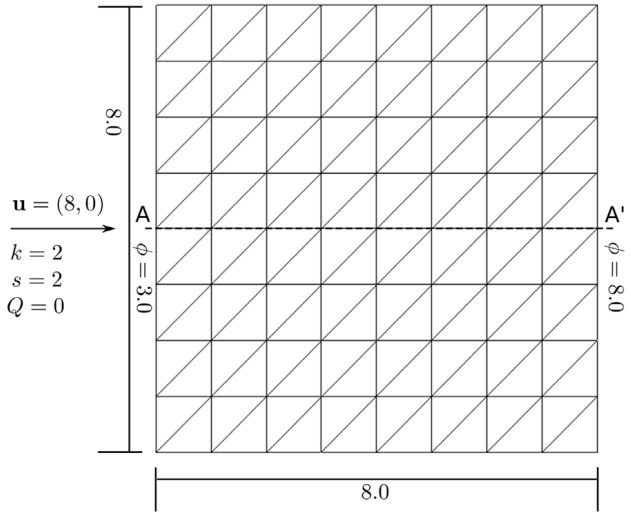

Fig. 1. Transient advection–diffusion–absorption problem. Square domain with linear velocity and zero source.

where Ω^e is the element area. For elements belonging to the boundary in meshes of 3-noded triangles we have chosen

$$l_{sc} = 2\sqrt{\Omega^e} \tag{47}$$

The expression of l_{sc} in Eq. (47) introduces a higher value of the shock-capturing term at the boundaries where sharp gradients exist in directions different from the velocity directions.

7. Examples

In the examples shown next the density ρ and the specific flux c are chosen such that $\rho c = 1$. We have also assumed an isotropic diffusion of value k.

7.1. Transient advection–diffusion–absorption problem

The analysis domain $(x, y) = [0, 8] \times [0, 8]$ is discretized into a regular mesh of $(2 \times 8) \times (2 \times 8)$ 3-noded triangles of unit rectangular side ($l_v = 1$) (Fig. 1). The advection, diffusion and reaction coefficients are chosen as $v_1 = 8$, $k = 2$ and $s = 2$. The transported variable is the temperature. The schematics of the problem can be seen in Fig. 1. The problem data yields the dimensionless numbers $\gamma_v = 2$ and $\omega_v = 1$.

The Dirichlet boundary conditions $\phi(x = 0) = 3$ and $\phi(x = 8) = 8$ are employed. The initial solution is chosen to have a linear profile. The transient solution was obtained iteratively using the implicit scheme of Eqs. (29)–(33) with $\theta = 1.0$ and a time step of $\Delta t = 0.0625$ s (Fig. 2). This corresponds to an element Courant number $C = 0.5$. An exponential layer gradually develops at the right boundary which triggers a global instability in the Galerkin FEM. As there is not significant dispersive phenomena this global instability is successfully controlled by the SUPG method (well-known result) and the FIC–FEM method developed in this work. Fig. 3 shows a perspective view of the quasi-steady-state solution for the temperature for $t = 2$ s. The steady state solution matches the 1D result reported in [45].

Next, the same problem is run with a non-uniform mesh. Fig. 4 shows the schematics of the case. The transient solution is also obtained iteratively using the implicit scheme of Eqs. (29)–(33) with $\theta = 1.0$ and a time step of $\Delta t = 0.0625$ s (Fig. 5). Results show a good behavior of the numerical scheme for non-uniform meshes. The lowest value at $t = 2$ s is virtually the same in both cases.

Fig. 6 shows a perspective view of the quasi-steady-state solution for the temperature for $t = 2$ s.

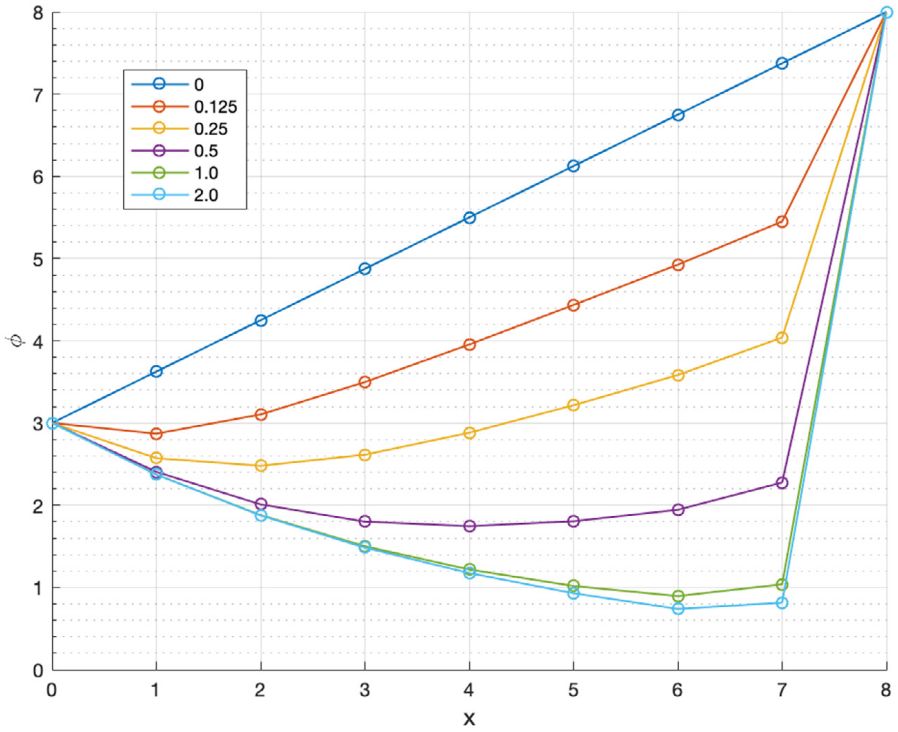

Fig. 2. Transient advection–diffusion–absorption problem. Transient FIC–FEM solution obtained with a structured mesh of 2 × 8 × 8 three-noded triangles. The transient solutions are plotted along line A-A' at times 0.0 s, 0.125 s, 0.25 s, 0.5 s, 1 s and 2 s.

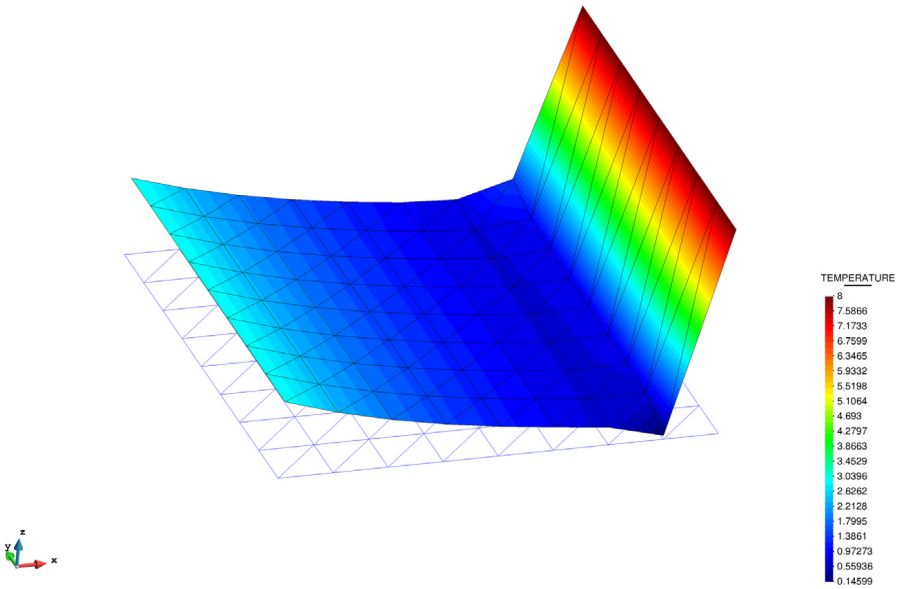

Fig. 3. Transient advection–diffusion–absorption problem. Solution obtained at$t = 2$ s.

7.2. *Skewed flow in a square domain with non-uniform boundary conditions*

The domain is $(x, y) = [0, 1] \times [0, 1]$. The problem data is: $\mathbf{v} = [-5 \cdot 10^6, -9 \cdot 10^6]^T$, $k = 1$, $\rho c = 1$, $s = 0$ and $Q = 0$. The transported variable is again the temperature. The boundary conditions are: $\phi = 1$ on $(x = 1, y > 0.7) \cup (x < 1, y = 1)$, $\phi = 0.5$ at $(x = 1, y = 0.7)$ and $\phi = 0$ on the rest of the boundary (Fig. 7). The transient solution was obtained using the implicit scheme here presented with $\theta = 0.8$ and a time

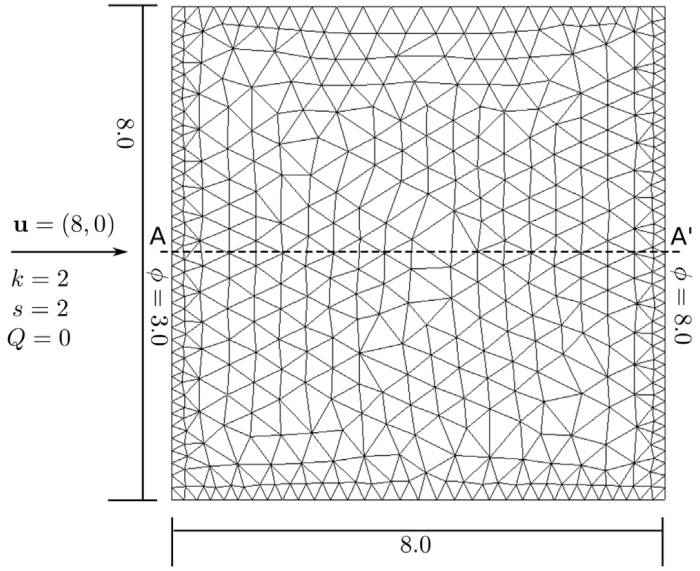

Fig. 4. Transient advection–diffusion–absorption problem with a non-uniform mesh. Square domain with linear velocity and zero source.

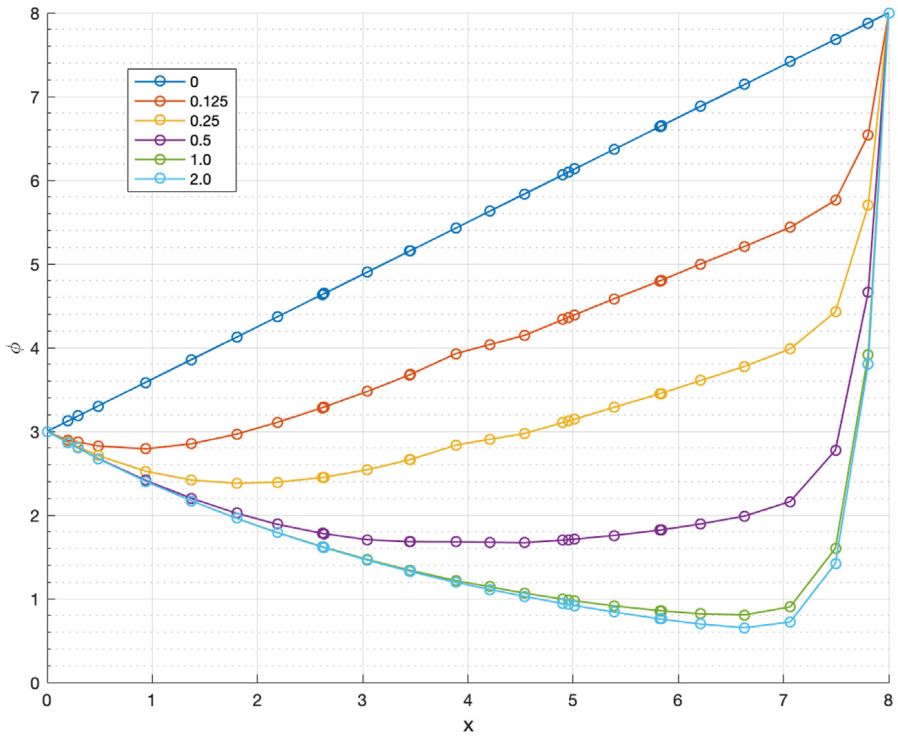

Fig. 5. Transient advection–diffusion–absorption problem. Transient FIC–FEM solution obtained with a non-uniform mesh of three-noded triangles. The transient solutions are plotted along line A-A' at times 0.0 s, 0.125 s, 0.25 s, 0.5 s, 1 s and 2 s.

step of Δt = 1e-09 s. Convergence within each time step was found in 2–3 iterations. The solution develops an exponential boundary layer at the outflow boundary and an internal characteristic layer (parabolic) which is skewed to the mesh and the boundary. Both layers are subgrid phenomena for the considered mesh resolution. Both the exponential and characteristic layers are reproduced in the FIC–FEM solution without spurious oscillations near the layers. The FIC–FEM result of the evolution of the solution in time towards steady state is shown in Fig. 8. Fig. 9 shows a perspective view of the quasi steady-state solution for t = 2e−07 s. The steady-state solution agrees with that reported in [16,41,46].

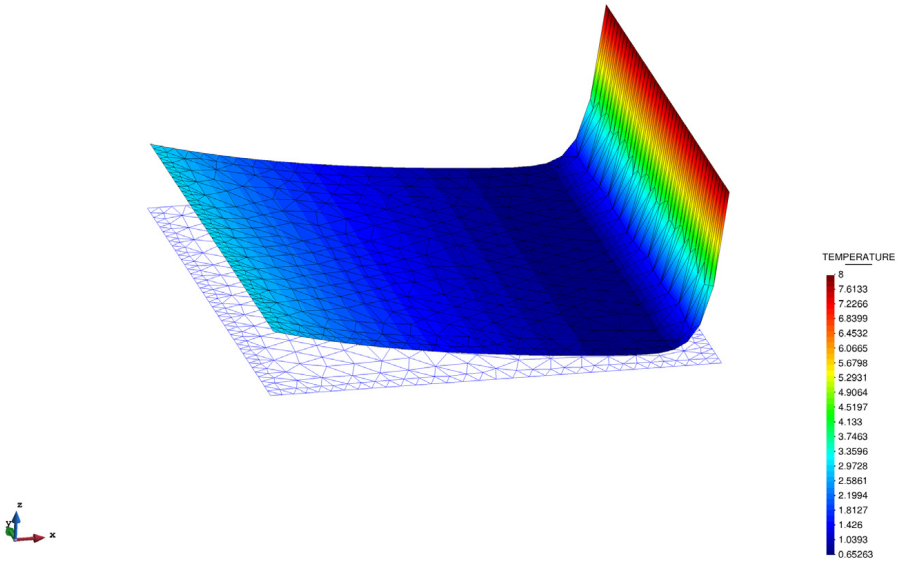

Fig. 6. Transient advection–diffusion–absorption problem with a non-uniform mesh. Solution obtained at t = 2 s.

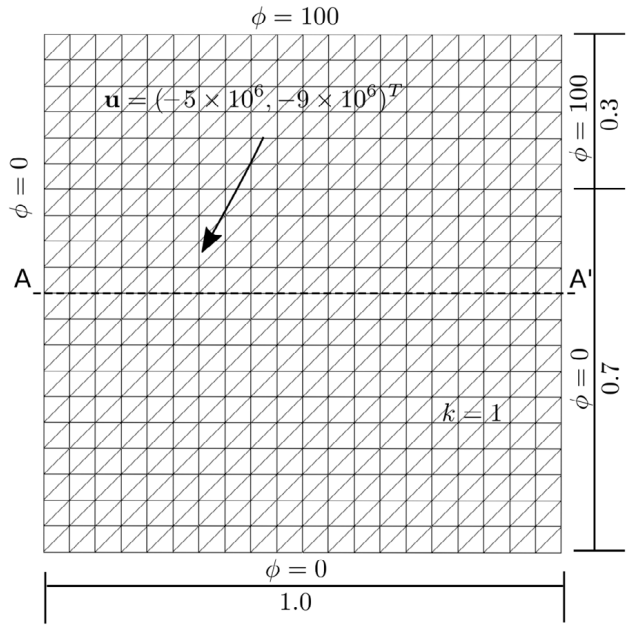

Fig. 7. Square domain with non-uniform Dirichlet conditions, downwards diagonal velocity and zero source. Mesh of 2 × 20 × 20 three-noded triangles.

7.3. Uniform advection problem with constant source

We study the uniform advection of a temperature field with a constant source term. The problem data is: $\mathbf{v} = [1, 0]^T$, $k = 10^{-8}$, $\rho c = 1$, $s = 0$ and $Q = 1$. The homogeneous boundary condition $\phi = 0$ is imposed everywhere as shown in Fig. 10. The solution develops an exponential layer at the outflow boundary $x = 1$ and parabolic layers at the boundaries $y = 0$ and $y = 1$. The FIC–FEM results of the transient solution towards steady-state are shown in Fig. 11. A perspective of the quasi steady-state solution at time $t = 1.5$ s is shown in Fig. 12. Both layers are subgrid phenomena for the considered mesh resolution. The transient solution was obtained iteratively using the implicit scheme presented in the paper with $\theta = 0.8$ and a time step of $\Delta t = 0.005$ s. Convergence within each time step was found in 2–3 iterations. The steady-state solution agrees with that reported in [46].

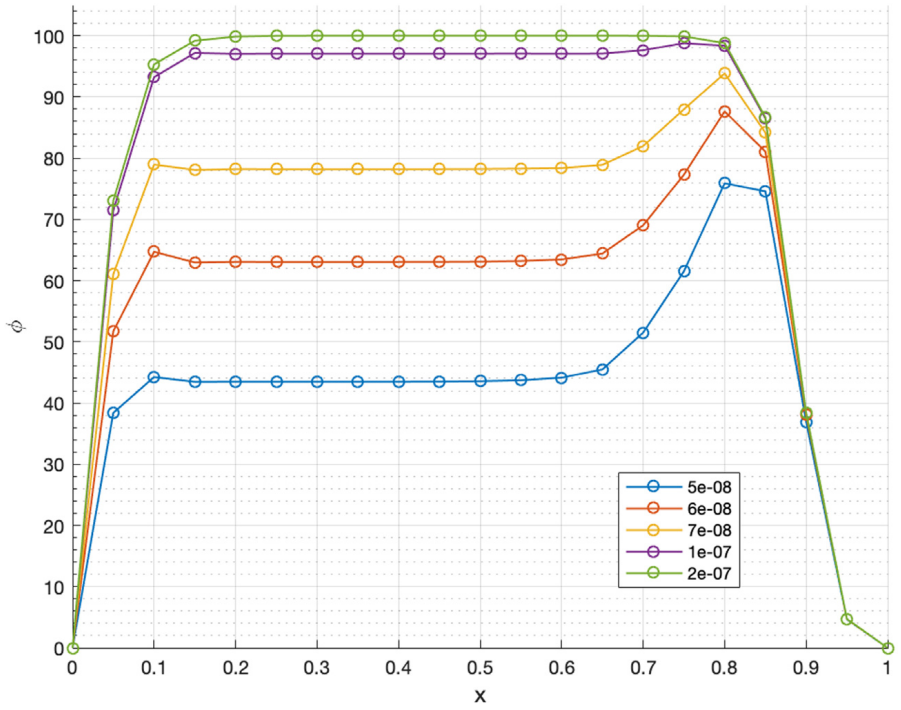

Fig. 8. Square domain with non-uniform Dirichlet conditions. FIC–FEM solution along line A-A'. The transient solutions are plotted at times 5e−08 s, 6e−08 s, 7e−08 s, 1e−07 s and 2e−07 s.

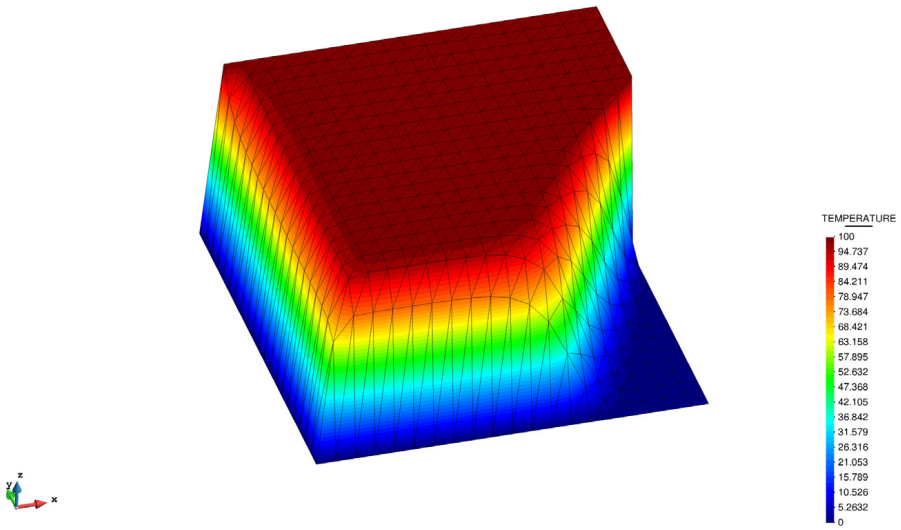

Fig. 9. Square domain with non-uniform Dirichlet conditions. Solution at time 2e−07 s.

7.4. Advective–diffusive transport of the temperature in a rectangular domain with Neumann and non-uniform Dirichlet conditions, rotational velocity field and zero source

The rectangular domain of sides 1×2 units and the boundary conditions are shown in Fig. 13. The rotational velocity field is defined as $\mathbf{u} = 10^4 \times [y(1-x^2), -x(1-y^2)]^T$. A unit isotropic diffusion is assumed. The value of the temperature (ϕ) is prescribed at part of the domain sides as shown in Fig. 13. In the rest of the sides, the

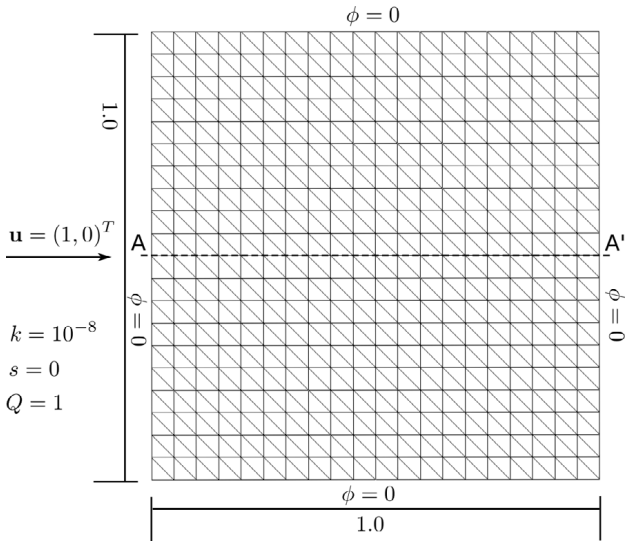

Fig. 10. Square domain with linear velocity and constant source. Structured mesh of 2 × 20 × 20 three-noded triangles.

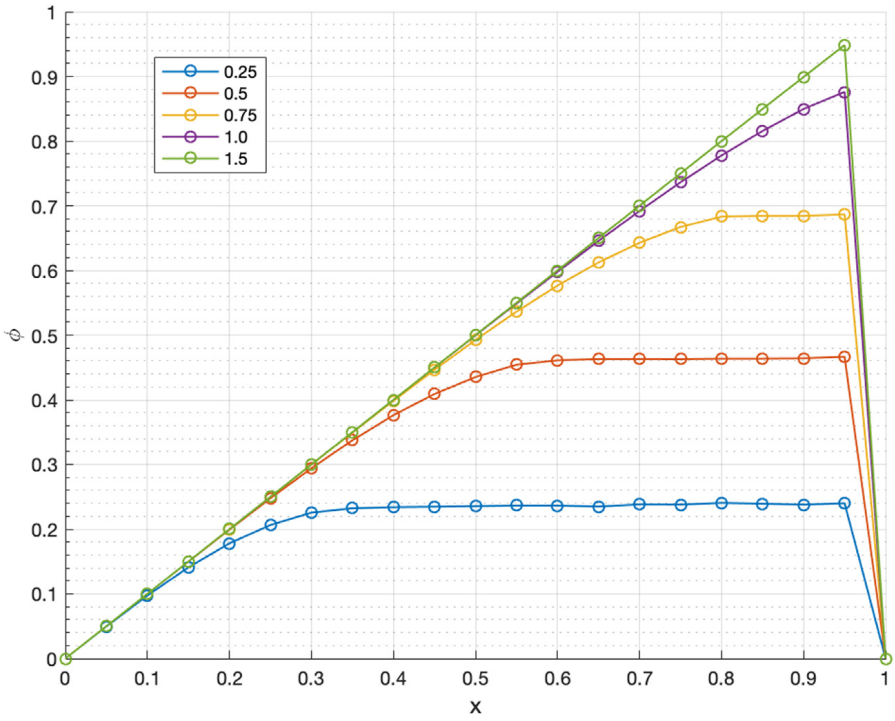

Fig. 11. Square domain with linear velocity and constant source. FIC solution obtained along line A-A'. The transient solutions are plotted at times 0.25 s, 0.5 s, 0.75 s, 1 s and 1.5 s.

Neumann condition ($q_n^p = 0$) is imposed. The problem was solved with the uniform mesh of 3-noded triangles shown in Fig. 13. The correct solution is a uniform plateau of $\phi = 100$ with a boundary layer at the right hand side where the solution drops towards the prescribed value of $\phi = 0$ and a circular sharp gradient region around the lower circular zone where the solution takes a zero value. The FIC–FEM results of the transient solution towards steady-state are shown in Fig. 14. A perspective of the quasi steady-state solution at time $t = 1e{-}03$ s is shown

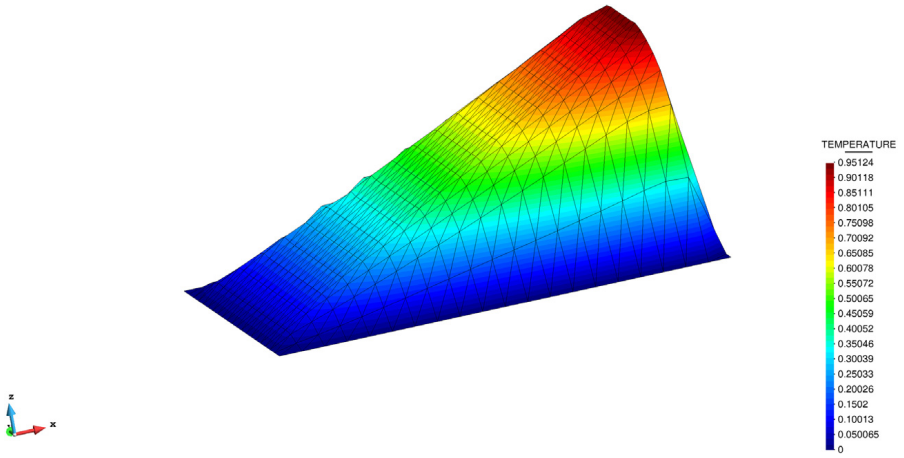

Fig. 12. Square domain with linear velocity and constant source. Solution at time 1.5 s.

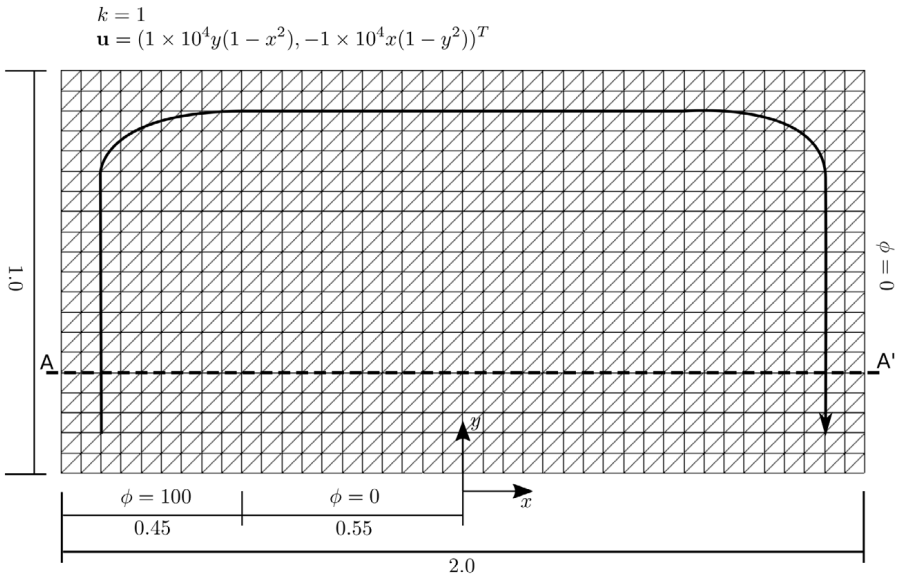

Fig. 13. Advective–diffusive transport of the temperature in a rectangular domain with Neumann and non-uniform Dirichlet conditions, rotational velocity and zero source. Structured mesh of $2 \times 40 \times 20$ three-noded triangles.

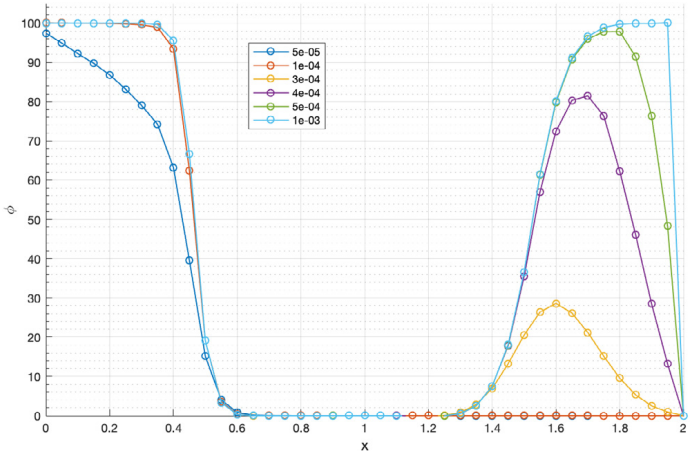

Fig. 14. FIC solution of the problem in Fig. 13. The transient solutions are plotted along line A-A' at times 5e−05 s, 1e−04 s, 3e−04 s, 4e−04, 5e−04 and 1e−03 s.

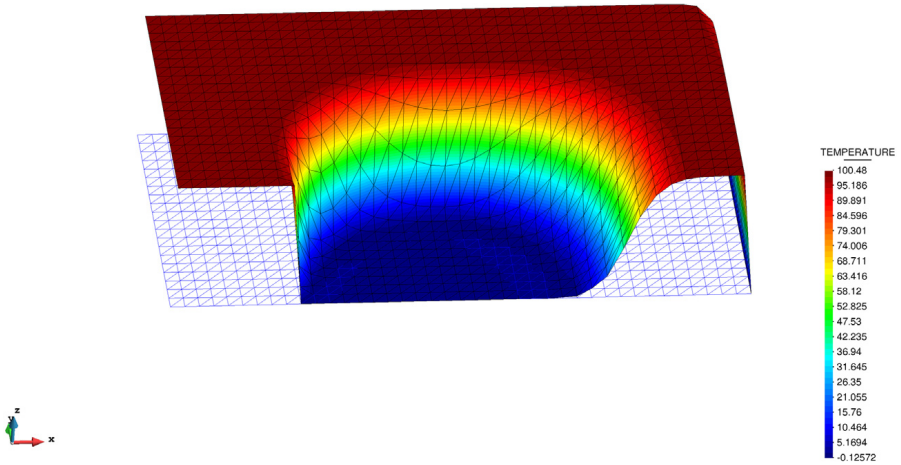

Fig. 15. Solution at 1e−03 s.

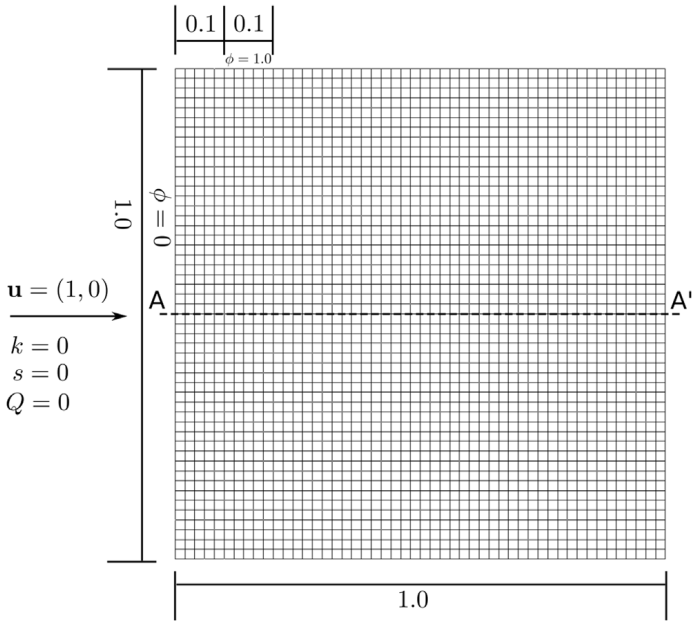

Fig. 16. Pure convection of a temperature plateau in a square domain with horizontal velocity. Structured mesh of 50 × 50 4-noded quadrilaterals.

in Fig. 15. The transient solution was obtained using the implicit scheme presented in this work with $\theta = 0.8$ and a time step of $\Delta t = 1\text{e}{-05}$ s. Convergence within each time step was found in 2–3 iterations. The steady-state solution agrees with that reported in [16].

7.5. Pure convection of a temperature plateau

We study the pure convection of an initial temperature plateau. The domain dimensions are $(x, y) = [0, 1]\times[0, 1]$. The problem data is: $\mathbf{v} = [1, 0]^T$, $k = 0$, $s = 0$, $\rho c = 1$ and $Q = 0$. The homogeneous boundary condition $\phi = 0$ is imposed at the left wall as shown in Fig. 16. The temperature plateau is generated by imposing a value of the temperature $\phi = 1.0$ from $x = 0.1$ to $x = 0.2$. The problem has been solved using a regular mesh of 50 × 50 four-noded quadrilateral elements. Shock capturing effects have not been taken into account in this case, as mentioned in the last part of Section 3. Figs. 17 and 18 show that the initial solution maintains its shape through the domain.

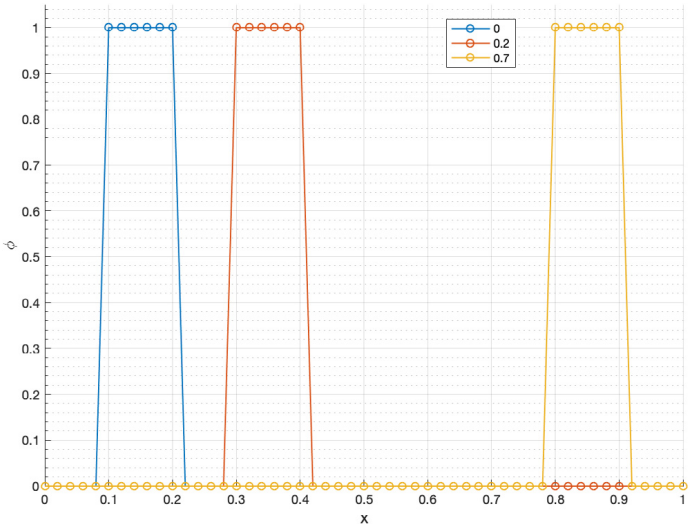

Fig. 17. Pure convection of a temperature plateau. FIC–FEM solution plotted along line A-A' at times 0 s, 0.2 s and 0.7 s.

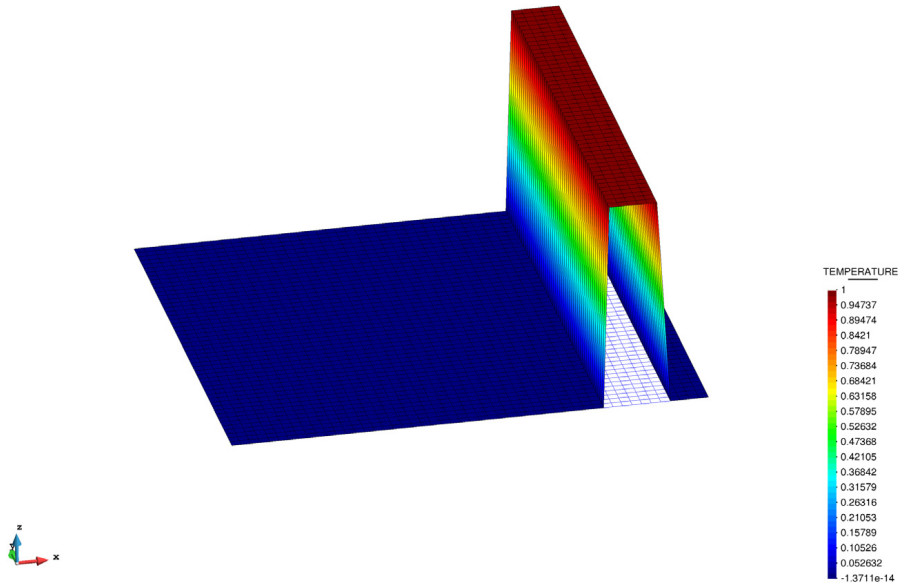

Fig. 18. Pure convective case. FIC–FEM solution at time 0.7 s.

The transient solution was obtained using the explicit scheme given in Eq. (34) and a time step of $\Delta t = 0.2$ s, giving an element Courant number of $C = 1$.

7.6. Advection–diffusion of a concentration field

In this problem we study the advection and diffusion of a concentration that is instantaneously released as a Dirac source in a point of a stream. This problem is generally known as the plume transport problem [68].

The domain dimensions are $(x, y) = [0, 35] \times [0, 10]$. The problem data is: $\mathbf{v} = [1, 0]^T$, $\rho c = 1$, $k = 0.1$, $s = 0$ and $Q = 0$. The homogeneous boundary condition $\phi = 0$ is imposed on the left wall as shown in Fig. 19. The value $\phi_0 = 1000$ is imposed as an initial value of the concentration at the node $(x, y) = (2, 5)$.

The analytical solution for this 2D problem is [68]

$$\phi(x, y, t) = \frac{\phi_0}{L_3 4\pi Dt} e^{-A} \tag{48a}$$

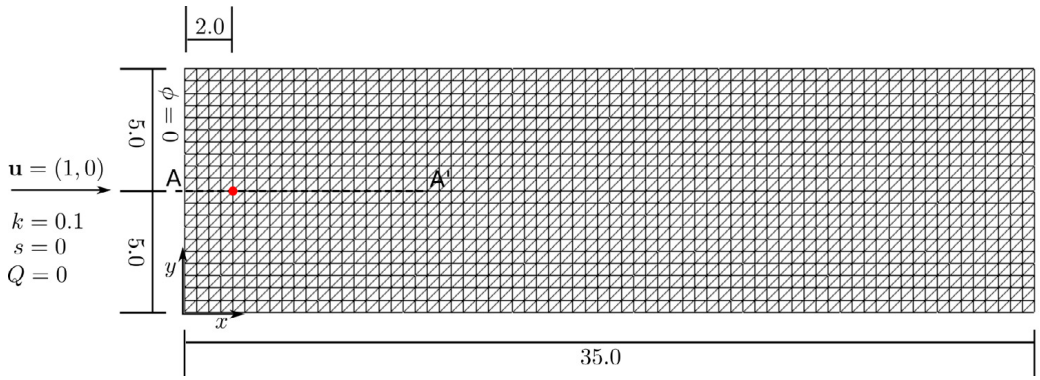

Fig. 19. Advection–diffusion of a concentration field. Rectangular domain with horizontal velocity. Structured mesh of 2 × 70 × 20 three-noded triangles.

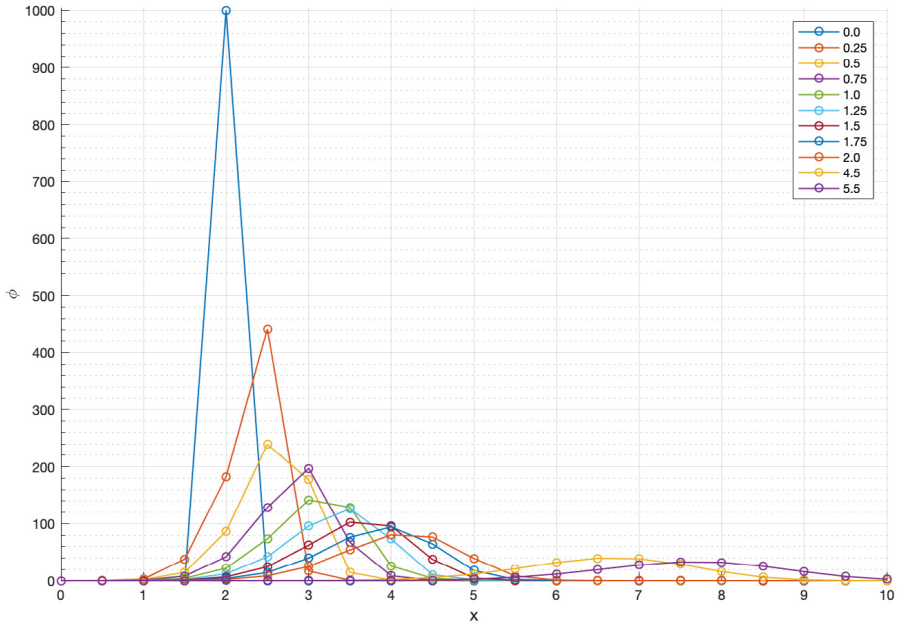

Fig. 20. Advection–diffusion of a concentration field. FIC–FEM solution along line A-A' obtained with the mesh of Fig. 19. Structured mesh of 2 × 70 × 20 three-noded triangles. Solution at times 0 s, 0.25 s, 0.5 s, 0.75 s, 1.0 s, 1.25 s, 1.5 s, 1.75 s, 2.0 s, 4.5 s and 5.5 s.

with

$$A = -\frac{1}{4Dt}\left\{[x_1 - (x_1^0 + v_1 t)]^2 + [x_2 - (x_2^0 + v_2 t)]^2\right\} \tag{48b}$$

In Eqs. (48) ϕ is the initial value of the concentration that is dropped at the point with coordinates $\mathbf{x}^0 = [x_1^0, x_2^0]^T$, L_3 is the vertical dimension of the analysis domain (in this problem we have taken $L_3 = 1$), v_1 and v_2 are the horizontal and vertical components of the velocity vector, respectively and $D = \frac{K}{\rho c}$ where K is the average diffusion defined in Section 2.1.

The transient solution was obtained using an implicit scheme with $\theta = 0.5$ and a time step of $\Delta t = 0.25$ s, giving a Courant number of $C = 0.5$. Once again, the shock-capturing terms were not taken into account for solving this problem following the argument given at the end of Section 3. On the other hand, the use of the consistent form of the mass matrix was essential for obtaining good results for this problem. Fig. 20 shows how the solution is advected and diffuses as time increases. The numerical results for the distribution of the contraction along line A-A' are in agreement with the analytical solution shown in Fig. 21. The graphs are taken along the A-A' line, which goes from (0, 5) to (10, 5). A comparison of the contours of the numerical and analytical distributions of the concentration at $t = 15$ s can be seen in Figs. 22 and 23, respectively.

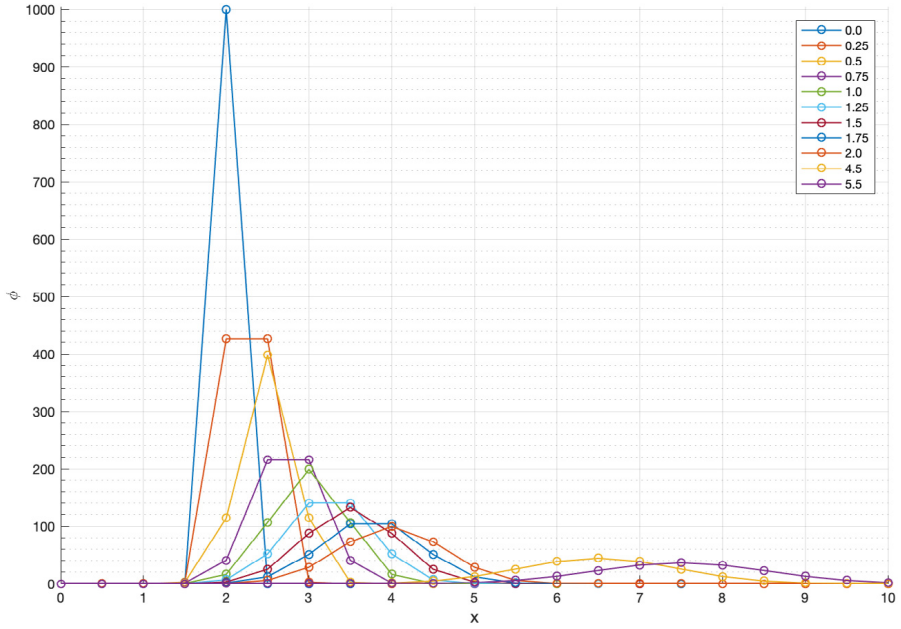

Fig. 21. Advection–diffusion of a concentration field. Analytical solution along line A-A' plotted on the structured mesh of Fig. 19. Solution at times 0 s, 0.25 s, 0.5 s, 0.75 s, 1.0 s, 1.25 s, 1.5 s, 1.75 s, 2.0 s, 4.5 s and 5.5 s.

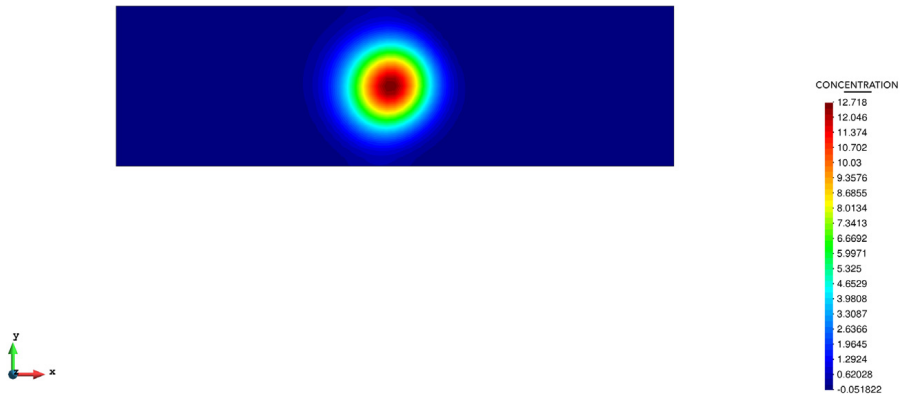

Fig. 22. Advection–diffusion of a concentration field. Contours of the FIC–FEM results at t = 15 s.

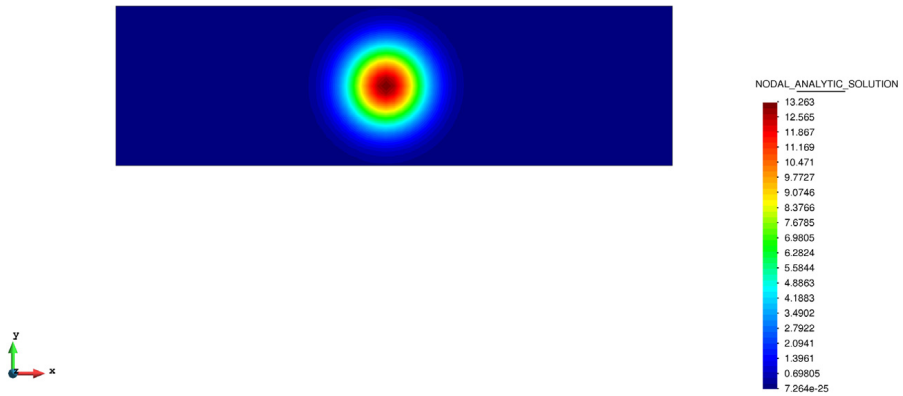

Fig. 23. Advection–diffusion of a concentration field. Contours of the analytical results at t = 15 s.

8. Concluding remarks

In this work we have extended the steady-state multidimensional FIC–FEM formulation reported in [46] to the transient case. The stabilized variational expression has the standard residual form typical of the FIC–FEM procedure. The stabilized terms introduced by the FIC approach depend on a characteristic element length and two stabilization parameters whose expression is obtained as an extension of the steady-state forms presented in [46]. A shock capturing term is introduced to account for the Gibbs oscillations across internal/boundary layers.

The good behavior of the FIC–FEM formulation has been verified for transient advection–diffusion–absorption problems with numerical solutions evolving to a steady-state, as well as to two fully transient problems.

The numerical results were obtained in most cases using an implicit scheme. An exception is the pure convection problem (Section 7.5) that was solved with an explicit scheme and a Courant number of $C = 1$. The shock capturing terms were not taken into account in the solution of the fully transient problems (Sections 7.5 and 7.6). We also remark the importance of using a consistent stabilized mass matrix in the concentration field example.

Acknowledgments

This research was partially funded by the PRECISE, Spain project (BIA2017-83805-R) of the National Research Plan of the Spanish Government. Support for this work was also provided from the Office for Naval Research Global (ONRG) of the US Navy through the NICE-SHIP project.The authors acknowledge financial support from the Spanish Ministry of Economy and Competitiveness through the Severo Ochoa Programme for Centres of Excellence in RTD (CEX2018-000797-S). We also acknowledge the financial support of the CERCA programme of the Generalitat de Catalunya (Spain).

References

[1] J. Donea, A. Huerta, Finite Element Method for Flow Problems, J. Wiley & Sons, 2003.
[2] O.C. Zienkiewicz, R.L. Taylor, P. Nithiarasu, The Finite Element Method for Fluid Dynamics, sixth ed., Elsevier, 2005.
[3] A.N. Brooks, T.J.R. Hughes, Streamline Upwind/Petrov–Galerkin formulations for the convective dominated flows with particular emphasis on the incompressible Navier–Stokes equations, Comput. Methods Appl. Mech. Engrg. 32 (1–3) (1982) 199–259.
[4] T.J.R. Hughes, A.N. Brooks, A theoretical framework for Petrov–Galerkin methods, with discontinuous weighting functions: application to the streamline upwind procedure, in: R.H. Gallagher, D.M. Norrie, J.T. Oden, O.C. Zienkiewicz (Eds.), Finite Elements in Fluids, Vol. IV, Wiley, Chichester, 1982.
[5] T.J.R. Hughes, M. Mallet, A new finite element formulations for computational fluid dynamics: III. The generalized streamline operator for multidimensional advective-diffusive systems, Comput. Methods Appl. Mech. Engrg. 58 (1986) 305–328.
[6] F. Kikuchi, T. Ushijima, Theoretical analysis of some finite element schemes for convective diffusion equations, in: R. Gallagher, D. Norrie, J. Oden, O.C. Zienkiewicz (Eds.), Finite Elements in Fluids, Vol. IV, John Wiley and Sons Ltd, Chichester, 1982.
[7] R. Löhner, K. Morgan, O.C. Zienkiewicz, The solution of non-linear hyperbolic equation systems by the finite element method, Internat. J. Numer. Methods Fluids 4 (1984) 1043–1063.
[8] R. Codina, A discontinuity-capturing crosswind-dissipation for the finite element solution of the convection–diffusion equation, Comput. Methods Appl. Mech. Engrg. 110 (1993) 325–342.
[9] P.A.B. de Sampaio, A.L.G.A. Coutinho, A natural derivation of discontinuity capturing operator for convection–diffusion problems, Comput. Methods Appl. Mech. Engrg. 190 (2001) 6291–6308.
[10] J. Douglas, T.F. Russell, Numerical methods for convection-dominated diffusion problems based on combining the method of characteristics with the finite element or finite difference procedures, SIAM J. Numer. Anal. 19 (1982) 871–885.
[11] E.G. Dutra do Carmo, G.B. Alvarez, A new upwind function in stabilized finite element formulations, using linear and quadratic elements for the scalar convection–diffusion problems, Comput. Methods Appl. Mech. Engrg. 193 (2004) 2383–2402.
[12] A.C. Galeão, E.G. Dutra do Carmo, A consistent approximate upwind Petrov–Galerkin method for the convection-dominated problems, Comput. Methods Appl. Mech. Engrg. 68 (1) (1988) 83–95.
[13] C. Johnson, A. Szepessy, P. Hansbo, On the convergence of shock-capturing streamline diffusion finite element methods for hyperbolic conservation laws, Math. Comp. 54 (1990) 107–129.
[14] P. Knobloch, Improvements of the Mizukami–Hughes method for convection–diffusion equations, Comput. Methods Appl. Mech. Engrg. 196 (2006) 579–594.
[15] A. Mizukami, T.J.R. Hughes, A Petrov–Galerkin finite element method for convection-dominated flows: An accurate upwinding technique for satisfying the maximum principle, Comput. Methods Appl. Mech. Engrg. 50 (2) (1985) 181–193.
[16] E. Oñate, F. Zarate, S.R. Idelsohn, Finite element formulation for the convective-diffusive problems with sharp gradients using finite calculus, Comput. Methods Appl. Mech. Engrg. 195 (2006) 1793–1825.
[17] T.J.R. Hughes, L.P. Franca, G.M. Hulbert, A new finite element formulation for computational fluid dynamics: VIII. The Galerkin/least-squares method for advective-diffusive equations, Comput. Methods Appl. Mech. Engrg. 73 (1989) 173–189.
[18] T.J.R. Hughes, G.R. Feijoo, L. Mazzei, J.B. Quincy, The variational multiscale method: a paradigm for computational mechanics, Comput. Methods Appl. Mech. Engrg. 166 (1998) 3–24.

[19] O.C. Zienkiewicz, R. Codina, A general algorithm for compressible and incompressible flows. Part I: the split, characteristic based scheme, Internat. J. Numer. Methods Fluids 20 (1995) 869–885.
[20] V. John, P. Knobloch, On spurious oscillations at layers diminishing (SOLD) methods for convection–diffusion equations: Part I - A review, Comput. Methods Appl. Mech. Engrg. 196 (2007) 2197–2215.
[21] S.R. Idelsohn, J.C. Heinrich, E. Oñate, Petrov–Galerkin methods for the transient advective-diffusive equation with sharp gradients, Internat. J. Numer. Methods Engrg. 39 (1996) 1455–1473.
[22] C.C. Yu, J.C. Heinrich, Petrov–Galerkin methods for the time-dependent convective transport equations, Internat. J. Numer. Methods Engrg. 23 (1986) 883–901.
[23] E. Burman, A. Ern, Nonlinear diffusion and discrete maximum principle for stabilized Galerkin approximations of the convection–diffusion–reaction equation, Comput. Methods Appl. Mech. Engrg. 191 (2002) 3833–3855.
[24] S.R. Idelsohn, N. Nigro, M. Storti, G. Buscaglia, A Petrov–Galerkin formulation for advective-reaction–diffusion problems, Comput. Methods Appl. Mech. Engrg. 136 (1996) 27–46.
[25] T.E. Tezduyar, Y.J. Park, Discontinuity-capturing finite element formulations for nonlinear convection–diffusion–reaction equations, Comput. Methods Appl. Mech. Engrg. 59 (1986) 307–325.
[26] L.P. Franca, E.G. Dutra do Carmo, The Galerkin gradient least-squares method, Comput. Methods Appl. Mech. Engrg. 74 (1989) 41–54.
[27] I. Harari, T.J.R. Hughes, Stabilized finite element methods for steady advection-diffusion with production, Comput. Methods Appl. Mech. Engrg. 115 (1994) 165–191.
[28] C. Baiocchi, F. Brezzi, L.P. Franca, Virtual bubbles and the GaLS, Comput. Methods Appl. Mech. Engrg. 105 (1993) 125–141.
[29] F. Brezzi, M.O. Bristeau, L.P. Franca, M. Mallet, G. Rogé, A relationship between stabilized finite element methods and the Galerkin method with bubble functions, Comput. Methods Appl. Mech. Engrg. 96 (1992) 117–129.
[30] F. Brezzi, A. Russo, Choosing bubbles for advection-diffusion problems, Math. Models Methods Appl. Sci. 4 (1994) 571–587.
[31] F. Brezzi, G. Hauke, L.D. Marini, G. Sangalli, Link-cutting bubbles for the stabilization of convection–diffusion–reaction problems, Math. Models Methods Appl. Sci. 13 (3) (2003) 445–461.
[32] L.P. Franca, C. Farhat, Bubble functions prompt unusual stabilized finite element methods, Comput. Methods Appl. Mech. Engrg. 123 (1995) 299–308.
[33] L.P. Franca, F. Valentin, On an improved unusual stabilized finite element method for the advective-reactive-diffusive equation, Comput. Methods Appl. Mech. Engrg. 190 (2001) 1785–1800.
[34] R. Codina, On stabilized finite element methods for linear systems of convection–diffusion–reaction equations, Comput. Methods Appl. Mech. Engrg. 190 (2000) 2681–2706.
[35] G. Hauke, A. García-Olivares, Variational subgrid scale formulations for the advection-diffusion–reaction equation, Comput. Methods Appl. Mech. Engrg. 190 (2001) 6847–6865.
[36] G. Hauke, A simple subgrid scale stabilized method for the advection-diffusion–reaction equation, Comput. Methods Appl. Mech. Engrg. 191 (2002) 2925–2947.
[37] G. Hauke, G. Sangalli, M.H. Doweidar, Combining adjoint stabilized methods for the advection-diffusion–reaction problem, Math. Models Methods Appl. Sci. 17 (2) (2007) 305–326.
[38] J. Principe, R. Codina, On the stabilization parameter in the subgrid scale approximation of scalar convection–diffusion–reaction equations on distorted meshes, Comput. Methods Appl. Mech. Engrg. 199 (21–22) (2010) 1386–1402.
[39] R. Codina, Comparison of some finite element methods for solving the diffusion-convection-reaction equation, Comput. Methods Appl. Mech. Engrg. 156 (1998) 185–210.
[40] E. Oñate, J. Miquel, G. Hauke, Stabilized formulation for the advection-diffusion-absorption equation using finite calculus and linear finite elements, Comput. Methods Appl. Mech. Engrg. 195 (33–36) (2006) 3926–3946.
[41] E. Oñate, J. Miquel, F. Zarate, Stabilized solution of the multidimensional advection-diffusion-absorption equation using linear finite elements, Comput. & Fluids 36 (2007) 92–112.
[42] C. Felippa, E. Oñate, Nodally exact Ritz discretizations of the 1D diffusion-absorption and Helmholtz equations by variational FIC and modified equation methods, Comput. Mech. 39 (2) (2007) 91–111.
[43] P. Nadukandi, E. Oñate, J. García Espinosa, A high-resolution Petrov–Galerkin method for the 1D convection–diffusion-reaction problem, Comput. Methods Appl. Mech. Engrg. 199 (9–12) (2010) 525–546.
[44] P. Nadukandi, E. Oñate, J. García Espinosa, A high-resolution Petrov–Galerkin method for the convection–diffusion-reaction problem. Part II. A multidimensional extension, Comput. Methods Appl. Mech. Engrg. 213–216 (2012) 327–352.
[45] E. Oñate, J. Miquel, P. Nadukandi, An accurate FIC-FEM formulation for the 1D advection–diffusion–reaction equation, Comput. Methods Appl. Mech. Engrg. 298 (2016) 373–406.
[46] E. Oñate, P. Nadukandi, J. Miquel, Accurate FIC-FEM formulation for the multidimensional steady-state advection–diffusion–absorption equation, Comput. Methods Appl. Mech. Engrg. 327 (2017) 352–368.
[47] E. Oñate, Derivation of stabilized equations for numerical solution of advective-diffusive transport and fluid flow problems, Comput. Methods Appl. Mech. Engrg. 151 (1998) 233–265.
[48] E. Oñate, M. Manzan, A general procedure for deriving stabilized space–time finite element methods for advective-diffusive problems, Internat. J. Numer. Methods Fluids 31 (1999) 203–221.
[49] E. Oñate, M. Manzan, Stabilization techniques for finite element analysis of convection–diffusion problems, in: B. Sundén, G. Comini (Eds.), Computational Analysis of Convection Heat Transfer, Vol. 2000, WIT Press, Southampton (UK), 2000, pp. 71–117.
[50] E. Oñate, A. Valls, J. García, FIC/FEM formulation with matrix stabilizing terms for incompressible flows at low and high Reynolds numbers, Comput. Mech. 38 (4–5) (2006) 440–455.

[51] E. Oñate, J. García, S.R. Idelsohn, F. Del Pin, FIC formulations for finite element analysis of incompressible flows. Eulerian, ALE and Lagrangian approaches, Comput. Methods Appl. Mech. Engrg. 195 (23–24) (2006) 3001–3037.
[52] E. Oñate, A. Valls, J. García, Modeling incompressible flows at low and high Reynolds numbers via a finite calculus-finite element approach, J. Comput. Phys. 224 (2007) 332–351.
[53] E. Oñate, P. Nadukandi, S. Idelsohn, J. García, C. Felippa, A family of residual-based stabilized finite element methods for Stokes flows, Int. J. Numer. Methods Fluids 65 (1–3) (2011) 106–134.
[54] E. Oñate, P. Nadukandi, S. Idelsohn, P1/P0+ elements for incompressible flows with discontinuous material properties, Comput. Methods Appl. Mech. Engrg. 271 (2014) 185–209.
[55] E. Oñate, J. García, A finite element method for fluid–structure interaction with surface waves using a finite calculus formulation, Comput. Methods Appl. Mech. Engrg. 191 (2001) 635–660.
[56] E. Oñate, S.R. Idelsohn, F. Del Pin, R. Aubry, The particle finite element method. An overview, Int. J. Comput. Methods 1 (2) (2004) 267–307.
[57] E. Oñate, S.R. Idelsohn, M.A. Celigueta, R. Rossi, Advances in the particle finite element method for the analysis of fluid-multibody interaction and bed erosion in free surface flows, Comput. Methods Appl. Mech. Engrg. 197 (19–20) (2008) 1777–1800.
[58] E. Oñate, R.L. Taylor, O.C. Zienkiewicz, J. Rojek, A residual correction method based on finite calculus, Eng. Comput. 20 (5/6) (2003) 629–658.
[59] E. Oñate, J. Rojek, R.L. Taylor, O.C. Zienkiewicz, Finite calculus formulation for incompressible solids using linear triangles and tetrahedra, Internat. J. Numer. Methods Engrg. 59 (2004) 1473–1500.
[60] E. Oñate, S.R. Idelsohn, C. Felippa, Consistent pressure Laplacian stabilization for incompressible continua via higher order finite calculus, Internat. J. Numer. Methods Engrg. 87 (1–5) (2011) 171–195.
[61] E. Oñate, S.R. Idelsohn, O.C. Zienkiewicz, R.L. Taylor, C. Sacco, A stabilized finite point method for analysis of fluid mechanics problems, Comput. Methods Appl. Mech. Engrg. 139 (1996) 315–346.
[62] E. Oñate, S.R. Idelsohn, A mesh-free finite point method for advective-diffusive transport and fluid flow problems, Comput. Mech. 23 (1998) 283–292.
[63] E. Oñate, C. Sacco, S.R. Idelsohn, A finite point method for incompressible flow problems, Comput. Vis. Sci. 2 (2000) 67–75.
[64] E. Oñate, F. Perazzo, J. Miquel, A finite point method for elasticity problems, Comput. Struct. 79 (2001) 2151–2163.
[65] E. Oñate, Possibilities of finite calculus in computational mechanics, Internat. J. Numer. Methods Engrg. 60 (1) (2004) 255–281.
[66] O.C. Zienkiewicz, R.L. Taylor, J.Z. Zhu, The Finite Element Method. The Basis, sixth ed., Elsevier, 2005.
[67] J. Donea, A Taylor–Galerkin method for convective transport problems, Internat. J. Numer. Methods Engrg. 20 (1984) 101–119.
[68] H. Fisher, J. List, C. Koh, J. Imberger, N. Brooks, Mixing in Inland and Coastal Waters, Elsevier, 2013.

Chapter 3

Semi-Lagrangian formulation for the advection-diffusion-absorption equation

3.1 Article data

Title: Semi-Lagrangian formulation for the advection-diffusion-absorption equation.

Authors: A. Puigferrat, M. Masó, I. de-Pouplana, G. Casas and E. Oñate

Journal: Computer Methods in Applied Mechanics and Engineering 380 (2021) 113807

Received: 17 July 2020 / Accepted: 13 March 2021 / Available online: 31 March 2021

DOI: 10.1016/j.cma.2021.113807

3.2 Introduction

Standard FEM techniques for solving convective transport problems based on the Eulerian description of the continuum suffer from instabilities if not endowed with the appropriate stabilization techniques [7, 34, 41]. These techniques, which are based on the addition of artificial diffusion terms, tend to spoil the accuracy of the numerical solution in cases where there is a (relatively small) physical diffusion. Thus, one is faced with a trade-off between stability and accuracy that is particularly restrictive for

high-Péclet flows.

Transport problems involving high-Péclet numbers (Pe) are common in many practical situations. Among these, we note the study of environmental pollution, either related to the quality of air or water [8], or the simulation of advection-diffusion in a microfluidics channel [92], just to name a few. High-Damköhler (Da) numbers arise in the study of flames [46] and other fast-reacting systems.

The convective transport of a physical quantity such as heat or a chemical concentration accounting for diffusion and absorption effects is a phenomenon that plays a central role in many applications of interest. Such phenomenon is well described by a differential equation of an advection-diffusion-absorption type. A large volume of scientific work has been devoted to the study of this equation and, in particular, to its solution by numerical means. The problem is well-studied for a variety of methods like finite differences [23], finite volumes [45] and the finite element method (FEM) [17, 18, 26, 29, 55, 56], among others.

The results obtained using the formulation developed in the thesis showed good behavior in the different chosen examples. Nonetheless, certain difficulties were observed: excessive diffusion was introduced for problems involving high-Péclet numbers. Also, some numerical instabilities were obtained for high-Damköhler numbers.

In order to overcome these difficulties in the thesis we have developed a new Lagrangian-Eulerian procedure. The combined method uses a Lagrangian approach based on the updated version of the classical Particle Finite Element Method (PFEM) [39, 40] is used to calculate advection effects. The Lagrangian approach is combined with a standard Eulerian strategy based on the Finite Element Method (FEM) in order to compute diffusion and absorption effects. The Eulerian FEM procedure is based on a FIC–FEM stabilized formulation explained in Chapter 2 [68, 70, 77].

The attached paper describes the most relevant features of each of the two computational approaches and the coupling scheme is explained. The semi-Lagrangian approach benefits from the FIC–FEM stabilized Eulerian method and the Lagrangian PFEM2 one. More specifically, the content of the paper is organized as follows. First, the Eulerian solution scheme using a FIC–FEM procedure is introduced. Next, the PFEM2 technique is described and the Eulerian-Lagrangian splitting strategy is detailed. Several examples are presented in order to show the advantages of using the new semi-Lagrangian

formulation versus the standard Eulerian approach: the evolution of a concentration field in a high-Péclet flow (no absorption) in 2D and in 3D and five other advective-diffusive-absorptive problems in 2D and 3D to validate the formulation. Among these we highlight the low and high-Damköhler numbers problems and the high Péclet 3D transport of a concentration.

3.3 Scientific contribution

In this chapter we explain the most relevant features of each computational approach and the coupling scheme is explained. Also, several problems are solved to validate the method: the evolution of a localized concentration field in two dimensions (2D), the evolution of a spherical field in 3D and three benchmark problems from the literature with high absorption.

Overall, the semi-Lagrangian approach benefits from the FIC–FEM stabilized Eulerian method and the Lagrangian PFEM2 one and simplifies the one explained in Chapter 2. It can be understood as a splitting method, which uses a set of particles to solve the pure convective transport problem (via the PFEM2 technique) and a stabilized FEM for solving the diffusive-reactive terms of the transport equations. The same fixed mesh is used for solving both the Lagrangian and Eulerian solution steps.

The results obtained with the semi-Lagrangian formulation have been validated with previous results for advection or absorption dominated problems. The goal was to show the noticeable improvement against the results obtained with the FIC–FEM Eulerian formulation, particularly in cases with a high Péclet and/or high Damköhler numbers.

Available online at www.sciencedirect.com
ScienceDirect
Comput. Methods Appl. Mech. Engrg. 380 (2021) 113807
Computer methods in applied mechanics and engineering
www.elsevier.com/locate/cma

Semi-Lagrangian formulation for the advection–diffusion–absorption equation

Albert Puigferrat[a], Miguel Masó[a], Ignasi de-Pouplana[a,b], Guillermo Casas[a,b], Eugenio Oñate[a,b,*]

[a] *Centre Internacional de Mètodes Numèrics en Enginyeria CIMNE, Barcelona, Spain*
[b] *Universitat Politècnica de Catalunya (UPC), Barcelona, Spain*

Received 17 July 2020; received in revised form 11 March 2021; accepted 13 March 2021
Available online 31 March 2021

Abstract

We present a numerical method for solving advective–diffusive–absorptive problems with high values of advection and absorption. A Lagrangian approach based on the updated version of the classical Particle Finite Element Method (PFEM) is used to calculate advection, while a Eulerian strategy based on the Finite Element Method (FEM) is adopted to compute diffusion and absorption. The Eulerian FEM procedure is based on a Finite Increment Calculus (FIC) stabilized formulation recently developed by the authors. The most relevant features of each computational approach are outlined and the coupling scheme is explained. Several problems are solved to validate the method: the evolution of a localized concentration field in two dimensions (2D), the evolution of a spherical field in 3D and three benchmark problems from the literature with high absorption.
© 2021 Published by Elsevier B.V.

Keywords: Convection–diffusion–reaction; Finite element method; FIC; PFEM; Eulerian; Lagrangian

1. Introduction

The convective transport of a physical quantity such as heat or a chemical concentration accounting for diffusion and absorption effects is a phenomenon that plays a central role in many applications of interest. Such phenomenon is well described by a differential equation of an advection–diffusion–absorption type. A large volume of scientific work has been devoted to the study of this equation and, in particular, to its solution by numerical means. The problem is well-studied for a variety of methods like finite differences [1], finite volumes [2] and the finite element method (FEM) [3–8], among others. Nonetheless, this numerical problem remains a challenging one, especially for high Péclet or Damköhler numbers, due to the numerical difficulties that arise as the highest-derivative term becomes overwhelmed by the other two.

Transport problems involving high-Péclet numbers (Pe) are common in many practical situations. Among these, we note the study of environmental pollution, either related to the quality of air or water [9], or the simulation of advection–diffusion in a microfluidics channel [10], just to name a few. High-Damköhler (Da) numbers arise in the study of flames [11] and other fast-reacting systems.

* Corresponding author at: Universitat Politècnica de Catalunya (UPC), Barcelona, Spain.
E-mail address: onate@cimne.upc.edu (E. Oñate).

https://doi.org/10.1016/j.cma.2021.113807
0045-7825/© 2021 Published by Elsevier B.V.

Standard FEM techniques for solving convective transport problems based on the Eulerian description of the continuum suffer from instabilities if not endowed with the appropriate stabilization techniques [12–14]. These techniques, which are based on the addition of artificial diffusion terms, tend to spoil the accuracy of the numerical solution in cases where there is a (relatively small) physical diffusion. Thus, one is faced with a trade-off between stability and accuracy that is particularly restrictive for high-Péclet flows.

Moreover, the numerical solution to the advection, diffusion and absorption problem is prone to exhibit global, Gibbs and dispersive oscillations, which require the application of specific stabilization techniques to control instabilities. The local Gibbs oscillations appear along the characteristic layers in advection-dominated problems. For absorption-dominated cases, Gibbs oscillations can be found near the Dirichlet boundaries and in regions where the distributed source term is nonregular. Also, the solution of the transient problem may exhibit dispersive oscillations when the initial solution and/or the distributed source term are nonregular [15]. Various techniques for solving these problems can be found in literature, such as the Petrov–Galerkin method [12–14,16,17], the Galerkin Least Squares (GLS) method [18,19], the Variational Multiscale (VMS) method [20] or the characteristic split procedure [21,22]. In this paper we will use the Finite Increment Calculus (FIC) stabilization technique which has been widely used to solve problems involving quasi and fully incompressible fluids and solids with the FEM [23–29]. The FIC technique is based on expressing the equations of balance of mass and momentum in a space/time domain of finite size and retaining higher-order terms in the Taylor series expansion used for expressing the change in the transported variables within the balance domain. In addition to the standard terms of infinitesimal theory, the FIC form of the balance equations contains derivatives of the classical differential equations multiplied by characteristic distances in space and/or time [23,24,26–29].

In the last decades, various authors have investigated ways of solving transient problems for high-Péclet numbers. For instance, Sevilla et al. [30] studied the influence of the number of integration points in the accuracy of the computations, using high-order curved finite elements and proved that they were one order of magnitude more precise than classical isoparametric FEM. In [31], the simulation of dispersing plumes and puffs was studied using a second-order closure model and a parameterized Eulerian approach.

From a different perspective, fully Lagrangian methods have been used for high-Péclet flows. For instance, in [32] good results for the convection–diffusion equations coupled to the incompressible flow equations were obtained using two Lagrangian methods.

A third option that exploits the benefits of a combined Eulerian–Lagrangian method has been studied by other authors to solve problems such as advection–diffusion [33–35], the solute transport in heterogeneous porous media [36] or the nanoparticle distribution in nanofluids [37]. Many of these studies have proved that a splitting of a Eulerian and a Lagrangian solution can solve the excessive numerical diffusion observed in Eulerian methods. These splittings aim to accurately solve the advective part of the transport equation using a Lagrangian method and then calculate the diffusion problem via a Eulerian technique.

A combination of the Backwards Method of Characteristics with various Eulerian methods such as finite differences or finite elements was studied in [38]. Good results were obtained for high Courant numbers but no clear conclusion was reached on the stability and convergence of the methods. Cady [34] used a Modified Method of Characteristics together with finite differences and the Galerkin method but found accuracy problems. In the following years, the problem of global mass conservation due to the integration of the mass balance equation was addressed. In 1998, Healy and Russell [39] proposed the finite volume Eulerian–Lagrangian localized method with a forward tracking of the characteristics that lead to better results in comparison with previous methods. The performance of four Eulerian–Lagrangian solvers that relied on different interpolators was studied in [36]. It was found that the taut spline interpolator was able to yield accurate solutions for high-Péclet numbers. This method, based on a forward tracking algorithm, proved to be more efficient than other methods, such as the Petrov–Galerkin technique, for this kind of problems. The accuracy of the Petrov–Galerkin method can however be improved with the FIC stabilization technique [15,40,41]. In 2000 and 2006, respectively, Young et al. studied several Eulerian–Lagrangian methods such as the Eulerian–Lagrangian Boundary Element Method [42], which provided the solution for low numerical diffusion, and the Eulerian–Lagrangian method of fundamental solutions [43], which is a mesh-free method that has the simplicity of a fixed grid from the Eulerian method and the computational power of the Lagrangian method. More recently, Wang et al. have studied a Eulerian–Lagrangian Discontinuous Galerkin Method [44,45] and a Modified Method of Characteristics with an adjusted advection procedure [46] for the transient advection–diffusion equations. In 2012, Al-Lawatia [47] developed a mass conservative Eulerian–Lagrangian control

volume scheme for the solution of the same equations in two dimensions (2D), based on the Eulerian–Lagrangian localized adjoint method [39].

In this work we present an alternative Eulerian–Lagrangian split formulation, termed *semi-Lagrangian formulation*, for the advection–diffusion–absorption equation that leads to accurate and stable results, and has neither convergence nor grid orientation problems. The Lagrangian part of the method is based on the Particle Finite Element Method — second generation (termed from here onwards PFEM2) [48,49], which has been successfully used to simulate problems of sediment transport [50], diffusion dominant problems [51] and free surface flows [52], while the Eulerian formulation follows the FIC–FEM procedure presented in [41].

The idea of combining a fixed mesh with particles moving for solving the advection–diffusion equation is not new, as shown in some of the works cited above [33–35]. One can even find in the literature works that also use the PFEM2 for the advective part of the advection–diffusion equation [48,49,51]. None of the above, however, include the absorption in the transport equations and thus, the main novelty of this paper is the derivation of a general semi-Lagrangian formulation for the solution of multi-dimensional transient advection–diffusion–absorption problems. The resulting numerical technique provides a general and straightforward procedure applicable to a wide range of problems, both from low to high Péclet and Damköhler numbers.

The semi-Lagrangian approach benefits from the FIC–FEM stabilized Eulerian method and the Lagrangian PFEM2 one. In this work we compare the benefits of the semi-Lagrangian method versus the standard Eulerian procedure for solving advection–diffusion–absorption problems.

The paper is organized as follows. First, the Eulerian solution scheme using a FIC–FEM procedure is introduced. Next, the PFEM2 technique is described and the Eulerian–Lagrangian splitting strategy is detailed. Several examples are presented in order to show the advantages of using the new semi-Lagrangian formulation versus the standard Eulerian approach: the evolution of a concentration field in a high-Péclet flow (no absorption) in 2D and in 3D and five other advective–diffusive–absorptive problems in 2D and 3D.

2. Eulerian approach

In this section, we present the Eulerian FIC–FEM formulation for solving the multidimensional advection–diffusion–absorption equations. The procedure follows the recent work of the authors [41].

2.1. Governing equations

Transport balance

The transport balance equation in a domain of area/volume Ω is expressed as

$$r_t = 0 \quad \text{in } \Omega \tag{1a}$$

with

$$r_t := \rho c \left(\frac{\partial \phi}{\partial t} + \mathbf{v}^T \nabla \phi \right) - \nabla^T \mathbf{D} \nabla \phi + s\phi - Q \tag{1b}$$

For 3D problems,

$$\mathbf{v} = \begin{bmatrix} v_1 \\ v_2 \\ v_3 \end{bmatrix}, \quad \mathbf{D} = \begin{bmatrix} k_1 & 0 & 0 \\ 0 & k_2 & 0 \\ 0 & 0 & k_3 \end{bmatrix}, \nabla = \begin{bmatrix} \partial/\partial x_1 \\ \partial/\partial x_2 \\ \partial/\partial x_3 \end{bmatrix} \tag{2}$$

In Eqs. (1a)–(1b)–(2) ϕ is the transported variable (i.e., the temperature in a heat transfer problem or the concentration in a mass transfer problem), v_i is the ith cartesian component of the velocity vector $\mathbf{v}$; ρ, c and k_i are the density, the specific flux parameter and the conductivity of the material along the ith global direction, respectively and s is the reaction parameter. In the following, and unless otherwise specified, we will assume that the problem parameters (ρ, c, k, s) are constant over the analysis domain Ω. In our work we define D = k/(ρc) as the normalized diffusivity, and R = s/(ρc) as the normalized absorption.

Boundary and initial conditions

The boundary conditions of the aforementioned equations are

$$\phi - \phi^p = 0 \quad \text{on } \Gamma_\phi \tag{3}$$

$$r_\Gamma = 0 \quad \text{on } \Gamma_q \tag{4}$$

with

$$r_\Gamma := -q_n + q_n^p \tag{5}$$

where

$$q_n = \mathbf{q}^T \mathbf{n} \quad , \quad \mathbf{q} = -\mathbf{D}\nabla\phi \tag{6}$$

In Eqs. (3)–(6) ϕ^p and q^p are the prescribed boundary fields of the transported variable and the outgoing diffusive flux at the Dirichlet and Neumann boundaries Γ_ϕ and Γ_q, respectively, with $\Gamma_\phi \cup \Gamma_q = \Gamma$, $\Gamma_\phi \cap \Gamma_q = \varnothing$, with Γ being the boundary of Ω and $\mathbf{n}$ its exterior unit normal.

The definition of the problem is completed with the *initial conditions*

$$\phi(\mathbf{x}, t_0) = \phi_0(\mathbf{x}) \tag{7}$$

where ϕ_0 is a known field.

2.2. Finite increment calculus (FIC) expressions

The governing Eqs. (1a) and (1b) and the boundary conditions (3)–(6) are expressed using the FIC theory as [53].

Transport balance

$$r_t - \underline{\frac{1}{2}\mathbf{h}^T \nabla r_t} = 0 \qquad \text{in } \Omega \tag{8}$$

with $\mathbf{h} = [h_1, h_2, h_3]^T$ in 3D.

Boundary conditions

$$\phi - \phi^p = 0 \quad \text{on } \Gamma_\phi \tag{9a}$$

$$r_\Gamma + \underline{\frac{1}{2} h_n r_t} = 0 \quad \text{on } \Gamma_q \quad , \quad \text{with } h_n = \mathbf{h}^T \mathbf{n} \tag{9b}$$

Eqs. (8) and (9b) are obtained by expressing the balance of fluxes in an arbitrary prismatic space domain of size $h_1 \times h_2 \times h_3$ within the global problem domain and at the Neumann boundary, respectively. The distances h_i are termed *characteristic lengths* of the FIC method. The variations of the transported variable within the balance domain are approximated by Taylor series expansions retaining one order higher terms than in the infinitesimal theory [23]. This higher-order expansions produce the underlined terms in Eqs. (8) and (9), which provide the necessary stability for the corresponding discretized equations.

Note that, as the characteristic length vector $\mathbf{h}$ tends to zero, the FIC governing equations tend to the standard infinitesimal form; that is, $r_t \to 0$ in Ω and $r_\Gamma \to 0$ on Γ_q as $\mathbf{h} \to \mathbf{0}$.

The characteristic lengths are small quantities which are defined in the context of the discrete problem and whose value influences the stability and accuracy of the FIC method. In practice, they are expressed as a proportion of a typical grid dimension [23]. The characteristic length vector is defined in [41] as the sum of the streamline characteristic vector $\mathbf{h}_v$, the absorption characteristic length vector $\mathbf{h}_r$ and the shock capturing characteristic length vector $\mathbf{h}_{sc}$, i.e.

$$\mathbf{h} = \mathbf{h}_v + \mathbf{h}_r + \mathbf{h}_{sc} \tag{10}$$

The FIC equations are the starting point for deriving different stabilized numerical methods. In combination with the Galerkin FEM, they yield the so-called FIC–FEM procedure [15,40] which has been successfully applied to problems of convective transport, fluid and solid mechanics such as advection–diffusion [23,54–56], diffusion–absorption and Helmholtz [57], advection–diffusion–absorption [53,58], advection–diffusion–reaction [40], incompressible fluid flow [59–63], fluid–structure-interaction [64–66], particle-laden flows and standard and incompressible solid mechanics [26,27,67]. The FIC approach has also been applied to a variety of problems in mechanics using the meshless finite point method [68–71].

2.3. Space and time integration

The system of Eqs. (8)–(9) has been discretized in space with the FEM and in time using an implicit Generalized Trapezoidal rule [72,73]. Details about the finite element matrices and vectors of the discretized problem can be found in [41]. The solution for the nodal values at a time instant is found using an incremental iterative strategy as

$$ {}^{i}\mathbf{H}^{n}\,\Delta\boldsymbol{\phi} = -{}^{i}\mathbf{r}_{t}^{n} \tag{11} $$

where $\Delta\boldsymbol{\phi}$ is the increment of the nodal variables, $(\cdot)^n$ denotes values at time $t = t_n$, ${}^{i}(\cdot)$ denotes values at the ith iteration and

$$ {}^{i}\mathbf{H}^{n} = \frac{1}{\theta\Delta t}\mathbf{M} + {}^{i}\mathbf{K}^{n} + \mathbf{C} + \mathbf{S} \tag{12} $$

$$ {}^{i}\mathbf{r}_{t}^{n} := \mathbf{M}\dot{\boldsymbol{\phi}} + [{}^{i}\mathbf{K}^{n} + \mathbf{C} + \mathbf{S}]{}^{i}\boldsymbol{\phi}^{n+\theta} - {}^{i}\mathbf{f}^{n} \tag{13} $$

In Eqs. (12) and (13), θ is a non dimensional time parameter ($0.5 < \theta \leq 1$ is required for the integration scheme to be unconditionally stable [22,72,73]).

The non-linearity of $\mathbf{K}$ is due to its dependence with ϕ when the equations are stabilized with the FIC procedure [41].

In Eq. (13) we define $\dot{\boldsymbol{\phi}} = \frac{\boldsymbol{\phi}^{n+\theta} - \boldsymbol{\phi}^{n}}{\theta\Delta t}$.

From the value of $\Delta\boldsymbol{\phi}$ obtained from Eq. (11) we compute the value of $\boldsymbol{\phi}^{n+\theta}$ at the $i+1$ iteration as

$$ {}^{i+1}\boldsymbol{\phi}^{n+\theta} = {}^{i}\boldsymbol{\phi}^{n+\theta} + \Delta\boldsymbol{\phi} \tag{14} $$

The iterative solution at t_{n+1} is obtained as

$$ {}^{i+1}\boldsymbol{\phi}^{n+1} = \frac{1}{\theta}{}^{i+1}\boldsymbol{\phi}^{n+\theta} + \left(1 - \frac{1}{\theta}\right)\boldsymbol{\phi}^{n} \tag{15} $$

The iterations proceed until convergence is achieved for both the unknown field ϕ and the residual $\mathbf{r}_t$ measured in a L_2 norm. A detailed explanation of each component of Eqs. (12) and (13) can be found in [41].

3. Semi-Lagrangian approach

Although good results were obtained in [41] when solving the advection–diffusion–absorption equations with the Eulerian FIC–FEM procedure, it was observed that excessive diffusion was obtained for problems involving high-Péclet numbers. This was the motivation for using the Lagrangian PFEM2 [49] to solve this type of problems, in view of its particular feature of non adding numerical diffusion for the advective problem. The PFEM2 technique can be understood as a splitting method, which uses a set of particles to solve the pure convective transport problem and a finite element mesh to solve the rest of the transport equations. In our work the PFEM2 is used to solve the advection equation. Following that, the diffusion–absorption equations are solved with the Eulerian FIC–FEM strategy.

Let us start by rewriting the transport balance Eq. (1b) using the total time derivative as

$$ r_t := \rho c\frac{D\phi}{Dt} - \nabla^{T}\mathbf{D}\nabla\phi + s\phi - Q = 0 \tag{16a} $$

$$ \frac{D\mathbf{x}}{Dt} = \mathbf{v} \tag{16b} $$

Eq. (16a) can be integrated using the trapezoidal rule explained in Section 2.3. Due to the dependence with Eq. (16b), a coupling between the time integration of both equations shall be defined.

3.1. Advection step

Let us consider a finite set of (point)-particles with which we uniformly seed the computational domain, such that their positions do not necessarily coincide with the locations of the finite element mesh nodes.

Remark 1. In this work the computational domain is initially seeded with fifteen to twenty particles per element, depending on whether it is 2D or 3D. This number does not remain constant during the simulation because particles can freely enter and exit finite elements as they move through the domain. Thereby, in order to properly perform the advection stage, every time step the domain is reseed with particles so as to ensure that a minimum number is present within each finite element. This number of particles was chosen to be four in 2D and six in 3D. Particles can also be eliminated from each finite element in order to limit the computational cost. In this case, the maximum number of particles allowed per finite element is sixteen in 2D and twenty-four in 3D. These particle thresholds were chosen as they have proven to give accurate results in previous works [49].

Let us assume that the particles move as material points and that each one stores the point concentration of the property $\phi_p = \phi(\mathbf{x}_p)$. Since the variables are not known for any arbitrary time t, but only for the discrete time steps $1,\ 2\ldots n,\ n+1\ldots$ defined in Section 2.3, the advection of a particle can be approximated using a θ-family discretization as:

$$\mathbf{x}_p^{n+1} = \mathbf{x}_n^p + (1-\theta)\int_{t_n}^{t_{n+1}} \mathbf{v}_n(\mathbf{x}_p^t)dt + \theta\int_{t_n}^{t_{n+1}} \mathbf{v}_{n+1}(\mathbf{x}_p^t)dt \tag{17}$$

If the velocity field is known, the system becomes explicit and the problem is reduced to moving the particles along the streamlines. The problem is solved using an explicit forward integration ($\theta = 0$) with substepping [48]. This method, also known as XIVAS [74,75], was initially applied to a variable velocity field.

After the particles are moved, the ones that leave the domain are removed.

3.2. Projection

When solving the advective step in Eq. (16a), the particles concentration at $\mathbf{x}_p^{n+1}$ is the same as at the onset of the time step ($\mathbf{x}_p^n$). This is equivalent to saying that the advective step assumes $\frac{D\phi}{Dt} = 0$. This modification in the field described by the particles needs to be transferred onto the finite element space. As usual in particle-based techniques, such as PFEM, a projection procedure is used to transfer the information from the particles to the finite elements in the underlying mesh. In our work we use

$$\phi^* = \mathcal{L}(\phi_p) \tag{18}$$

where $\mathcal{L}$ is the projection operator from the particles to the finite element space and ϕ^* is the result of the advection at the time step $n+1$. In this case, a first order explicit projection has been used and all the particles in the elements surrounding a node contribute to that node, i.e.

$$\phi_i^* = \frac{\Sigma_e \Sigma_{p_e} w_p \phi_p}{\Sigma_e \Sigma_{p_e} w_p} \quad \text{with} \quad w_p = N_{ei}(\mathbf{x}_p) \tag{19}$$

where the index i runs over all the mesh nodes, where e runs over the elements sharing node i and where p_e runs over the particles contained in element e.

3.3. Diffusion–absorption stage

Once the advection problem is solved explicitly in the particles and the results are transferred to the mesh nodes, the Lagrangian residual (Eq. (16a)) is solved in a fixed grid with a Eulerian FIC–FEM technique. The spatial discretization and the time integration scheme follows the procedure explained in Section 2.3. Details are given in [41].

Note that the advective term $\mathbf{C}$ from Eq. (13) vanishes as advection is modelled with the Lagrangian approach and the time derivative $\dot{\phi}$ denotes now the total derivative (Eq. (16a)).

The total time derivative is computed as

$$\dot{\phi} = \frac{\phi^{n+\theta} - \phi^*}{\theta \Delta t} \tag{20}$$

Eq. (20) includes the contribution of the advection computed with the particles.

As explained in Section 3.1, the advection is calculated separately from the diffusion and the absorption with the PFEM2 procedure. As the equations solved with a Eulerian approach are free from advective instabilities, this

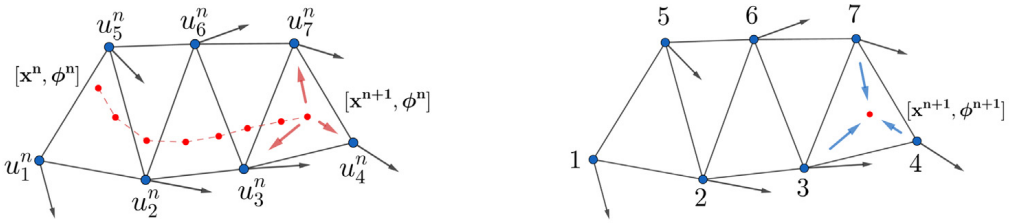

(a) Explicit advection stage using particles (in red). Next, the particles' information is transferred to the mesh nodes (in blue).

(b) Diffusion-absorption stage. Contribution of the finite element nodes to the particles.

Fig. 1. Illustration of the two main steps of the PFEM2 framework.

splitting simplifies the equations in the following way. The parameter $\mathbf{h}_v$, which helps solving global advective instabilities is set to zero as the advection is calculated through a particles method. $\mathbf{h}_{sc}$, which is used to attenuate Gibbs oscillations that appear along characteristic layers is also set to zero as these oscillations do not appear in the PFEM2 method. Finally, the advective components of $\mathbf{h}_r$, are set to zero as the velocity is computed in previous steps and does not intervene in the diffusion–absorption stage. The characteristic length parameter from Eq. (10) needed for the FIC–FEM Eulerian solution is then computed as

$$\mathbf{h} = \mathbf{h}_r = \frac{2}{r_t}\mathbf{D_s}\nabla\phi \tag{21}$$

where matrix $\mathbf{D}_s$ takes care of the instabilities induced by the irregularity of the triangular mesh near boundaries that develop parabolic layers for high values of the absorption parameter [15].

The new characteristic length (Eq. (21)) leads to the disappearance of the non-linearity seen in Eqs. (12) and (13), which simplifies the resolution of the advection–diffusion–absorption equation.

3.4. Particles update

The last step of the PFEM2 algorithm is to add the contribution of the solution of Eq. (16a) to the particles. To avoid the accumulation of projection errors and additional diffusion, the information from the particles is updated using an incremental scheme. This step only involves the evaluation of the unknown at each particle position in the finite element mesh as:

$$\phi_p^{n+1} = \phi_p^n + \phi(\mathbf{x}_p^{n+1}) - \phi(\mathbf{x}_p^*) \tag{22}$$

The basic steps of the PFEM2 procedure can be seen in Fig. 1.

Properties of the PFEM2 procedure

Apart from removing the numerical diffusion added from the FEM Eulerian approach, PFEM2 has proven to be very accurate when large time-steps and/or coarse meshes are used [49]. However, due to the projection of the information, as well as the updating of the particles, the method does not guarantee conservation of the transported variable. In Section 4.1 we have evaluated the evolution in time of the concentration value in order to assess the conservation features of the algorithm after 15 s of simulation. Negligible concentration changes were observed for this problem. This is a distinct feature of PFEM [29] and will be studied in more detail in further work.

4. Examples

We present seven examples of application of the semi-Lagrangian formulation: the transport of a concentration of a solute in a fluid domain (both in 2D and 3D), a high-Damköhler number example (both in 2D and 3D), one low-Dämkohler number example in 3D and two other advective–diffusive–absorptive problems with a manufactured solution. These examples are used to validate the method both high-Péclet and high-Damköhler number cases as well as those complex ones with a manufactured solution.

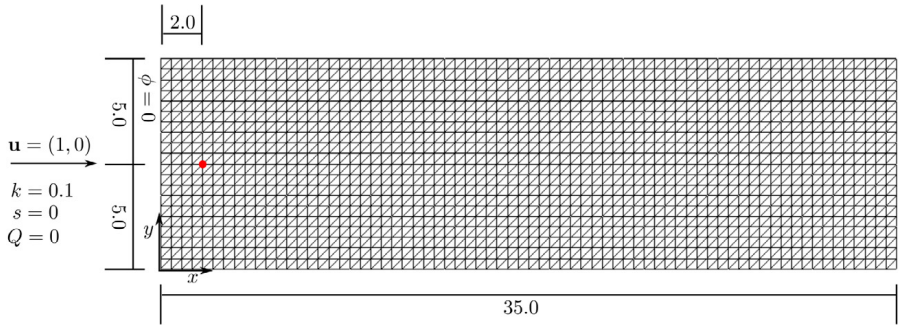

Fig. 2. 2D transport of a concentration. Finite element mesh. The initial concentration is depicted in red at point (2, 5).

4.1. 2D transport of a concentration

4.1.1. Introduction

We study the evolution of an initially point-like concentration of solute as it is transported and diffused from a point source in a fluid with a known velocity field. The main interest is to compare the accuracy of a purely Eulerian approach versus the semi-Lagrangian method previously described from low to very high Péclet numbers.

We consider a uniform velocity field parallel to the x-axis of 1 m/s. Two different values are considered for the diffusivity: $D = 0.1$ m^2/s for the low-Péclet ($Pe = 2.5$) example and $D = 0$ for the high-Péclet one ($Pe \to \infty$). The Péclet number is defined as follows: $Pe = \frac{ul}{2D}$, where u is the horizontal velocity, l is the characteristic length and D is the normalized diffusivity. In this and in the following 3D example we have considered $\rho c = 1$ J/m^{3}K. The analysis domain $(x, y) \in [0, 35] \times [0, 10]$ m is discretized into a regular mesh of 3-noded triangles with a mesh size $h = 0.5$ m, which gives a domain of $2 \times (70 \times 20)$ elements.

The Dirichlet boundary condition $\phi = 0$ at $x = 0$ m and the initial concentration $\phi(x_0, y_0, 0) = 1000$ kg/m^2 at $\mathbf{x}^0 = (2, 5)$ m are considered. Fig. 2 shows a diagram of the whole set-up (note that the point $(2, 5)$ is made to coincide with a mesh node).

For the numerical solution, the initial condition is defined by the value of the concentration at a single node ($\phi_0 = 1000$ kg/m^2 at node (2, 5), 0 everywhere else) as a single shape function whose maximum concentration coincides with ϕ_0. This corresponds to a total mass of 250 kg for the numerical simulation.

The numerical solution is compared to an analytical one that consists in the transport and diffusion of a Gaussian density distribution [76]. The initial conditions in this case are defined as

$$\phi(x, y, t) = \frac{\phi_0}{L_3 4\pi D\hat{t}} e^{-A} \tag{23a}$$

with

$$A = \frac{1}{4D\hat{t}} \left\{ [x_1 - (x_1^0 + u_1(\hat{t} - t^0))]^2 + [x_2 - (x_2^0 + u_2(\hat{t} - t^0))]^2 \right\} \tag{23b}$$

where t^0 is calculated such that at $\hat{t} = t^0$, ϕ corresponds to a Gaussian whose height is equal to 1000 kg/m^2 and is centred at the node (2, 5) and such that the initial total mass coincides with the one imposed as the initial condition in the numerical solution.

We have an initial error that comes from the idealized representation of a concentrated mass. We are simply comparing a Gauss bell to a pyramid with the same total mass and height and how they evolve in time.

L_3 is the vertical dimension of the analysis domain (we have taken $L_3 = 1$), u_1 and u_2 are the horizontal and vertical components of the velocity vector and D is the normalized diffusivity. In all cases, the density ρ and the specific flux c are chosen such that $\rho c = 1$ J/m^{3}K. We have also assumed isotropic diffusion. Several cases have been studied to see the effect of the advective and diffusive terms on the result.

The time-integration parameters are $\theta = 0.5$ and $\Delta t = 0.5$ s. Taking into account these parameters the Courant number is $C = 1$.

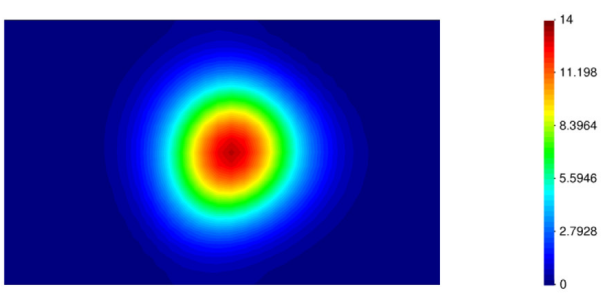

(a) Eulerian solution for $Pe = 2.5$.

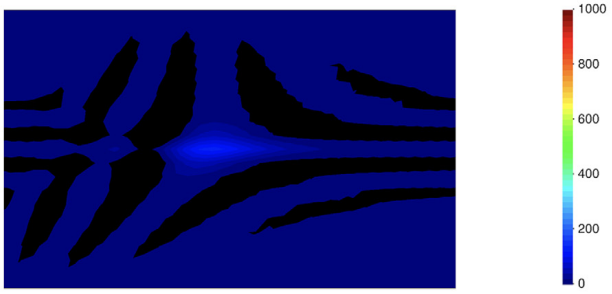

(b) Eulerian solution for $Pe \to \infty$.

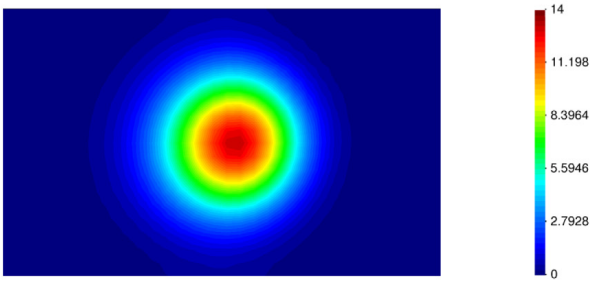

(c) Semi-Lagrangian solution for $Pe = 2.5$.

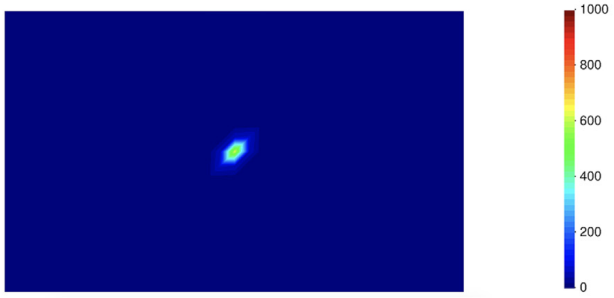

(d) Semi-Lagrangian solution for $Pe \to \infty$.

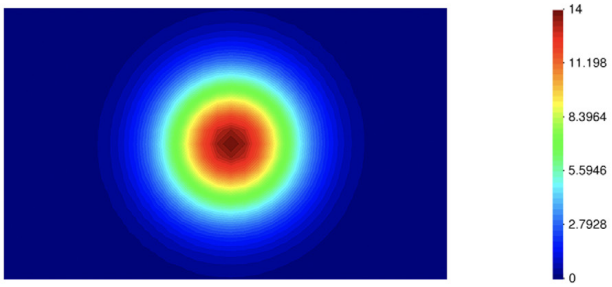

(e) Analytical solution for $Pe = 2.5$.

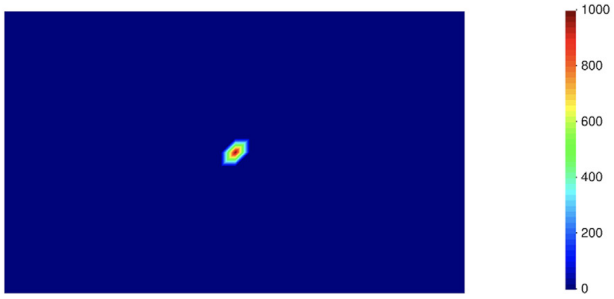

(f) Analytical solution $Pe \to \infty$.

Fig. 3. 2D transport of a concentration. Eulerian, semi-Lagrangian and analytical results compared at $t = 15$ s.

4.1.2. Results

The results obtained with the Eulerian and the semi-Lagrangian methods are presented next.

- Eulerian and semi-Lagrangian solutions for $Pe = 2.5$
  We have compared the Eulerian and semi-Lagrangian solutions with the analytical one. Numerical results show a slight difference of concentration versus the analytical values. While in the Eulerian method a maximum concentration value of 13.234 kg/m^2 is obtained, using the semi-Lagrangian approach this value is 13.085 kg/m^2. The maximum analytical value for the same case at $t = 15$ s is $\phi = 13.089$ kg/m^2 (Fig. 3e), which represents a percentual gain of 1.11% in the Eulerian case (Fig. 3a) and 0.03% loss in the semi-Lagrangian one (Fig. 3c). In both cases, the concentration difference is small and thus we can conclude that both methods work well for this Péclet number but the semi-Lagrangian shows a substantially higher accuracy. Looking at the concentration contour at Fig. 3a, we can observe a small deformation of the resulting shape for the Eulerian case due to the slightly higher numerical diffusion.
- Eulerian and semi-Lagrangian solutions for $Pe \to \infty$
  In this case, the effect of the diffusive component vanishes. The Eulerian result in Fig. 3b shows a solution which is not representative of the analytical one and keeps on diffusing as the simulation advances. On the

Table 1
2D transport of a concentration. Maximum concentration values of each method for different Péclet numbers.

		Maximum concentration value [kg/m^2]		
		Analytical	*Semi-Lagrangian*	*Eulerian*
Pe	$\to \infty$	1000.00	626.55	129.92
	2.5e06	999.92	626.53	129.92
	2.5e05	999.25	626.36	129.90
	2.5e04	992.52	624.61	129.73
	2.5e03	929.89	607.60	128.03
	2.5e02	570.131	470.390	113.910
	2.5e01	117.098	118.130	65.081
	4.55	23.570	25.835	24.687
	3.33	17.360	17.372	17.410
	2.50	13.089	13.085	13.234

other hand, the semi-Lagrangian result in Fig. 3d, shows no loss of the amount of concentration transport as it evolves in time, similarly as in the analytical solution for the same Pe (Fig. 3f). The maximum value of the semi-Lagrangian method is 626.55 kg/m^2, which corresponds to the projection of the maximum concentration from the particles to the mesh. Hence, as expected, there is a slight concentration loss (due to the projection from the particles to the mesh nodes) towards the adjacent elements from the point where the concentration is assigned. The sum of the concentrations on these adjacent elements coincides with the initial maximum value of 1000 kg/m^2. While in this case the interpolation error is 0, the first projection smoothens out completely the spike, since no particle coincides with the spike position exactly.

4.1.3. Sensitivity analysis

In this section we run several cases varying the value of the diffusivity between the lowest and highest Péclet number of the examples (from $Pe = 2.5$ to $Pe \to \infty$).

Table 1 presents the maximum concentration values for each of the methods with different diffusivities. The reference values obtained with the analytical solutions are included for comparison.

Clearly, the semi-Lagrangian approach, which benefits from the particle Lagrangian motion, works very well for purely advective situations, as well as for the range of Péclet numbers considered in this study.

On the other hand, we observe that the Eulerian FIC–FEM method solves stability problems, especially in the most diffusive cases. The solutions coincide with the semi-Lagrangian results.

Fig. 4 shows the maximum concentration in terms of the Péclet number. Note how the Eulerian approach presents a huge numerical diffusion for high-Péclet numbers. The semi-Lagrangian approach yields more accurate results. The difference between the analytical solution and the semi-Lagrangian results is assessed in Section 4.1.4.

Note that for $Pe \lesssim 2.5$, the Eulerian solution begins to gain relevance and the results are comparable to those obtained with the semi-Lagrangian approach.

4.1.4. Numerical diffusion analysis

This section studies the examples of Section 4.1.2, which are now plotted along time to see their relative impact in the numerical diffusion.

Fig. 5 shows that, although the first four seconds of the example differ slightly, the results are quite identical at $t = 15$ s.

The case for $Pe \to \infty$ is shown in (Fig. 6). We can see that the semi-Lagrangian method presents no diffusion loss whatsoever in the maximum transported value, except from that introduced by the projection of the nodal concentration from the particles to the adjacent elements.

4.2. Transient advection–diffusion–absorption problem with sharp boundary layers

The analysis domain $(x, y) \in [0, 8] \times [0, 8]$ is discretized into a regular mesh of $2 \times (8 \times 8)$ 3-noded triangles of unit rectangular side ($l = 1$) (Fig. 7). The advection, diffusion and absorption coefficients are $u = 8$ m/s, $D = 2$

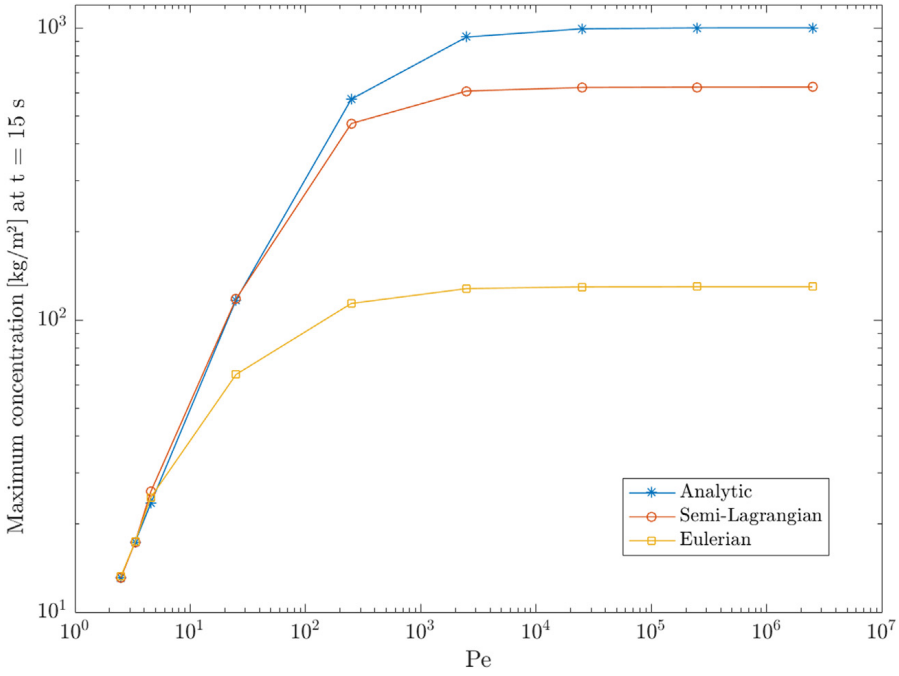

Fig. 4. 2D transport of a concentration. Comparison of the analytical, semi-Lagrangian and Eulerian methods in terms of the Péclet number.

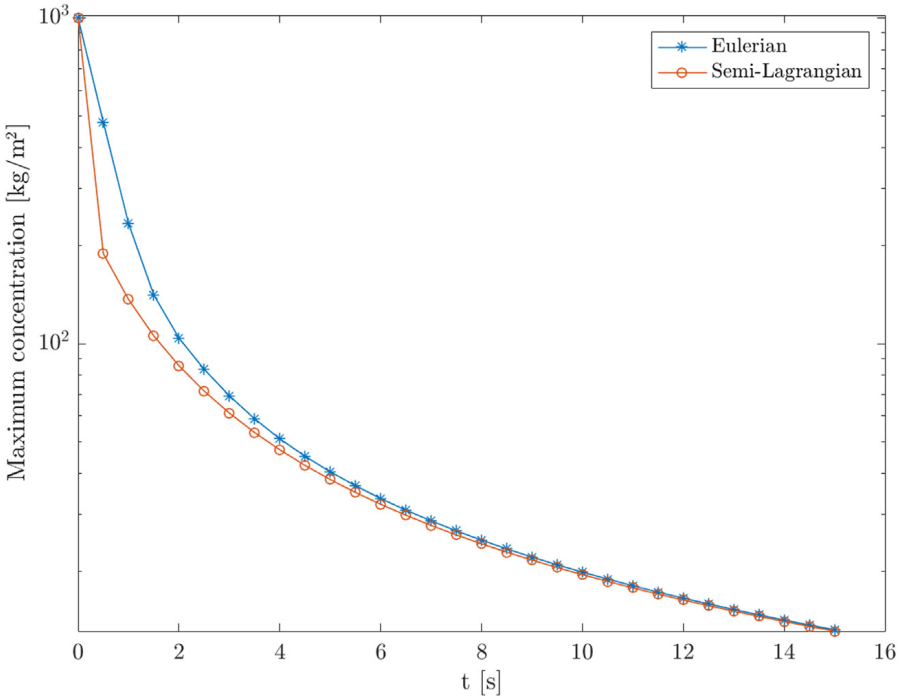

Fig. 5. 2D transport of a concentration. Comparison of the maximum transported value from $t = 0$ s to $t = 15$ s using the semi-Lagrangian and Eulerian methods ($Pe = 2.5$).

m^2/s and $R = 2000.0$ s^{-1}. The transported variable is the mass, in Kg and $\rho c = 1$ J/m^3K. The schematics of the problem can be seen in Fig. 7. The problem data yields a Péclet number of $Pe = 2.0$ and a Damköhler number of $Da = 250.0$. The Damköhler number is defined as $Da = \frac{sl}{u}$, where s is the reaction parameter (or absorption coefficient R, as ρc equals 1.0), l is the characteristic length and u the velocity.

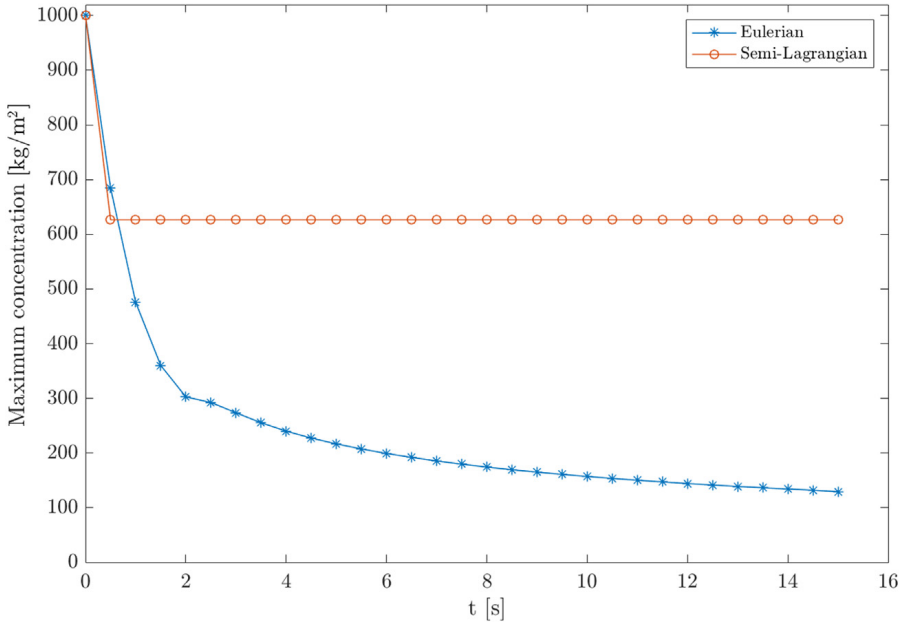

Fig. 6. 2D transport of a concentration. Comparison of the maximum transported value from $t = 0$ s to $t = 15$ s using the semi-Lagrangian and Eulerian methods ($Pe \to \infty$).

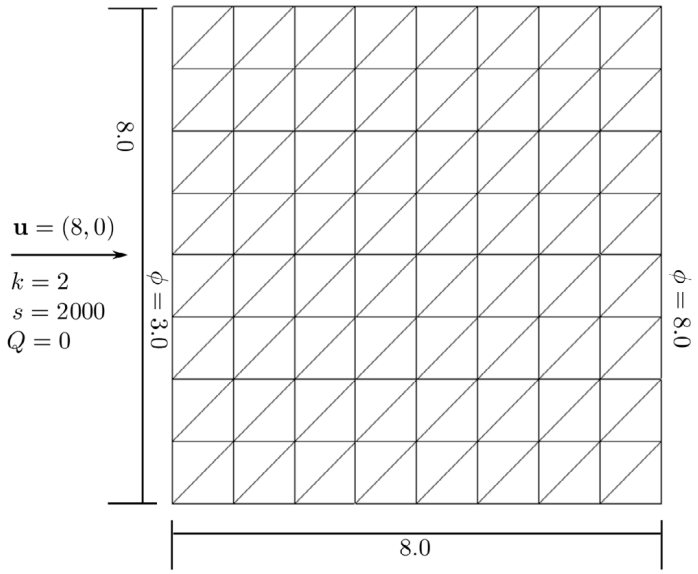

Fig. 7. Transient advection–diffusion–absorption problem. Square domain with constant velocity and zero source.

The Dirichlet boundary conditions $\phi(x = 0) = 3$ and $\phi(x = 8) = 8$ kg/m^2 are employed. The initial solution is chosen to have a linear profile. The transient solution was obtained with the implicit iterative scheme explained in Section 2.3 with $\theta = 1.0$ and a time step of $\Delta t = 0.0625$ s. This corresponds to an element Courant number of $C = 0.5$. An exponential layer gradually develops at the right boundary which is attenuated thanks to the absorptive stabilization features introduced by the FIC–FEM procedure (Fig. 8).

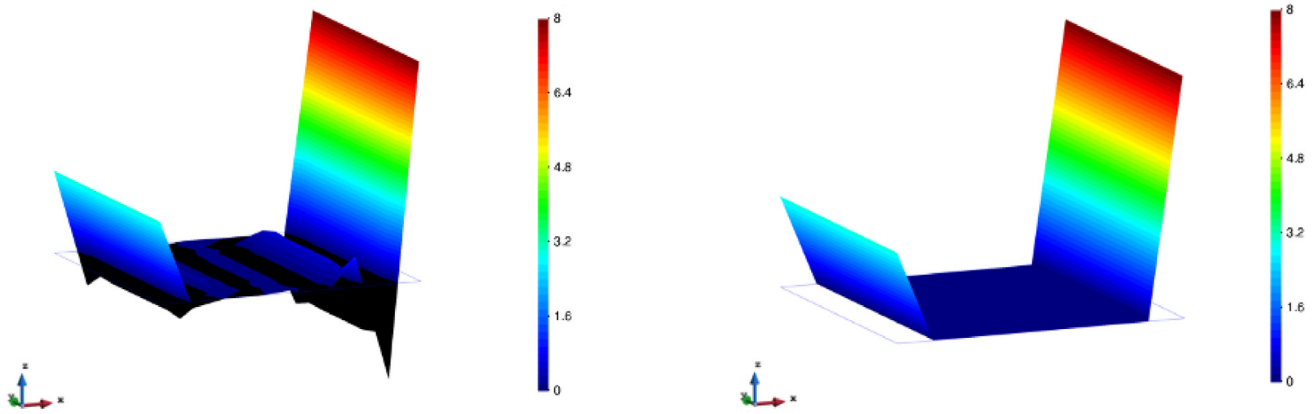

(a) Result without absorption stabilization. **(b)** Result with absorption stabilization.

Fig. 8. Transient advection–diffusion–absorption with sharp boundary layer. Results at $t = 2$ s.

Table 2
Manufactured advective–diffusive–absorptive problem. Damköhler and Péclet numbers for each of the cases studied.

	Damköhler numbers			Péclet numbers
	R = 100 1/s	R = 1000 1/s	R = 10 000 1/s	
l = *1/32* m	3.13	31.25	312.50	1.56
l = *1/64* m	1.56	15.63	156.25	0.78
l = *1/128* m	0.78	7.81	78.13	0.39
l = *1/256* m	0.39	3.91	39.06	0.20

4.3. Transient advection–diffusion–absorption problem with a manufactured solution

This example consists in solving a low-diffusive advective–absorptive problem using the manufactured solution stated in Eq. (24). This problem was solved by Duan et al. [77,78].

$$\phi(x,y) = \left(\frac{x^2}{2u_1} + \frac{Dx}{u_1^2}\left(\frac{1}{2u_1} + \frac{D}{u_1^2}\right)\frac{\exp\frac{-u_1}{D} - \exp\left[\frac{-u_1}{D}(1-x)\right]}{1-\exp\frac{-u_1}{D}}\right)\times \left(\frac{y^2}{2u_2} + \frac{Dy}{u_2^2}\left(\frac{1}{2u_2} + \frac{D}{u_2^2}\right)\frac{\exp\frac{-u_2}{D} - \exp\left[\frac{-u_2}{D}(1-y)\right]}{1-\exp\frac{-u_2}{D}}\right) \tag{24}$$

Introducing Eq. (24) into Eq. (1b) yields the non-homogeneous source-like term Q that is used, in turn, to solve the advective–diffusive–absorptive equation with the semi-Lagrangian procedure.

We will consider a uniform velocity field of $\mathbf{u} = (u_1, u_2)^T := (1/2, \sqrt{3}/2)^T$. A value of $D =$ 1e-2 m^2/s and R $= s/\rho c = 10^i$ 1/s with $i = 2, 3, 4$ have been taken.

These cases have been run with $\rho c = 1$ J/m^{3}K. The analysis domain $\Omega := (x, y) \in [0, 1]\times[0, 1]$ m is discretized in a regular mesh of $2\times(1/2^i \times 1/2^i)$ 3-noded triangles with a characteristic length $l = 1/2^i$ m, being $i = 5, 6, 7, 8$.

A Dirichlet boundary condition of $\phi = 0$ kg at the whole boundary is considered. The time-integration parameters are chosen as: $\theta = 1.0$ and $\Delta t =$ 1e-4 s.

An image of the numerical result and the exact solution can be seen in Fig. 10. Excellent agreement is obtained.

Table 2 shows the Damköhler numbers corresponding to each of the cases considered in the study.

Table 3 shows the root-mean-square error for each case analysed. Taking the last two values (belonging to the finest mesh examples), the convergence has also been calculated.

Fig. 9 displays a graph of the results of Table 3.

Table 3
Manufactured advective–diffusive–absorptive problem. Root-mean-square error (RMSE) and order of convergence for different values of R = s/(ρc).

	RMSE		
	R = 100 1/s	R = 1000 1/s	R = 10 000 1/s
l = 1/32 m	0.00906573	0.00842561	0.00836711
l = 1/64 m	0.00420981	0.00370434	0.00362029
l = 1/128 m	0.00153896	0.00127547	0.00122659
l = 1/256 m	0.00056077	0.00038503	0.00036025
Convergence order	1.46	1.73	1.77

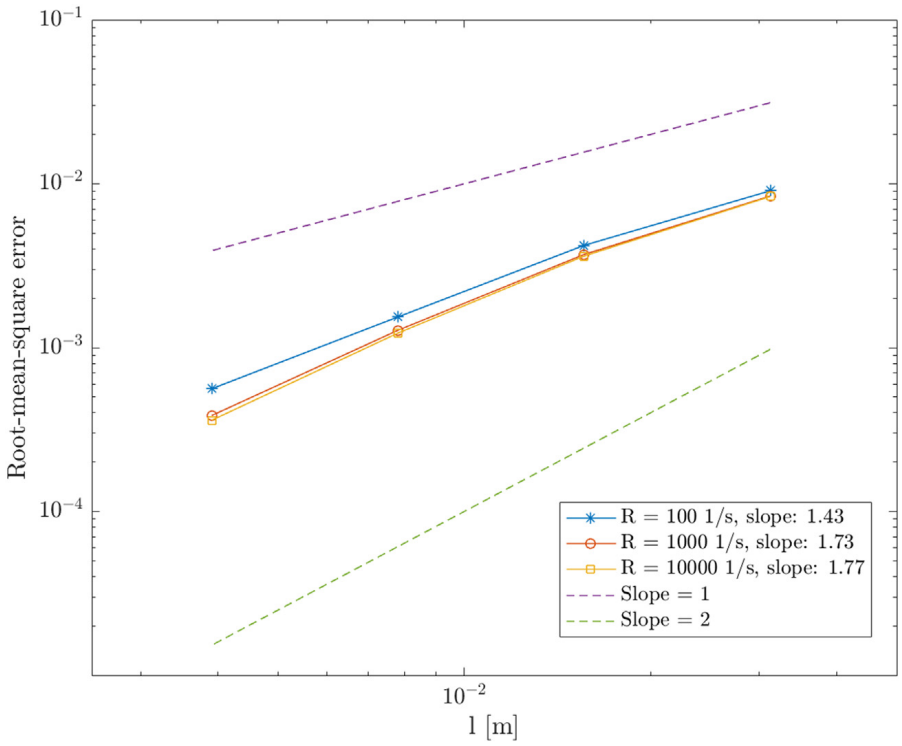

Fig. 9. Manufactured advective–diffusive–absorptive problem. Root-mean-square error versus the characteristic length l. Lines with slope = 1 and 2 are plotted for reference.

4.4. Manufactured transient advection–diffusion–absorption hump problem

This last example, taken from [77], consists in a hump moving in a domain changing its height periodically leading to the appearance of a strong interior layer adjacent to the hump walls. The exact solution is given by Eq. (25). This solution is introduced into Eq. (1b) to yield the manufactured unhomogeneous source-like function Q used for solving the advection–diffusion–absorption equation with the semi-Lagrangian procedure.

$$\phi(t,x,y) = 16\sin(\pi t)x(1-x)y(1-y)\times \left(\frac{1}{2} + \frac{\arctan[2\varepsilon^{-1/2}(0.25^2-(x-0.5)^2-(y-0.5)^2)]}{\pi}\right) \tag{25}$$

We have considered a uniform velocity field of $\mathbf{u} = (2,3)^T$. A value of D = 1e-6 m^2/s has been chosen for the normalized diffusivity and R = 1000 1/s for the normalized absorption.

These cases have been run with ρc = 1 J/m^{3}K. The analysis domain $\Omega := (x,y) \in [0,1]\times[0,1]$ m is discretized in a regular mesh of 2 × (64 × 64) 3-noded triangles with a characteristic length l = 1/64 m.

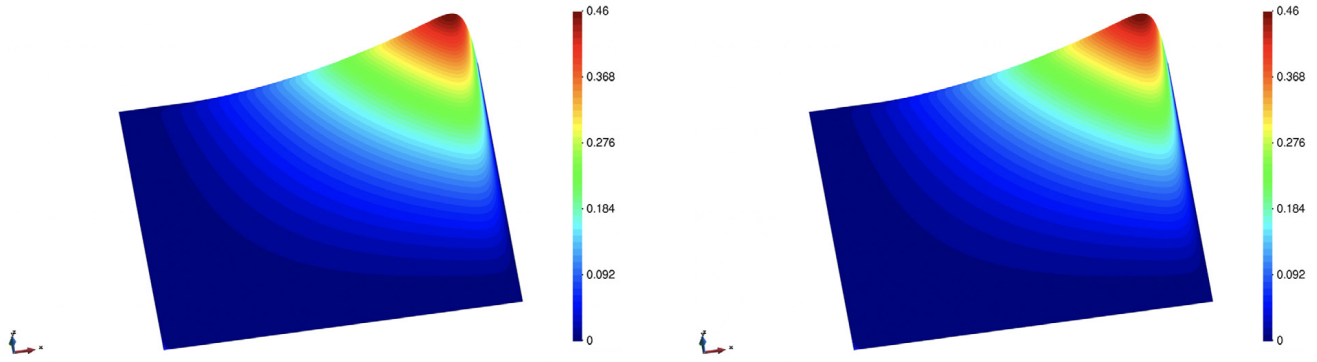

(a) Numerical solution. **(b)** Analytical solution.

Fig. 10. Advective–diffusive–absorptive problem with manufactured solution. Elevation plot at $t = 0.08$ s with a $h = 1/256$, $D =$ 1e-2 m^2/s and a $R = 10^4$ 1/s giving $Pe = 0.20$ and $Da = 39.06$.

A Dirichlet boundary condition $\phi = 0$ kg at $\partial\Omega$ has been considered. The initial condition is $\phi = 0$ kg at $t = 0$ s. The time-integration parameters are chosen as: $\theta = 0.8$ and $\Delta t =$ 1e-3 s.

Results of the simulation can be seen in Fig. 11.

The results show that the solution is stable and does not exhibit spurious oscillations near the interior layer region. Some minor oscillations – $\approx$ 2% of the maximum value — can be spotted on the top-right side of the domain.

A qualitative comparison with the examples in [77] shows that the semi-Lagrangian procedure is highly competitive with the best methods in that paper.

4.5. 3D advection–diffusion–absorption problem for a low Damköhler number

The analysis domain $(x, y, z) \in [0, 8] \times [0, 8] \times [0, 8]$ is discretized into a regular mesh of $2 \times (16 \times 16 \times 16)$ 4-noded tetrahedra of rectangular side $l = 0.5$. The advection, diffusion and absorption coefficients are chosen as $u = 8$ m/s, $D = 2$ m^2/s and $R = 2.0$ s^{-1}. The transported variable is the mass, in Kg and $\rho c = 1$ J/m^{3}K. The schematics of the problem are shown in Fig. 12. The problem data yields a Péclet number of $Pe = 1.0$ and a Damköhler number of $Da = 0.125$.

The Dirichlet boundary conditions of $\phi = 100$ kg/m^3 on the surfaces $\overline{AA'B'B}$, $\overline{BCC'B'}$ and $\overline{CDD'C'}$ and $\phi = 0$ kg/m^3 on the surfaces $\overline{DD'E'E}$ and $\overline{EE'A'A}$ are employed. The initial solution is chosen to have a linear profile (Fig. 13). The transient solution was obtained with the implicit iterative scheme explained in Section 2.3 with $\theta = 1.0$ and a time step of $\Delta t = 0.0625$ s. This corresponds to an element Courant number $C = 1.0$.

Fig. 14 shows the evolution of the solution on a plane at $y = 4$ and Fig. 15 a perspective view of the quasi-steady-state solution for the transported variable for $t = 2$ s. Accurate stabilized results are obtained, thanks to the stabilization features of the FIC–FEM approach.

4.6. 3D advection–diffusion–absorption problem for a high Damköhler number

The analysis domain $(x, y, z) \in [0, 8] \times [0, 8] \times [0, 8]$ is, again, discretized into a regular mesh of $2 \times (16 \times 16 \times 16)$ 4-noded tetrahedra of rectangular side $l = 0.5$. The advection, diffusion and absorption coefficients are chosen as $u = 8$ m/s, $D = 2$ m^2/s and $R = 2000.0$ s^{-1}. The transported variable is the mass, in Kg and $\rho c = 1$ J/m^{3}K. The schematics of the problem can be seen in Fig. 16. The problem data yields a Péclet number of $Pe = 1.0$ and a high Damköhler number of $Da = 125$.

The Dirichlet boundary conditions of $\phi = 3$ and $\phi = 8$ kg/m^3 are imposed on the surfaces $x = 0$ and $x = 8$, respectively. The initial solution is chosen to have a linear profile (Fig. 17). The transient solution was obtained with the implicit iterative scheme explained in Section 2.3 with $\theta = 1.0$ and a time step of $\Delta t = 1e - 4$ s. This corresponds to an element Courant number $C = 8e - 4$.

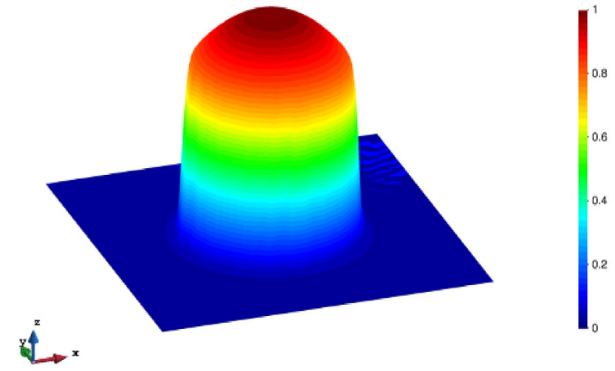

(a) Numerical solution.

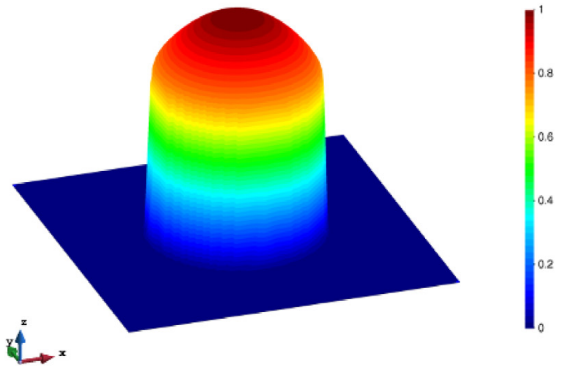

(b) Analytical solution.

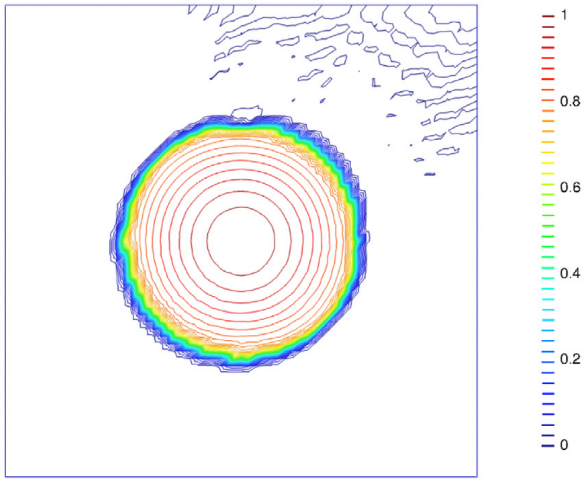

(c) Top view of the numerical solution.

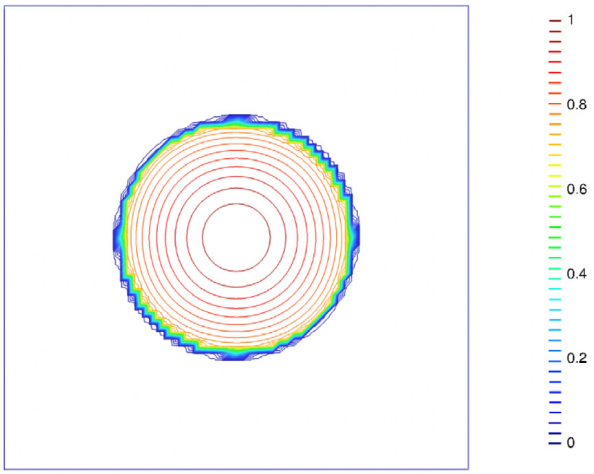

(d) Top view of the analytical solution.

Fig. 11. Manufactured hump problem. Hump geometry at $t = 0.5$ s with $h = 1/64$, $D =$ 1e-6 m^2/s and $R = 1000$ 1/s, which corresponds to $Pe = 1.56e4$ and $Da = 15.63$.

Fig. 18 shows the cubic domain along with two slices of it at the final time step ($t = 5e-3s$), it can be seen that the values in the central part of the domain are quickly absorbed. The steady state solution is free from boundary unstabilities.

Fig. 19 shows the evolution of the solution on a line from (0, 4, 4) to (8, 4, 4). A stable steady state is reached quickly and corresponds to the 1D and 2D solution.

4.7. Pure 3D advection of a spherical concentration

A 3D problem similar to the point concentration in 2D has been studied in this section. It consists in the pure advective transport ($Pe \to \infty$) of a uniform spherical blob with a concentration $\phi = 100$ kg/m^3. The spherical blob has a radius of 1.0 m and is initially centred at $(x, y, z) = (1.25, 2.5, 1.25)$. A helicoidal velocity field of $\mathbf{u} = (0.5, 0.5(z - 2.5), 0.5(y - 2.5))$ m/s is prescribed on the domain. For this problem we have chosen a normalized diffusivity $D = 0.0$ (pure advection) and a normalized absorption $R = 0.0$. The analysed domain $(x, y, z) \in [0, 15] \times [0, 5] \times [0, 5]$ m is discretized into a regular mesh of $(150 \times 50 \times 50)$ 4-noded linear tetrahedra. The Courant number in the x direction is $C = 2.5$. The schematics of the problem are shown in Fig. 20.

In Fig. 21 a typical streamline that the spherical blob follows during the simulation is shown.

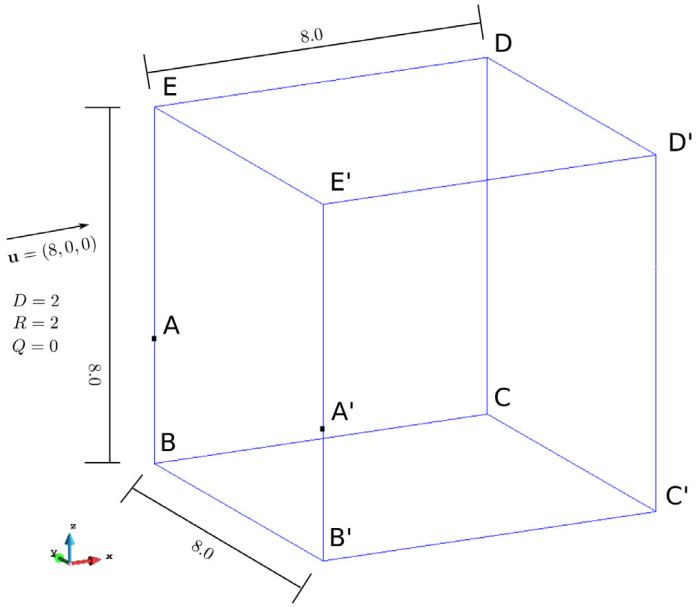

Fig. 12. Transient 3D advection–diffusion–absorption problem. Cubic domain with constant velocity and zero source.

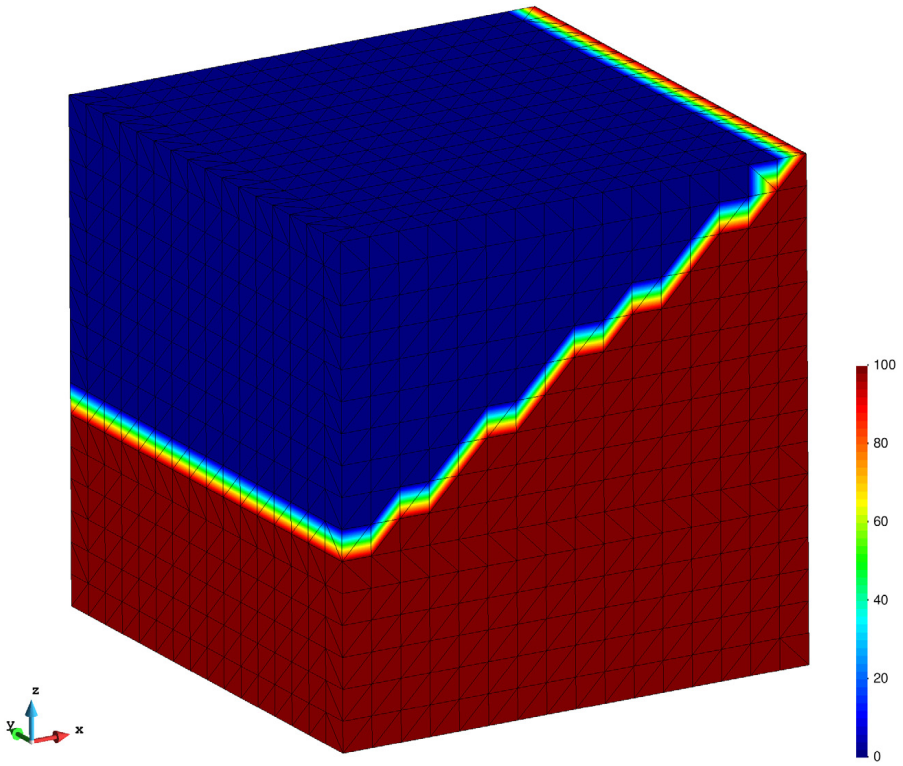

Fig. 13. Transient 3D advection–diffusion–absorption problem. Mesh of the cubic domain with the initial boundary conditions.

In Fig. 22 a 3D view of the transported sphere can be seen. Several time steps have been overlayed for the reader's ease. The results show no concentration loss except from the one derived from the projection of the initial conditions from the particles to the adjacent elements, which is $\approx 6.5\%$. This can be quantified by averaging the values of the concentration in the transported sphere of radius 1 m (Fig. 23). The projection loss in this case is directly related to the surface-to-volume ratio of a sphere, which is proportional to the inverse of the radius like $3/r$, with r denoting the radius. Therefore, such loss could be reduced either by increasing the radius of the spherical

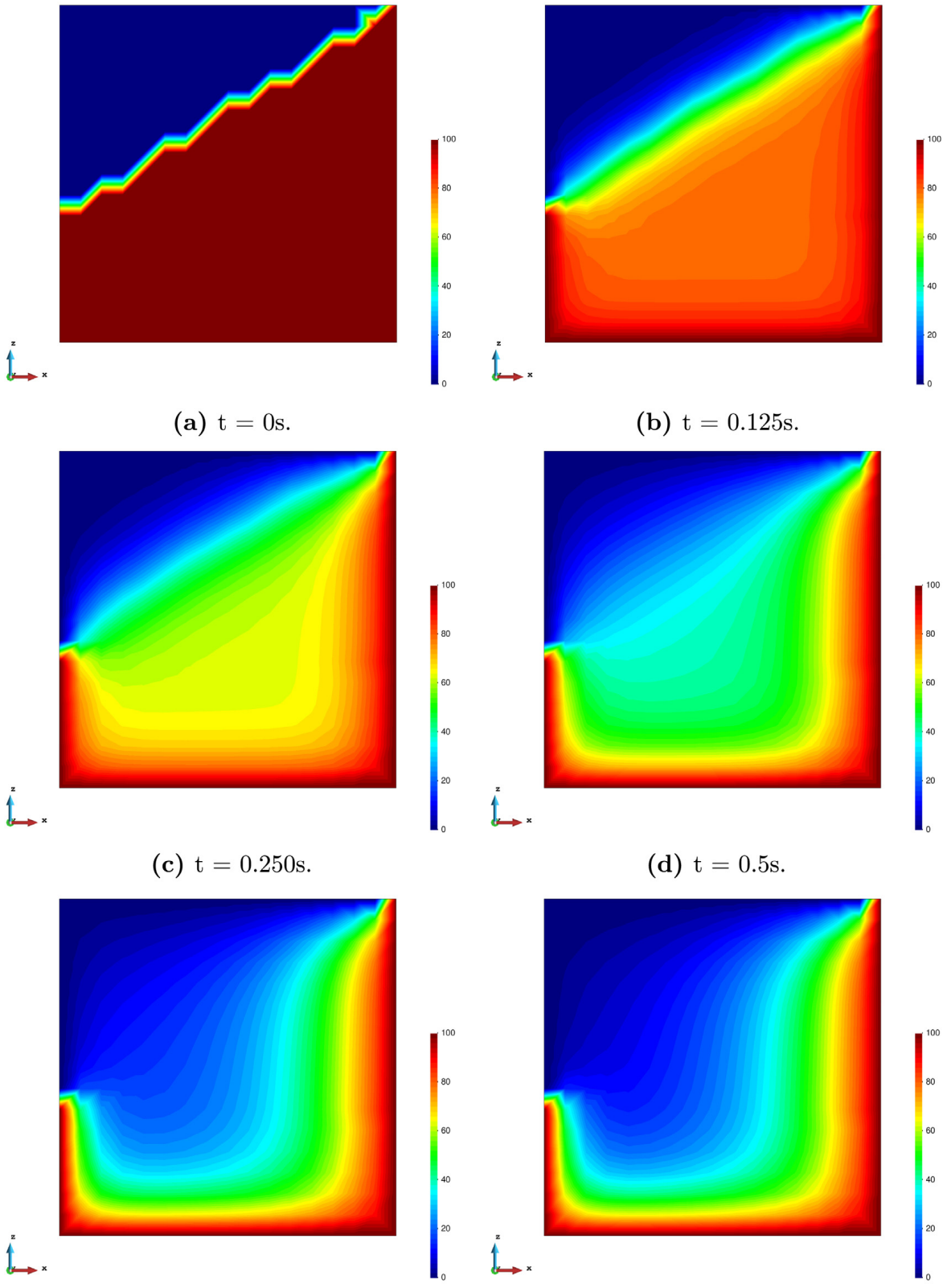

(a) t = 0s. (b) t = 0.125s.

(c) t = 0.250s. (d) t = 0.5s.

(e) t = 1s. (f) t = 2s.

Fig. 14. Transient 3D advection–diffusion–absorption evolution on a middle cut of the domain ($y = 4$).

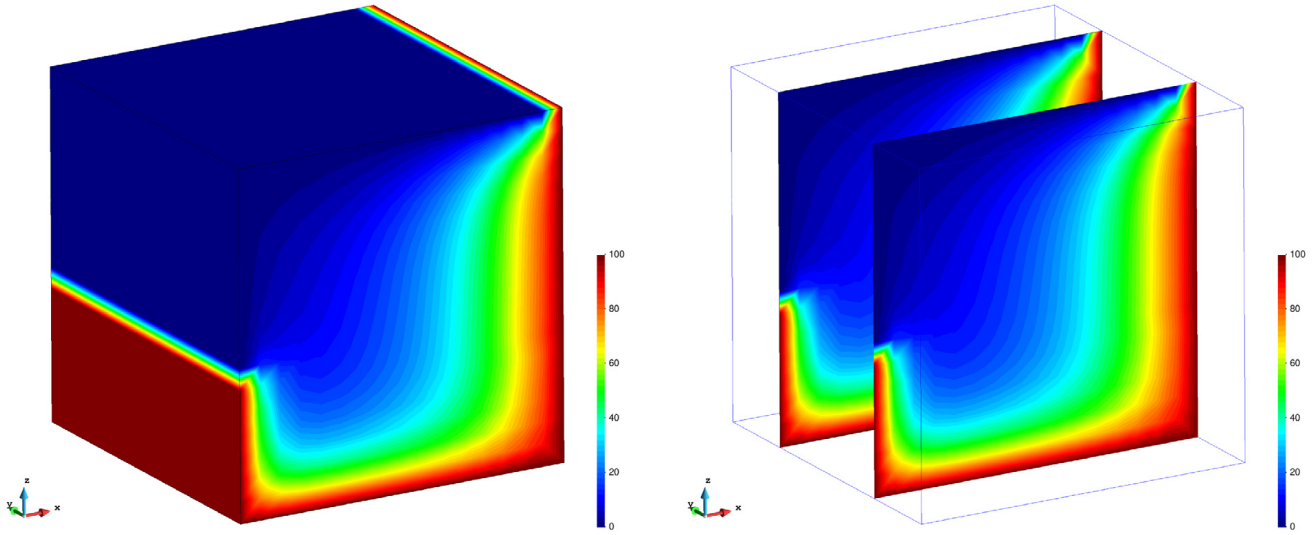

Fig. 15. Transient 3D advection–diffusion–absorption solution at $t = 2$ s: full domain and slices of it.

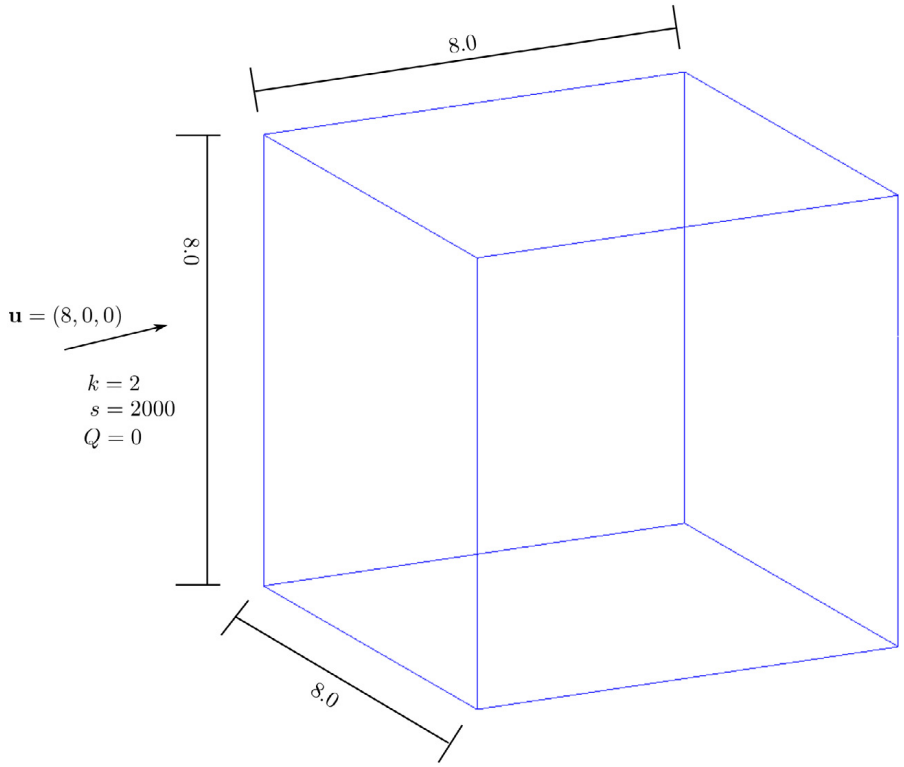

Fig. 16. Transient 3D sharp advection–diffusion–absorption problem. Cubic domain with constant velocity and zero source.

blob, or by decreasing the size of the finite element discretization. Here we have a combination of interpolation error and projection error. In this case, the mass loss error is due to the initial interpolation of the spherical shape onto the finite element mesh, which dominates all other sources of error. Note how consequently, after the first step, no significant losses are observed in Fig. 23.

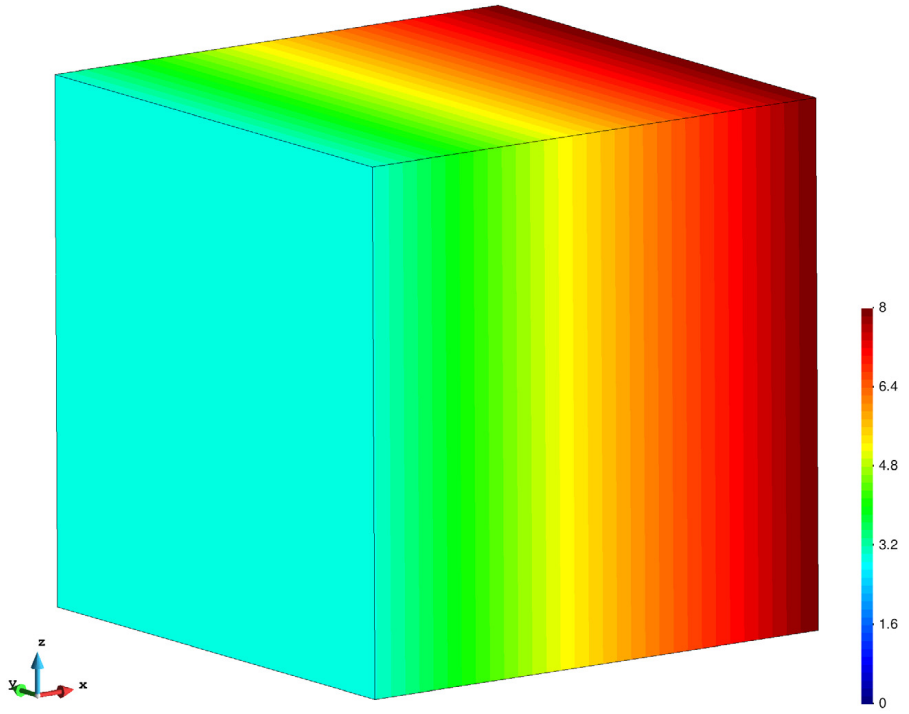

Fig. 17. Transient 3D sharp advection–diffusion–absorption problem. Cubic domain with initial conditions.

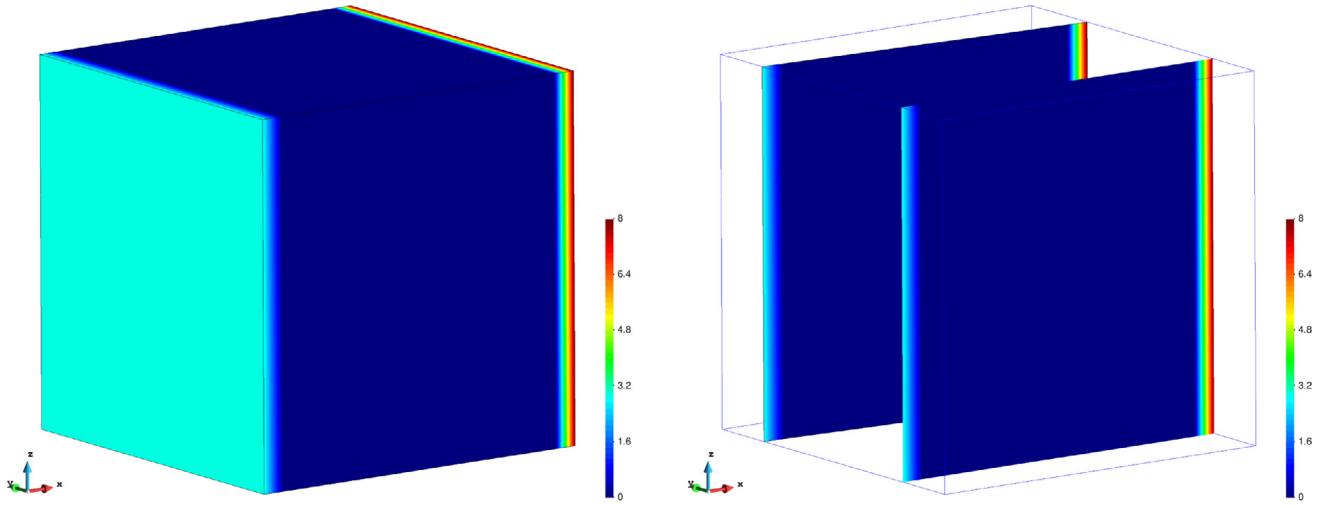

Fig. 18. Transient 3D sharp advection–diffusion–absorption solution at $t = 5e - 3s$: full domain and slices of it.

5. Concluding remarks

We have presented numerical method that combines a FIC–FEM stabilized Eulerian procedure with a semi-Lagrangian PFEM2-based approach that splits the advection–diffusion–absorption equation into a combination of a pure advective problem and a diffusive–absorptive one. The goal is the solution of advection–diffusion–absorption transport problems at high-Péclet and high-Damköhler numbers.

The presented method involves a more complex algorithm than the one in [41] but removes the non-linearity introduced by the previous stabilization. Low numerical diffusion is achieved due to the use of a Lagrangian method in the advection step. However, mass conservation in the domain is not guaranteed.

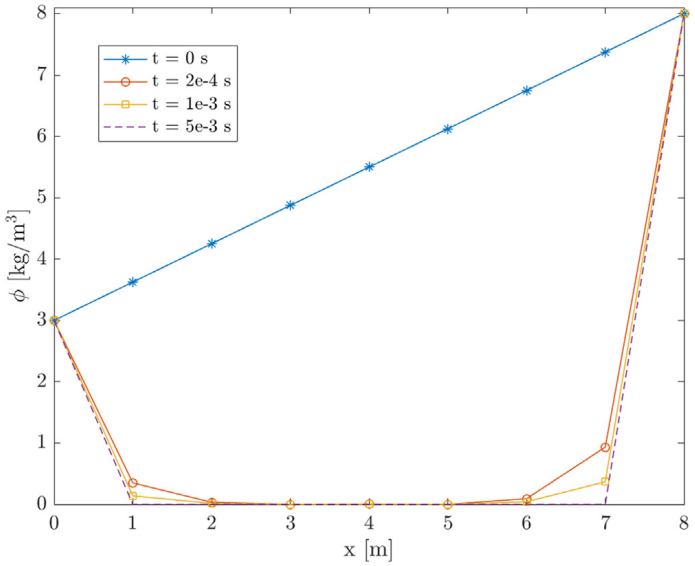

Fig. 19. Transient 3D sharp advection–diffusion–absorption problem. Concentration evolution on a middle point.

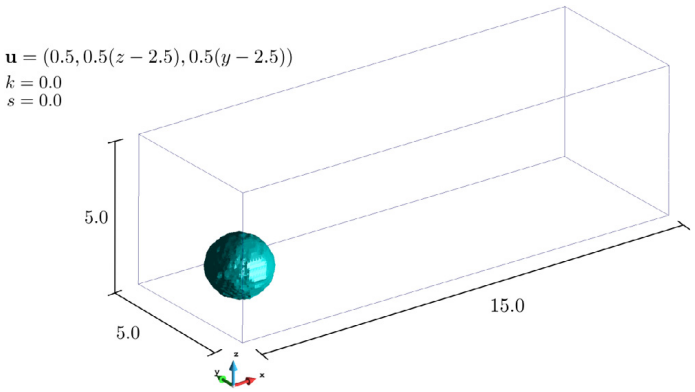

Fig. 20. Sphere advection problem set-up.

We first solved a 2D pure transport example to assess the behaviour of the mixed formulation when compared to a Eulerian one from advection-dominated cases to highly diffusive ones. The results show that, although the Eulerian base formulation behaves well for highly diffusive problems, it fails to accurately transport the heat/mass concentration in problems with high-Péclet numbers ($Pe > 5.0$) due to the high numerical diffusion introduced by the formulation. In contrast, the semi-Lagrangian approach remains accurate, without any numerical loss, even for $Pe \to \infty$.

We also have solved the transport of a sphere of heat/mass concentration and verified that the semi-Lagrangian approach is just as accurate for 3D problems.

After that, we studied three problems with higher Damköhler numbers in order to verify that the semi-Lagrangian method gives accurate and stable results for highly absorptive problems.

The first of these examples showed the benefits of the absorption stabilization in a problem where a boundary layer develops at the boundary due to the effect of absorption. Furthermore, our proposed algorithm was tested using two complex benchmarks from the literature with known analytical solutions. Its performance was satisfactory in both cases, indicating that it is a very robust method, suitable for its use for the solution of general advection–diffusion–absorption problems.

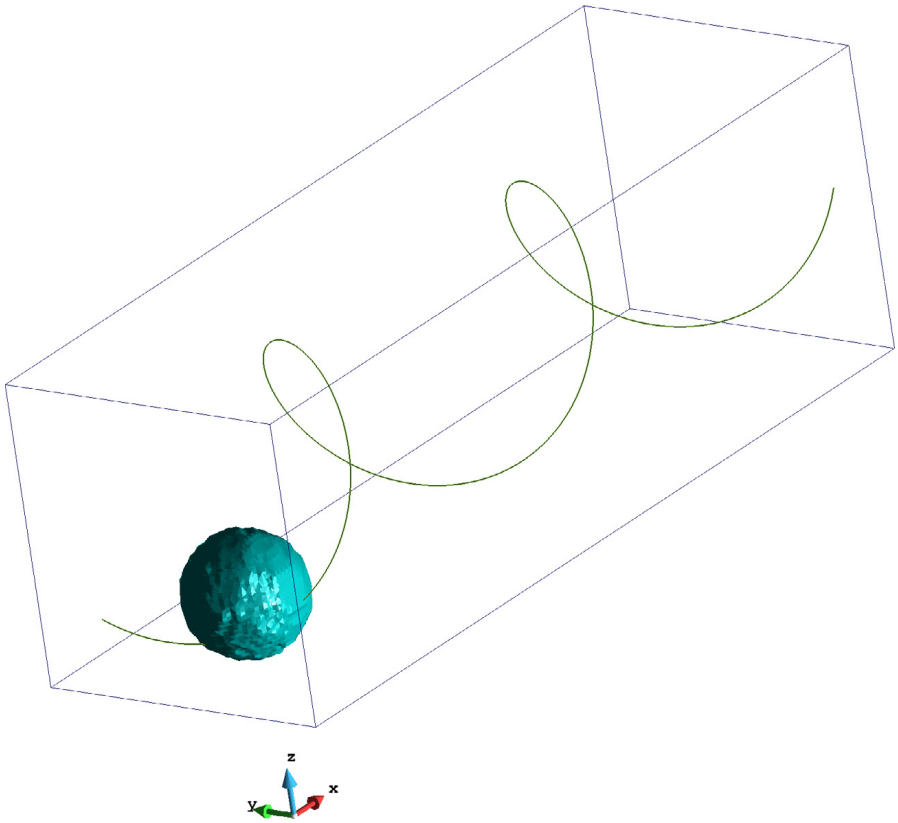

Fig. 21. Streamline that the spherical blob follows in the simulation.

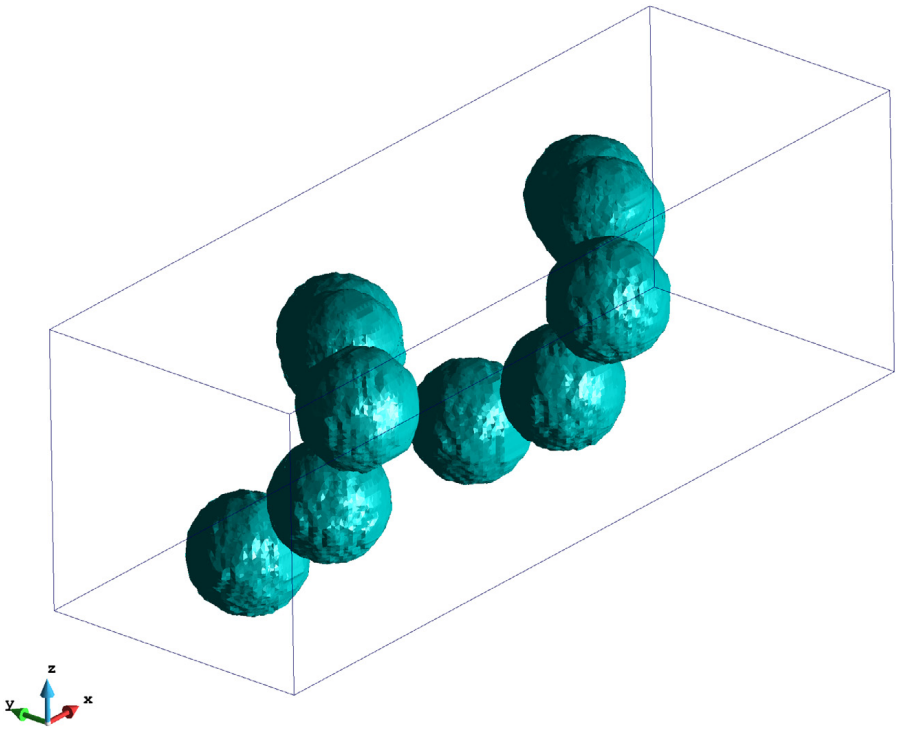

Fig. 22. 3D view of the sphere at several time steps.

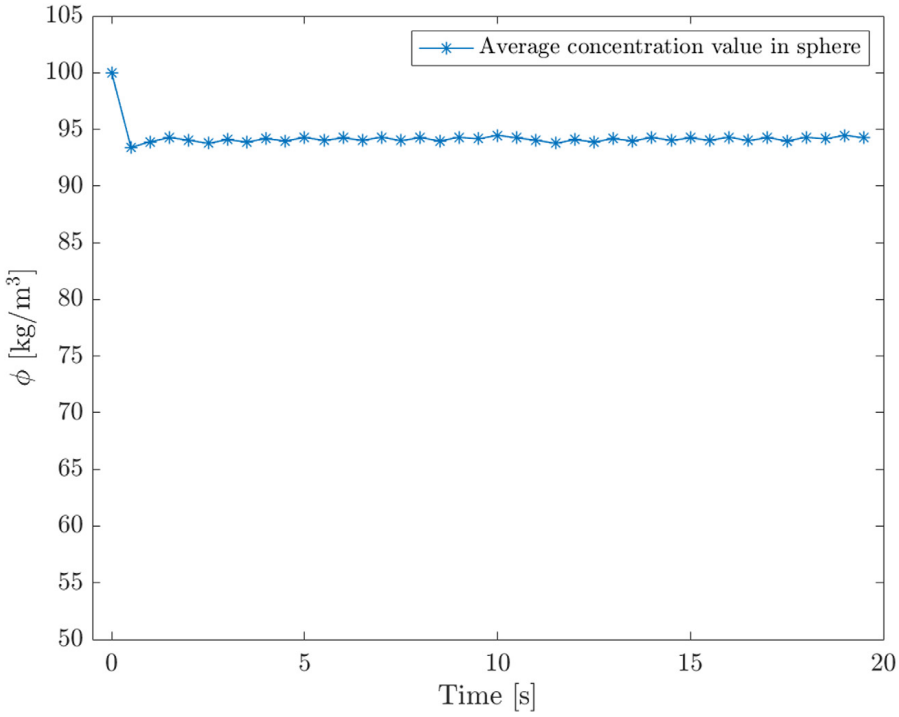

Fig. 23. 3D average of concentration values in the moving sphere at several time steps.

Declaration of competing interest

The authors declare that they have no known competing financial interests or personal relationships that could have appeared to influence the work reported in this paper.

Acknowledgements

This research was partially funded by the projects PRECISE (BIA2017-83805-R) and PARAFLUIDS (PID2019-104528RB-I00) of the Natural Research Plan of the Spanish Government. The authors also acknowledge the financial support from the CERCA programme of the Generalitat de Catalunya, Spain, and from the Spanish Ministry of Economy and Competitiveness, through the "Severo Ochoa Programme for Centres of Excellence in R&D", Spain (CEX2018-000797-S).

References

[1] J. Douglas, T.F. Russell, Numerical methods for convection-dominated diffusion problems based on combining the method of characteristics with the finite element or finite difference procedures, SIAM J. Numer. Anal. 19 (1982) 871–885.

[2] R.D. Lazarov, I.D. Mishev, P.S. Vassilevski, Finite volume methods for convection–diffusion problems, SIAM J. Numer. Anal. 33 (1) (1996) 31–55.

[3] R. Codina, Comparison of some finite element methods for solving the diffusion-convection-reaction equation, Comput. Methods Appl. Mech. Engrg. 156 (1998) 185–210.

[4] R. Codina, On stabilized finite element methods for linear systems of convection–diffusion–reaction equations, Comput. Methods Appl. Mech. Engrg. 190 (2000a) 2681–2706.

[5] L.P. Franca, F. Valentin, On an improved unusual stabilized finite element method for the advective-reactive-diffusive equation, Comput. Methods Appl. Mech. Engrg. 190 (2001) 1785–1800.

[6] I. Harari, TJR. Hughes, Stabilized finite element methods for steady advection-diffusion with production, Comput. Methods Appl. Mech. Engrg. 115 (1994) 165–191.

[7] P. Nadukandi, E. Oñate, J. García Espinosa, A high-resolution Petrov–Galerkin method for the 1D convection–diffusion-reaction problem, Comput. Methods Appl. Mech. Engrg. 199 (9–12) (2010) 525–546.

[8] P. Nadukandi, E. Oñate, J. García Espinosa, A high-resolution Petrov–Galerkin method for the convection–diffusion-reaction problem. Part II. A multidimensional extension, Comput. Methods Appl. Mech. Engrg. 213–216 (2012) 327–352.

[9] H.C. Burridge, D.A. Parker, E.S. Kruger, J.L. Partridge, P.F. Linden, Conditional sampling of a high Péclet number turbulent plume and the implications for entrainment, J. Fluid Mech. 823 (2017) 26–56.
[10] J.W. van de Meent, I. Tuval, R.E. Goldstein, Nature's microfluidic transporter: rotational cytoplasmic streaming at high Péclet numbers, Phys. Rev. Lett. 101 (17) (2008) 178102.
[11] E. Lee, K.Y. Huh, Zone conditional modeling of premixed turbulent flames at a high Damköhler number, Combustion and flame 138 (3) (2004) 211–224.
[12] A.N. Brooks, TJR. Hughes, Streamline upwind/Petrov–Galerkin formulations for the convective dominated flows with particular emphasis on the incompressible Navier–Stokes equations, Comput. Methods Appl. Mech. Engrg. 32 (1–3) (1982) 199–259.
[13] T.J.R. Hughes, A.N. Brooks, A theoretical framework for Petrov–Galerkin methods, with discontinuous weighting functions: application to the streamline upwind procedure, in: R.H. Gallagher, D.M. Norrie, J.T. Oden, O.C. Zienkiewicz (Eds.), Finite Elements in Fluids, IV, Wiley, Chichester, 1982.
[14] F. Kikuchi, T. Ushijima, Theoretical analysis of some finite element schemes for convective diffusion equations, in: R. Gallagher, D. Norrie, J. Oden, O.C. Zienkiewicz (Eds.), Finite Elements in Fluids, IV, John Wiley and Sons Ltd, Chichester, 1982.
[15] E. Oñate, P. Nadukandi, J. Miquel, Accurate FIC-FEM formulation for the multidimensional steady-state advection–diffusion–absorption equation, Comput. Methods Appl. Mech. Engrg. 327 (2017) 352–368.
[16] T.J.R. Hughes, M. Mallet, A new finite element formulations for computational fluid dynamics: III. The generalized streamline operator for multidimensional advective-diffusive systems, Comput. Methods Appl. Mech. Engrg. 58 (1986a) 305–328.
[17] R. Löhner, K. Morgan, O.C. Zienkiewicz, The solution of non-linear hyperbolic equation systems by the finite element method, Internat. J. Numer. Methods Fluids 4 (1984) 1043–1063.
[18] L.P. Franca, E.G. Dutra do Carmo, The Galerkin gradient least-squares method, Comput. Methods Appl. Mech. Engrg. 74 (1989) 41–54.
[19] T.J.R. Hughes, L.P. Franca, G.M. Hulbert, A new finite element formulation for computational fluid dynamics: VIII. The Galerkin/least-squares method for advective-diffusive equations, Comput. Methods Appl. Mech. Engrg. 73 (1989) 173–189.
[20] T.J.R. Hughes, G.R. Feijoo, L. Mazzei, J.B. Quincy, The variational multiscale method: a paradigm for computational mechanics, Comput. Methods Appl. Mech. Engrg. 166 (1998) 3–24.
[21] O.C. Zienkiewicz, R. Codina, A general algorithm for compressible and incompressible flows. Part I: the split, characteristic based scheme, Internat. J. Numer. Methods Fluids 20 (1995) 869–885.
[22] O.C. Zienkiewicz, R.L. Taylor, P. Nithiarasu, The Finite Element Method for Fluid Dynamics, 6th ed., Elsevier, 2005.
[23] E. Oñate, Derivation of stabilized equations for numerical solution of advective-diffusive transport and fluid flow problems, Comput. Methods Appl. Mech. Engrg. 151 (1998) 233–265.
[24] E. Oñate, A stabilized finite element method for incompressible viscous flows using a finite increment calculus formulation, Comput. Methods Appl. Mech. Engrg. 182 (3–4) (2000) 355–370.
[25] M. Chiumenti, Q. Valverde, C.A. De Saracibar, M. Cervera, A stabilized formulation for incompressible elasticity using linear displacement and pressure interpolations, Comput. Methods Appl. Mech. Engrg. 191 (46) (2002) 5253–5264.
[26] E. Oñate, R.L. Taylor, O.C. Zienkiewicz, J. Rojek, A residual correction method based on finite calculus, Eng. Comput. 20 (5/6) (2003) 629–658.
[27] E. Oñate, J. Rojek, R.L. Taylor, O.C. Zienkiewicz, Finite calculus formulation for incompressible solids using linear triangles and tetrahedra, Internat. J. Numer. Methods Engrg. 59 (11) (2004) 1473–1500.
[28] E. Oñate, S.R. Idelsohn, C. Felippa, Consistent pressure laplacian stabilization for incompressible continua via higher-order finite calculus, Internat. J. Numer. Methods Engrg. 87 (1–5) (2011) 171–195.
[29] E. Oñate, A. Franci, J.M. Carbonell, Lagrangian formulation for finite element analysis of quasi-incompressible fluids with reduced mass losses, Internat. J. Numer. Methods Fluids 74 (10) (2014) 699–731.
[30] R. Sevilla, S. Fernández-Méndez, A. Huerta, Comparison of high-order curved finite elements, Internat. J. Numer. Methods Engrg. 87 (8) (2011) 719–734.
[31] D.J. Thomson, Eulerian analysis of concentration fluctuations in dispersing plumes and puffs, Phys. Fluids 9 (8) (1997) 2349–2354.
[32] L.F. Rossi, A comparative study of Lagrangian methods using axisymmetric and deforming blobs, SIAM J. Sci. Comput. 27 (4) (2006) 1168–1180.
[33] R. Cady, S.P. Neuman, Three-dimensional adaptive Eulerian-Lagrangian finite element method for advection–dispersion, Dev. Water Sci. 36 (1988) 183–193.
[34] R. Cady, An adaptive multi-dimensional Eulerian-Lagrangian finite element method for simulating advection–dispersion, 1989.
[35] S.P. Neuman, S. Sorek, Eulerian-Lagrangian methods for advection–dispersion, Finite Elements in Water Resources (1982) 849–876.
[36] F. Ruan, D. McLaughlin, An investigation of Eulerian-Lagrangian methods for solving heterogeneous advection-dominated transport problems, Water Resour. Res. 35 (8) (1999) 2359–2373.
[37] M. Bahiraei, Studying nanoparticle distribution in nanofluids considering the effective factors on particle migration and determination of phenomenological constants by Eulerian–Lagrangian simulation, Advanced Powder Technology 26 (3) (2015) 802–810.
[38] Baptista, AEDM. Solution of Advection-Dominated Transport by Eulerian-Lagrangian Methods using the Backwards Method of Characteristics (Doctoral dissertation), Massachusetts Institute of Technology, 1987.
[39] R.W. Healy, T.F. Russell, Solution of the advection–dispersion equation in two dimensions by a finite-volume Eulerian-Lagrangian localized adjoint method, Adv. Water Resour. 21 (1) (1998) 11–26.
[40] E. Oñate, J. Miquel, P. Nadukandi, An accurate FIC-FEM formulation for the 1D advection–diffusion–reaction equation, Comput. Methods Appl. Mech. Engrg. 298 (2016) 373–406.
[41] A. Puigferrat, I. de Pouplana, E. Oñate, FIC–FEM formulation for the multidimensional transient advection–diffusion–absorption equation, Comput. Methods Appl. Mech. Engrg. 365 (2020) 112984.

[42] D.L. Young, Y.F. Wang, T.I. Eldho, Solution of the advection–diffusion equation using the Eulerian–Lagrangian boundary element method, Eng. Anal. Bound. Elem. 24 (6) (2000) 449–457.
[43] D.L. Young, C.M. Fan, C.C. Tsai, C.W. Chen, K. Murugesan, Eulerian-Lagrangian Method of Fundamental Solutions for Multi-Dimensional Advection-Diffusion Equation (Doctoral dissertation), National Taiwan University, 2006.
[44] K. Wang, H. Wang, M. Al-Lawatia, An Eulerian-Lagrangian discontinuous Galerkin method for transient advection-diffusion equations, Numer Methods Partial Differ. Equ. Int. J. 23 (6) (2007) 1343–1367.
[45] K. Wang, A uniform optimal-order estimate for an Eulerian-Lagrangian discontinuous Galerkin method for transient advection–diffusion equations, Numer. Methods Partial Differ. Equ. Int. J. 25 (1) (2009) 87–109.
[46] K. Wang, H. Wang, A uniform estimate for the MMOC for two-dimensional advection-diffusion equations, Numer. Methods Partial Differ. Equ. Int. J. 26 (5) (2010) 1054–1069.
[47] M. Al-Lawatia, An Eulerian-Lagrangian control volume scheme for two-dimensional unsteady advection-diffusion problems, Numer. Methods Partial Differential Equations 28 (5) (2012) 1481–1496.
[48] S.R. Idelsohn, N.M. Nigro, A. Limache, E. Oñate, Large time-step explicit integration method for solving problems with dominant convection, Comput. Methods Appl. Mech. Engrg. 217–220 (2012) 168–185.
[49] S. Idelsohn, E. Oñate, N. Nigro, P. Becker, J. Gimenez, Lagrangian versus Eulerian integration errors, Comput. Methods Appl. Mech. Engrg. 293 (2015) 191–206.
[50] R. Bravo, P. Ortiz, S. Idelsohn, P. Becker, Sediment transport problems by the particle finite element method (PFEM), Comput. Part. Mech. 7 (1) (2020) 139–149.
[51] J. Gimenez, N. Nigro, S. Idelsohn, Improvements to solve diffusion-dominant problems with PFEM-2, 2012.
[52] J.M. Gimenez, L.M. González, An extended validation of the last generation of particle finite element method for free surface flows, J. Comput. Phys. 284 (2015) 186–205.
[53] E. Oñate, J. Miquel, F. Zarate, Stabilized solution of the multidimensional advection-diffusion-absorption equation using linear finite elements, Comput. & Fluids 36 (2007) 92–112.
[54] E. Oñate, M. Manzan, A general procedure for deriving stabilized space–time finite element methods for advective-diffusive problems, Internat. J. Numer. Methods Fluids 31 (1999) 203–221.
[55] E. Oñate, M. Manzan, Stabilization techniques for finite element analysis of convection–diffusion problems, in: B. Sundén, G. Comini (Eds.), Computational Analysis of Convection Heat Transfer 2000, WIT Press, Southampton (UK), 2000, pp. 71–117.
[56] E. Oñate, F. Zarate, S.R. Idelsohn, Finite element formulation for the convective-diffusive problems with sharp gradients using finite calculus, Comput. Methods Appl. Mech. Engrg. 195 (2006) 1793–1825.
[57] C. Felippa, E. Oñate, Nodally exact ritz discretizations of the 1D diffusion-absorption and Helmholtz equations by variational FIC and modified equation methods, Comput. Mech. 39 (2) (2007) 91–111.
[58] E. Oñate, J. Miquel, G. Hauke, Stabilized formulation for the advection-diffusion-absorption equation using finite calculus and linear finite elements, Comput. Methods Appl. Mech. Engrg. 195 (33–36) (2006) 3926–3946.
[59] E. Oñate, A. Valls, J. García, FIC/FEM formulation with matrix stabilizing terms for incompressible flows at low and high Reynolds numbers, Comput. Mech. 38 (4–5) (2006) 440–455.
[60] E. Oñate, J. García, S.R. Idelsohn, F. Del Pin, FIC Formulations for finite element analysis of incompressible flows. Eulerian, ALE and Lagrangian approaches, Comput. Methods Appl. Mech. Engrg. 195 (23–24) (2006) 3001–3037.
[61] E. Oñate, A. Valls, J. García, Modeling incompressible flows at low and high Reynolds numbers via a finite calculus-finite element approach, J. Comput. Phys. 224 (2007) 332–351.
[62] E. Oñate, P. Nadukandi, S. Idelsohn, J. García, C. Felippa, A family of residual-based stabilized finite element methods for Stokes flows, Int. J. Num. Meth. Fluids 65 (1–3) (2011) 106–134.
[63] E. Oñate, P. Nadukandi, S. Idelsohn, P1/P0+ elements for incompressible flows with discontinuous material properties, Comput. Methods Appl. Mech. Engrg. 271 (2014) 185–209.
[64] E. Oñate, J. García, A finite element method for fluid–structure interaction with surface waves using a finite calculus formulation, Comput. Methods Appl. Mech. Engrg. 191 (2001) 635–660.
[65] E. Oñate, S.R. Idelsohn, F. Del Pin, R. Aubry, The particle finite element method. An overview, Int. J. Comput. Methods 1 (2) (2004) 267–307.
[66] E. Oñate, S.R. Idelsohn, M.A. Celigueta, R. Rossi, Advances in the particle finite element method for the analysis of fluid-multibody interaction and bed erosion in free surface flows, Comput. Methods Appl. Mech. Engrg. 197 (19–20) (2008) 1777—1800.
[67] E. Oñate, S.R. Idelsohn, C. Felippa, Consistent pressure Laplacian stabilization for incompressible continua via higher order finite calculus, Internat. J. Numer. Methods Engrg. 87 (1–5) (2011) 171—195.
[68] E. Oñate, S.R. Idelsohn, O.C. Zienkiewicz, R.L. Taylor, C. Sacco, A stabilized finite point method for analysis of fluid mechanics problems, Comput. Methods Appl. Mech. Engrg. 139 (1996) 315–346.
[69] E. Oñate, S.R. Idelsohn, A mesh-free finite point method for advective-diffusive transport and fluid flow problems, Comput. Mech. 23 (1998) 283–292.
[70] E. Oñate, C. Sacco, S.R. Idelsohn, A finite point method for incompressible flow problems, Comput. Vis. Sci. 2 (2000) 67–75.
[71] E. Oñate, F. Perazzo, J. Miquel, A finite point method for elasticity problems, Comput. Struct. 79 (2001) 2151–2163.
[72] J. Donea, A taylor-Galerkin method for convective transport problems, Internat. J. Numer. Methods Engrg. 20 (1984) 101–119.
[73] O.C. Zienkiewicz, R.L. Taylor, J.Z. Zhu, The Finite Element Method. the Basis, 6th ed., Elsevier, 2005.
[74] S. Idelsohn, N. Nigro, J. Gimenez, R. Rossi, J. Marti, A fast and accurate method to solve the incompressible Navier–Stokes equations, Eng. Comput. Int. J. Comput. Aided Eng. 30 (2013) 197–222.
[75] S.R. Idelsohn, J. Marti, P. Becker, E. Oñate, Analysis of multifluid flows with large time steps using the particle finite element method, Internat. J. Numer. Methods Engrg. 75 (2014) 621–644.

[76] Nepf H. 1.061 / 1.61 Transport Processes in the Environment. Massachusetts Institute of Technology: MIT OpenCourseWare https://ocw.mit.edu/License: Creative Commons BY-NC-SA.

[77] H.Y. Duan, P.W. Hsieh, R.C. Tan, S.Y. Yang, Analysis of a new stabilized finite element method for the reaction–convection–diffusion equations with a large reaction coefficient, Comput. Methods Appl. Mech. Engrg. 247 (2012) 15–36.

[78] H.Y. Duan, F. Qiu, A new stabilized finite element method for advection-diffusion-reaction equations, Numer. Methods Partial Differential Equations 32 (2) (2016) 616–645.

Chapter 4

Numerical prediction of the distribution of black carbon in a street canyon using a semi-Lagrangian finite element formulation

4.1 Article data

Title: Numerical prediction of the distribution of black carbon in a street canyon using a semi-Lagrangian finite element formulation.

Authors: A. Puigferrat, I. de-Pouplana, F. Amato and E. Oñate

Journal: Building and Environment (2021) 107910

Received: 17 July 2020 / Accepted: 13 March 2021 / Available online: 31 March 2021

DOI: 10.1016/j.buildenv.2021.107910

4.2 Introduction

The objective of this section of the thesis is to bring the procedure implemented in the previous chapters to the practical field. To do this, a coupling method for the fluid and the transport equations has been developed. The coupling algorithm has been validated

using an academic study and a practical case. This chapter describes the coupling strategy as well as the results obtained when the method has been applied to a practical situation.

The academic study is shown in Appendix A. The evolution of the velocity vectors and the distribution of an inert pollutant in a street canyon with a height / width ratio of 1 has been seen. The results have been compared with those obtained in [49, 100] among others with good agreement.

The attached paper describes the coupling strategy developed and its application to the transport of black carbon (BC) in a street canyon. More specifically the content of the paper is organized as follows. First, the general procedure for coupling the fluid and transport equations is introduced. Next, the overall solution strategy for the flow and transport equations is outlined. Details of the fluid flow solution using the stabilized FEM and the solution of the transport problem using the semi-Lagrangian method are given. In the last part of the paper, the coupled formulation is applied to the prediction of the transport of BC in a street canyon in Barcelona. First, a simulation in 2D with good results is presented. Then a 3D simulation, which corresponds to a 2D extrusion, is shown to demonstrate that three-dimensional phenomena are captured correctly with the proposed semi-Lagrangian formulation.

4.3 Scientific contribution

Having validated the semi-Lagrangian formulation in Chapter 3, the last part of the thesis' work has focussed on the development and validation of a procedure for coupling the fluid and transport equations. The coupled formulation has been used to model the distribution of a pollutant in a street in Barcelona.

The presented method implies coupling the equations for advection-diffusion-absorption transport of a substance with those of a fluid (the air), accounting for temperature effects in the flow. For the numerical solution of the fluid flow problem, we have used standard stabilized FEM procedures. More specifically, the Quasi-Static Variational Multiscale (QS-VMS) technique has been used for the numerical solution of the fluid equations with the FEM. This residual-based stabilization procedures allows the modelling of high gradients in the fluid flow (such as those induced by turbulence) in a simple and

effective way [19, 20]. Thermal effects in the flow have been modelled via the Boussinesq assumption. A one-way coupling of the thermal and flow effects has been considered in this research work.

The air velocities obtained in the fluid flow problem are used as input data for solving the transport of both the temperature and the pollution substances in air using the semi-Lagrangian procedure explained in Chapter 3.

We note that the transport of substances in turbulent air flows can be a computationally intense problem, especially when the domain of analysis is of large dimensions.

After the implementation of the coupling between the fluid flow for the air and the transport equations for the substances, several examples of transport of a pollutant in air have been run to show the capability of the model for solving practical problems. A problem chosen in the thesis is the air transport of a pollutant (black carbon) in a street canyon. Experimental results for this problem are available [2] and have been used to validate the numerical methods developed in the thesis.

The good results obtained in the validation examples have demonstrated the accuracy and applicability of the numerical methods developed in the thesis for solving problems related to the transport of pollutants in fluids and, more specifically, air pollution transport problems in urban environments.

Building and Environment 199 (2021) 107910

Contents lists available at ScienceDirect

Building and Environment

journal homepage: www.elsevier.com/locate/buildenv

Numerical prediction of the distribution of black carbon in a street canyon using a semi-Lagrangian finite element formulation

Albert Puigferrat [a], Ignasi de-Pouplana [a,b], Fulvio Amato [c], Eugenio Oñate [a,b,*]

[a] Centre Internacional de Mètodes Numèrics en Enginyeria CIMNE, Barcelona, Spain
[b] Universitat Politècnica de Catalunya (UPC), Barcelona, Spain
[c] Institute of Environmental Assessment and Water Research (IDAEA), Spanish Research Council (CSIC), Barcelona, Spain

ARTICLE INFO

Keywords:
Convective transport
Convection–diffusion–reaction
Transient
Finite element method
FIC
PFEM
Eulerian
Lagrangian

ABSTRACT

We present a procedure for coupling the fluid and transport equations to model the distribution of a pollutant in a street canyon, in this case, black carbon (BC). The fluid flow is calculated with a stabilized finite element method using the Quasi-Static Variational Multiscale (QS-VMS) technique. For the temperature and pollutant transport we use a semi-Lagrangian procedure, based on the Particle Finite Element Method (PFEM) combined with an Eulerian method based on a Finite Increment Calculus (FIC) formulation. Both methods are implemented on the open-source KRATOS Multiphysics platform. The coupled numerical formulation is applied to the prediction of the transport of BC in a street canyon, which can be a useful tool to lessen the impact of pollutants on pedestrians. Two test cases have been studied: a 2D simplified case and a more complex 3D one. The main goal of this study is to propose a useful tool to study the effect of pollution on pedestrians in a street-level scale. Good comparison with experimental results is obtained.

1. Introduction

Outdoor air pollution is linked to an estimated 4.2 million premature deaths worldwide every year [1]. Over 80% of people living in urban areas are exposed to levels of pollution above the limits established by the World Health Organization [2].

The growing concern to improve sustainability and air quality in urban areas has made numerical prediction of pollution transport increasingly important in deciding how to build and design these areas. Knowing how a pollutant is distributed in a street canyon over hours, days or months will help to design or re-think the streets so that pedestrians, terraces and windows suffer the least possible impact from city pollution [3,4].

One of the main pollutants in the air is the fine particle matter ($PM_{2.5}$) which measures less than 2.5 micrometres. More specifically, black carbon (BC) is a fraction of $PM_{2.5}$ closely related to traffic emissions and linked to adverse health effects. Several studies show that BC causes tissue irritation and the release of toxic chemical intermediates from scavenger cells. Soot particles also act as carriers for the organic compounds that can be allergens, mutagens, or carcinogens [5].

The formation of urban airflows in a street canyon is essential for human health as well as for the thermal comfort of the different buildings and their efficiency. The distribution of these buildings, as well as their geometry, can vary the temperature within the street canyon up to around 1 °C [6,7]. These temperature changes and the wind highly affect the natural ventilation that occurs within the street canyon, influencing, this way, the concentration of pollutants in air [6,7]. The street temperature, which is generally higher than the ambient temperature due to the sunlight and the traffic on it, creates buoyancy effects that modify the velocity field within the street canyon and, therefore, affects the distribution of the pollutants [8–10].

Traffic emissions are one of the most important sources of pollution in cities where streets are narrow and the configuration of the buildings create street canyons in which pollutants accumulate. The accurate prediction of the transport of these pollutants is basic for the design of solutions to minimize the exposure of citizens to traffic pollution.

The numerical prediction of the distribution of a pollutant in a street canyon is an important and complex environmental problem, as well as an architectural one. The transport of pollutant particles in air has been studied by several authors [8,9,11,12]. In these kind of problems microscale – that is the street scale – processes dominate the solution [13].

Pollutants come mainly from the exhaust pipes of the vehicles moving on the street and are dispersed through air by means of advection, diffusion and absorption. There are different factors to consider in predicting these effects. First, the temperature of the facades of buildings and the street cause thermal effects that affect the wind

* Corresponding author at: Centre Internacional de Mètodes Numèrics en Enginyeria CIMNE, Barcelona, Spain.
E-mail address: onate@cimne.upc.edu (E. Oñate).

https://doi.org/10.1016/j.buildenv.2021.107910
Received 26 January 2021; Received in revised form 16 April 2021; Accepted 17 April 2021
Available online 24 April 2021
0360-1323/© 2021 Elsevier Ltd. All rights reserved.

Nomenclature

α	Thermal expansion coefficient
$\dot{\boldsymbol{u}}_s$	Small scale acceleration
$\boldsymbol{\sigma}$	Stress tensor
$\boldsymbol{f}$	External forces acting on the domain
$\boldsymbol{g}'$	Reduced gravity
$\boldsymbol{g}$	Gravity
$\boldsymbol{n}$	Domain outer vector
$\boldsymbol{t}$	Prescribed surface traction
$\boldsymbol{u}$	Velocity vector
$\boldsymbol{u}_0$	Initial velocity
$\boldsymbol{u}_D$	Imposed velocity
Γ_D	Dirichlet boundary
Γ_N	Neumann boundary
μ	Dynamic viscosity of air
Ω	Domain of area/volume
ϕ	Transported variable
ϕ^p	Prescribed transported variable
ϕ_0	Initial value of the transported variable
ϕ_p	Transported variable on the particle
$\rho\boldsymbol{g}$	Gravitational body force
ρ	Air density
τ_p	Pressure stabilization parameter
τ_u	Velocity stabilization parameter
C	Courant number
c	Specific flux parameter
err_i	Relative error
h	Characteristic length
H/W	Height-to-width ratio
k_i	Thermal conductivity in the ith space direction
q^p	Outgoing diffusive flux
s	Reaction parameter
T	Temperature
t_0	Initial value of time
T_{amb}	Ambient temperature
D	Diagonal thermal conductivity matrix
BC	Black Carbon
D	Diffusivity
DNS	Direct Numerical Simulation
FEM	Finite Element Method
FIC	Finite Increment Calculus
l	Mesh size
LES	Large Eddy Simulation
MAPE	Mean Absolute Percentage Error
PFEM	Particle Finite Element Method
PFEM2	Particle Finite Element Method - second generation
$PM_{2.5}$	Fine Particle Matter
Q-ASGS	Quasi-Static Algebraic Sub-Grid Scales
QS-VMS	Quasi-Static Variational Multi- scale
R	Absorption
RANS	Reynolds-Averaged Numerical simulations
VMS	Variational Multiscale
$\hat{x}_i\|_{sim}$	Simulated value at each point
$\hat{x}_i\|_{exp}$	Experimental value at each point

speed field [14]. Secondly, the importance of thermal effects versus the diffusivity induced by air turbulence must be studied. The relationship between thermal effects and turbulence is taken into account by the Richardson's number [8,15]. The wind speed and its direction plays an important role in the dispersion of a pollutant. Finally, the mathematical and computational models used are an important decision when simulating these processes.

Various mathematical models have been used in the past to study air quality in urban areas and can be classified in three main family models: Gaussian, Lagrangian and Eulerian dispersion models. Gaussian parametrical models are based on the well known analytical solution for the Gaussian plume distribution [16] and they provide reliable results at the mesoscale. Gaussian models include AERMOD [17], CTDM [18] and ADMS [19–21], among others. AERMOD is a steady-state dispersion model developed by the US Environmental Protection Agency (EPA) and is generally used to simulate plumes in the mesoscale. The EPA also developed the Complex Terrain Dispersion Model (CTDM), which is able to get rid of the simulation cost of the mesoscale wind computation. ADMS is a British atmospheric dispersion modelling system which can take into account different locations (urban, coastal or mountain areas) and is able to calculate the interaction of several plumes in an urban area accounting for chemical processes. Since Gaussian plume models are not based on the fluid mechanics equations, they do not provide accurate results for more complex problems [22]. Also, they provide poor results in situations in which the Péclet number is low i.e. diffusive dominant [23] and they cannot account for chemical reactions [24]. As the geometry gets more complex at the microscale range, other models based on the numerical solution of the fluid flow equations at the street level have appeared.

Lagrangian and Eulerian methods are generally used for smaller scale numerical simulations. Eulerian methods aim to solve the fluid transport equations in a fixed reference frame. The Micro Scale Air Pollution Model (MISCAM) [25], for instance, is an Eulerian model used to study dispersion of pollutants in dense urban areas. GEOS-Chem is an Eulerian model which can be used to solve mixing of chemical components in the atmosphere at a regional scale [26]. Another Eulerian modelling system is the WRF-Chem, which takes into account chemical reactions, turbulence, emissions and the meteorological data at urban and regional scales [27]. The Community Multi-scale Air Quality (CMAQ) is yet another model used to predict air quality simulations at urban and regional scales [28]. Although these models work on various scales, most of them focus on larger domains than the microscale. Lagrangian methods, on the other hand, transport a property using single point particles, which simplifies and reduces numerical diffusion in advection-dominant processes, many times at the expense of increasing the computational cost. They are used primarily for long-range calculations. Two examples of Lagrangian methods are the NAME and the FLEXPART models, used in smoke tracking and epidemic situations [29,30].

A more extensive classification of dispersion models can be found in [31].

In this work we first calculate the turbulent fluid equations using a stabilized Eulerian Finite Element Method (FEM) based on a Quasi-Static Variational Multiscale (QS-VMS) procedure [32]. This method decomposes the variables into a large and a small scale and resembles a Large Eddy Simulation (LES) procedure. Then the calculated velocity field is exported to an Eulerian–Lagrangian split formulation, termed here *semi-Lagrangian formulation*, for solving the temperature evolution and the pollution transport problems accounting for advection–diffusion–absorption effects. The resulting coupled numerical procedure leads to accurate and stable results [33]. The Lagrangian part of the pollution transport solution (i.e. the advective part) is

based on the Particle Finite Element Method — second generation (PFEM2) [34,35]. For the solution of the Eulerian diffusion–absorption transport equation, we use a stabilized FEM using a Finite Increment Calculus (FIC) procedure recently developed by the authors [36–38]. The semi-Lagrangian approach therefore benefits from the best features of a combined Eulerian and Lagrangian FEM-type formulation: low numerical diffusion is achieved thanks to the use of a Lagrangian method in the advection step and the formulation only needs absorption stabilization. Thus, this method has proven to be accurate for solving the transport equation, particularly in high-Péclet cases, which are the ones we want to tackle [33].

The paper is organized as follows. First, the general procedure for coupling the fluid and transport equations is introduced. Next, the overall solution strategy for the flow and transport equations is outlined. Details of the fluid flow solution using the stabilized FEM and the solution of the transport problem using the semi-Lagrangian method are given. In the last part of the paper, the coupled formulation is applied to the prediction of the transport of an inert tracer (black carbon) in a street canyon in Barcelona. Good results are obtained in agreement with experimental data.

2. Modelling and simulation of air pollution transport

When simulating the movement in air of an inert tracer in a street canyon, one must take into account the different phenomena that occur in the transport of this tracer. This tracer is transported in several ways, namely due to advection, diffusion and absorption effects. Chemical reaction effects are neglected in this work, as black carbon is an inert pollutant. Depending on the conditions, the tracer will be forced by the air buoyancy caused by the temperature difference [8,10], or turbulent diffusivity will prevail over the other effects. Turbulent diffusivity is due to the eddy motion of a fluid. It is a parametrization of the diffusion that appears from fluid turbulence at that scale [9,39–41].

While a uniform fluid transports a scalar without any distortion, a non-uniform fluid can produce important effects on transport. The cause of this change between both types of fluid is the differential advection: as soon as a fluid presents turbulence, it brings parts of the fluid close to others with different concentrations of pollutant. This causes concentration gradients to intensify and induces additional diffusion [40].

In the case of a direct numerical simulation (DNS), in which the Navier–Stokes equations are solved without any turbulent model [42], all ranges of turbulence, whether spatial or temporal, are computed. In the case of the Reynolds-Averaged Numerical simulations (RANS), on the other hand, the turbulence is fully modelled. The kinetic energy modelled with the RANS procedure is much higher than the kinetic energy modelled by a Large Eddy Simulation (LES) method. The DNS procedure needs no additional terms to be added in the transport equation. However, for RANS modelling, additional turbulent diffusivity is required to be considered in the transport equation as all turbulent effects are modelled [43].

Given the previous considerations, the approach followed in this paper uses a Quasi-Static Variational Multiscale model to gauge the velocity field in which the sub-grid turbulence is calculated with a Quasi-Static Algebraic Sub-grid Scales formulation [44]. This model provides very accurate results without the need of the mesh resolution of DNS. The QS-VMS and the semi-Lagrangian formulation are implemented on the open-source platform KRATOS Multiphysics, which allows an easy coupling. Thermal effects due to buoyancy have been taken into account in the flow using the Boussinesq approximation [45]. The velocity, thus, is affected by the difference of temperature given by the ambient temperature and the street one. In this work we have not considered addition of a turbulent diffusivity in the BC transport equation [12,43,46].

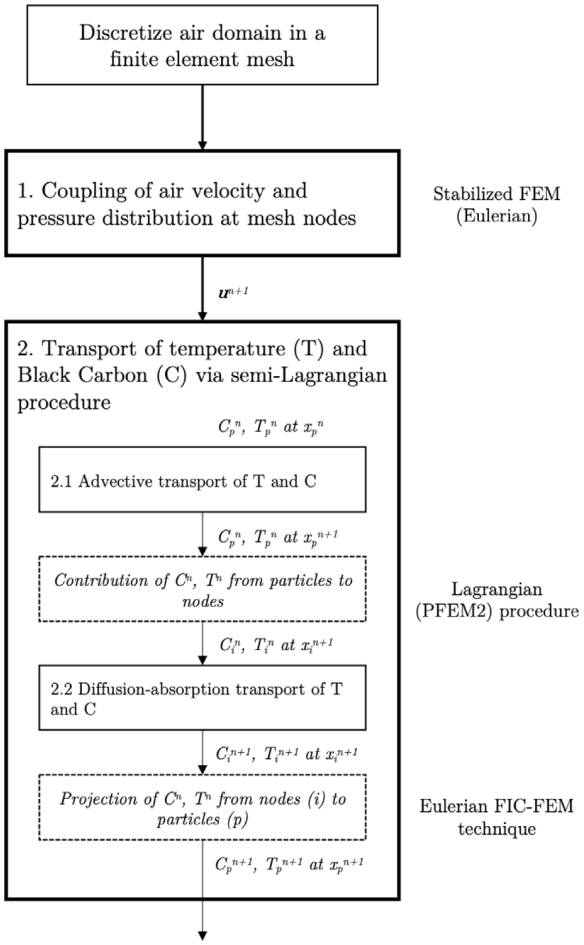

Fig. 1. Flowchart for the numerical solution strategy.

3. Numerical solution strategy

Fig. 1 shows a flowchart of the numerical solution strategy used for solving the transport of an inert substance, such as BC, in an air flow accounting for temperature effects.

The first step is the discretization of the air domain in a mesh of finite elements. In our work we use standard three-noded linear triangles and four-noded linear tetrahedra for 2D and 3D problems, respectively. Then the boundary and inlet conditions for the air flow, the temperature and the transported BC field are imposed.

Starting from a known initial field at time $t = t^n$ of velocity and pressure in the air and the distribution of temperature and BC in the air domain, the following computations are performed.

The velocity and pressure fields in the air at time t^{n+1} are computed using a stabilized Eulerian FEM based on a VMS formulation. The temperature field in the air is assumed to be constant during the air flow computations.

The air velocities obtained at time t^{n+1} are used for computing the distribution of temperature and BC at t^{n+1} using a semi-Lagrangian method. This is based on the advection of the transported variables using a particle-based Lagrangian technique (the PFEM2). The computation of the diffusion and absorption effects is carried out using a stabilized FEM based on a Finite Calculus procedure. Both the advection and diffusion–absorption steps are performed in the same fixed mesh used for the air flow computations.

Details of the different steps for computing the air flow and transported variables (temperature and BC) are given in the next section.

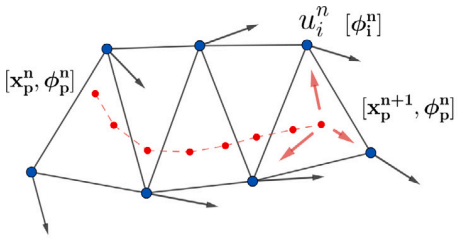

(a) **Step 1:** Advection step using particles (in red). **Step 2:** The particles' information is transferred to the mesh nodes (in blue)

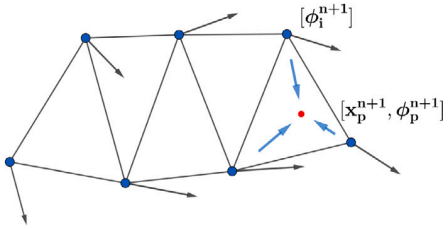

(b) **Step 3:** Diffusion-absorption step. **Step 4:** Contribution of the finite element nodes to the particles.

Fig. 2. Main steps of the semi-Lagrangian procedure.

Fig. 3. Satellite and map of the studied region (in red) and neighbourhood.

4. Governing equations

4.1. Air flow equations

Air motion is described by the incompressible Navier–Stokes equations. They state the balance of linear momentum (1) and the mass balance (2) in the air domain Ω as

$$\rho\partial_t \boldsymbol{u} + \rho\boldsymbol{u}\cdot\nabla\boldsymbol{u} - \nabla\cdot\boldsymbol{\sigma} = \boldsymbol{f} \qquad \text{in } \Omega\times[0,T) \tag{1}$$

$$\nabla\cdot\boldsymbol{u} = 0 \qquad \text{in } \Omega\times[0,T) \tag{2}$$

where ρ is the air density, $\boldsymbol{u}$ is the velocity vector, $\boldsymbol{\sigma}$ is the stress tensor and $\boldsymbol{f}$ contains any external force acting on the domain, such as the gravitational body force $\rho\boldsymbol{g}$.

The effect of temperature variations on the air is accounted for via the Boussinesq approximation [47]. It states that the density variation only affects the buoyancy term, i.e. in the body force term $\rho\boldsymbol{g}$. Consequently, Eqs. (1) and (2) are solved using a constant density ρ and replacing the gravity $\boldsymbol{g}$ by a reduced gravity $\boldsymbol{g}'$ as

$$\boldsymbol{g}' = \boldsymbol{g}\left[1 - \alpha\left(T - T_{amb}\right)\right] \tag{3}$$

where α is the coefficient of thermal expansion, T is the temperature at any point in the domain, and T_{amb} is the ambient temperature. The coefficient of thermal expansion has been taken as $\alpha = 1/T_{amb}$, the definition for ideal gases. In this work the temperature is assumed to be constant during the computation of the air velocity and pressure fields within each time step.

The stress tensor $\boldsymbol{\sigma}$ for Newtonian fluids reads

$$\boldsymbol{\sigma} = -p\mathbf{1} + 2\mu\left[\nabla^s\boldsymbol{u} - \frac{1}{3}(\nabla\cdot\boldsymbol{u})\mathbf{1}\right] \tag{4}$$

with $\mathbf{1}$ being the second order identity tensor, μ is the dynamic viscosity of the air, and where $\nabla^s\boldsymbol{u}$ is the symmetric gradient of the velocity.

The Navier–Stokes equations are completed with suitable initial and boundary conditions, namely,

$$\boldsymbol{u} = \boldsymbol{u}_0 \qquad \text{in } \Omega\times[0] \tag{5}$$

$$\boldsymbol{u} = \boldsymbol{u}_D \qquad \text{on } \Gamma_D\times[0,T) \tag{6}$$

$$\boldsymbol{\sigma}\cdot\boldsymbol{n} = \boldsymbol{t} \qquad \text{on } \Gamma_N\times[0,T) \tag{7}$$

where $\boldsymbol{u}_0$ is the initial velocity, $\boldsymbol{u}_D$ is the velocity imposed on the Dirichlet boundary Γ_D, $\boldsymbol{n}$ is the outer normal vector to the analysis domain and $\boldsymbol{t}$ is the prescribed surface traction acting on the Neumann boundary Γ_N.

4.2. Temperature and pollutant transport equations

The transport balance equation in a domain of area/volume Ω is expressed in a Lagrangian frame as

$$r_t = 0 \quad \text{in } \Omega \tag{8a}$$

with

$$r_t := \rho c\frac{D\phi}{Dt} - \boldsymbol{\nabla}^T\mathbf{D}\boldsymbol{\nabla}\phi + s\phi - Q = 0 \tag{8b}$$

$$\frac{D\mathbf{x}}{Dt} = \mathbf{u} \tag{8c}$$

In Eq. (8), ϕ is the transported variable (i.e., the BC in the problem considered in this work), u_i is the ith cartesian component of the velocity vector $\mathbf{u}$; ρ, c and s are the density, the specific flux parameter, the reaction parameter, respectively, and $\mathbf{D}$ is a diagonal thermal conductivity matrix with $D_{ii} = k_i$, with k_i being the thermal conductivity in

Fig. 4. AE-51 micro-aethalometers (Aethlabs) used for BC measurements [48].

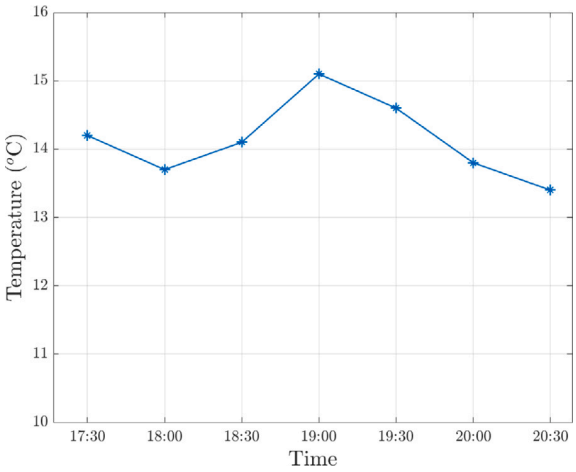

Fig. 5. Temperature in a nearby station in the studied period of time [49].

the ith space direction. In the following, and unless otherwise specified, we will assume that the problem parameters (ρ, c, k_i, s) are constant over the analysis domain Ω. In our work we define D = k/(ρc) as the diffusivity, and R = s/(ρc) as the absorption. These parameters depend on the transported variable and are chosen according to its nature. For instance, in a mass transport problem we would say carbon dioxide in air has a mass diffusivity (D) of 16 mm^2/s.

The time derivative in Eq. (8b) is the total derivative which is computed as $\frac{D\phi}{Dt} = \frac{\phi^{n+1}-\phi^n}{\Delta t}$, as typically done in Lagrangian schemes.

Eq. (8c) defines the velocity field in the Lagrangian frame. This equation is used for computing the trajectory of a set of particles representing the temperature and pollutant fields in the air domain following the air streamlines.

The boundary conditions of the aforementioned equations are

$$\phi - \phi^p = 0 \quad \text{on } \Gamma_D \tag{9a}$$

$$r_\Gamma = 0 \quad \text{on } \Gamma_N \tag{9b}$$

with

$$r_\Gamma := -q_n + q_n^p \tag{9c}$$

where

$$q_n = \mathbf{q}^T \mathbf{n} \quad , \quad \mathbf{q} = -\mathbf{D}\nabla\phi \tag{10}$$

In Eqs. (9) and (10), ϕ^p and q^p are the prescribed boundary fields of the transported variable and the outgoing diffusive flux at the Dirichlet and Neumann boundaries Γ_D and Γ_N of the analysed domain, respectively, and $\mathbf{n}$ its exterior unit normal. Eq. (9b) allows us to impose a face heat flux on the street surface.

The definition of the problem is completed with the initial conditions

$$\phi(\mathbf{x}, t_0) = \phi_0(\mathbf{x}) \tag{11}$$

where ϕ_0 is a known field at time t_0.

5. Air flow solution using a stabilized FEM formulation

The solution for the velocity and pressure fields in the air is coupled using a stabilized Eulerian FEM. Among the different choices for stabilized FEM we have chosen in this work a Variational Multiscale (VMS) approach.

The VMS technique [50,51] has been widely used to stabilize finite element formulations in fluid dynamics [52,53] and in solid mechanics [54,55]. The method is based on the hypothesis that the velocity and pressure fields can be separated into two different components: one for the large scale $(\cdot)_h$, and the other for the small scale $(\cdot)_s$, also referred as subscale as

$$\boldsymbol{u} = \boldsymbol{u}_h + \boldsymbol{u}_s \tag{12}$$

$$p = p_h + p_s \tag{13}$$

The large scale $(\cdot)_h$ corresponds to the part of the solution that can be described in the finite element space, whereas the subscale $(\cdot)_s$ stands for the small nuances of the solution that cannot be captured by the discrete finite element interpolation. Both spaces are complementary and conform the whole space of solutions. Since the large scale is represented by a finite space, the subscale space is infinite and must be approximated in order to obtain a feasible solution. The choice of the approximate subscale space leads to the final form of the stabilization method.

In this work we consider the Quasi-Static Algebraic Sub-Grid Scales (Q-ASGS) variant of the VMS approach [44,51] which neglects all terms involving the small scale acceleration $\dot{\boldsymbol{u}}_s$.

After discretizing the system of Eqs. (1) and (2) in the standard finite element fashion [56] and applying the aforementioned Q-ASGS method, the following system of equations in matrix form is obtained

$$\boldsymbol{M}\left(\tau_u, \boldsymbol{u}\right)\dot{\boldsymbol{U}} + \boldsymbol{K}\left(\tau_u, \tau_p, \boldsymbol{u}\right) + \boldsymbol{G}\left(\tau_u, \boldsymbol{u}\right)\boldsymbol{P} = \boldsymbol{F}\left(\tau_u, \boldsymbol{u}\right) \tag{14}$$

$$\boldsymbol{Q}_m\left(\tau_u\right)\dot{\boldsymbol{U}} + \boldsymbol{D}\left(\tau_u, \boldsymbol{u}\right)\boldsymbol{U} + \boldsymbol{Q}_p\left(\tau_u\right)\boldsymbol{P} = \boldsymbol{Q}_f\left(\tau_u\right) \tag{15}$$

where τ_u and τ_p are stabilization parameters defined as

$$\tau_u = \left(\frac{8\mu}{h^2} + \frac{2\rho\|\boldsymbol{u}\|}{h}\right)^{-1}, \tau_p = \mu + \frac{\|\boldsymbol{u}\|h}{4}$$

and h is a characteristic length of each finite element in the mesh.

The description of all the matrices and vectors in Eqs. (14) and (15) can be found in [44].

The resulting discrete problem does not suffer from the numerical instabilities that affect the Galerkin problem [57] and allows us to work with linear finite elements interpolators for both the velocity and the pressure.

Eqs. (14) and (15) are integrated in time using a standard Bossak scheme [58]. The output of the computation are the air velocity and pressure fields at t^{n+1}. These values are used for computing the transport of temperature and BC using the semi-Lagrangian technique described below.

Fig. 6. 2D section of the street canyon. View from Google Maps.

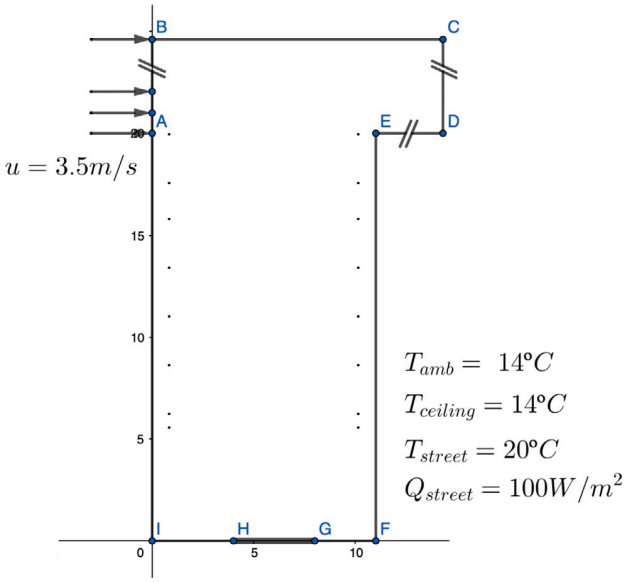

Fig. 7. Schematics of the 2D street canyon geometry.

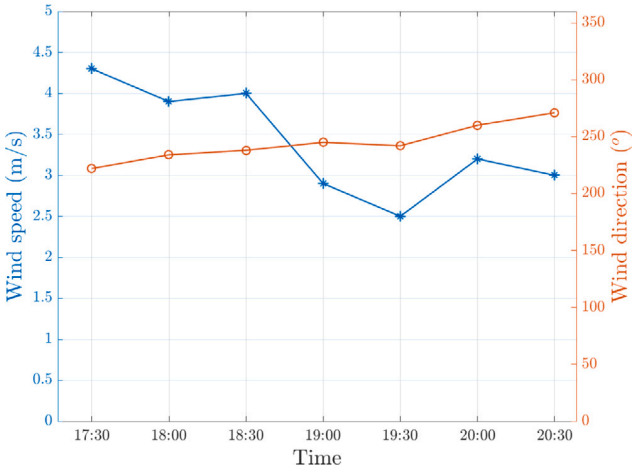

Fig. 8. Wind speed and direction in a nearby station in the studied period of time.

6. Semi-Lagrangian solution of the transport equation

The numerical method used to solve the transport of the temperature and pollutant fields is based on the semi-Lagrangian formulation developed by Puigferrat et al. [33]. This procedure calculates advection effect first using a Lagrangian approach based on the PFEM2 technique [34,35]. An Eulerian strategy based on the FEM is adopted to compute the diffusion and absorption effects in a second step. The Eulerian numerical solution is based on a stabilized FEM using a Finite Increment Calculus (FIC) technique [38].

The Semi-Lagrangian approach can be understood as a splitting method which uses a set of particles for transporting the advected variables within a fixed mesh and a FEM to solve the rest of the transport effects (diffusion and absorption) in the same fixed mesh.

The semi-Lagrangian procedure was originally introduced in [33] for solving the transient advection–diffusion–absorption equation for high Péclet numbers.

We outline below the main steps of the semi-Lagrangian procedure.

6.1. Solution steps of the semi-Lagrangian procedure

Once the air velocities have been obtained using the stabilized FEM, as described in Section 4.1, the transport of the temperature and the pollutant fields is computed using the following steps:

Step 1. Advection. Eq. (8c) is solved to transport the motion of a set of particles along the air streamlines. Each particle carries with itself the point concentration of the transported field (i.e. either the temperature or the concentration of BC) $\phi_p = \phi(\mathbf{x}_p)$.

Step 2. Projection. The values of the transported field at time t^{n+1} are transferred from the particles to the nodes of the finite element mesh.

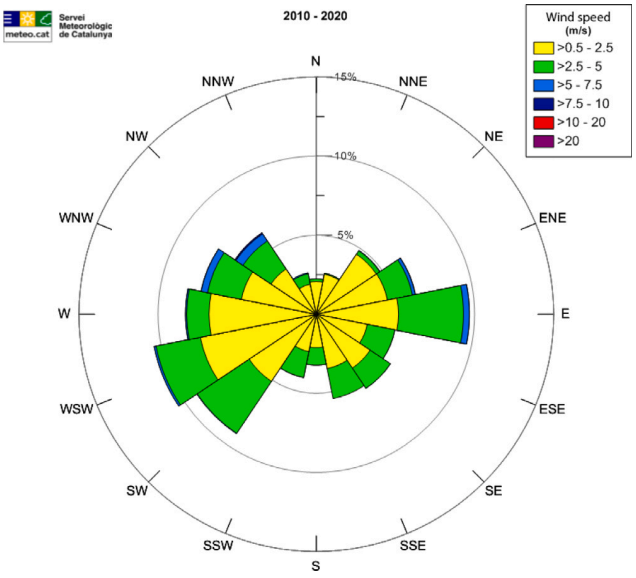

Fig. 9. Main directions of the wind in a nearby station.

Step 3. Diffusion–absorption. The diffusion and/or absorption of the pollutant is computed by solving the standard diffusion–reaction transport equation in a fixed grid with the FIC-FEM technique described in Section 6.2.

Step 4. Particles update. The values of the transported field are transferred from the nodes of the finite element mesh to the particles.

The steps of the Semi-Lagrangian procedure are shown in Fig. 2.

6.2. Computation of diffusion–absorption transport using a FIC-FEM technique

Eq. (8) and the boundary conditions (Eqs. (9) and (10)) are expressed in the fixed mesh using the FIC approach as [59].

Transport balance.

$$r_t - \underline{\frac{1}{2}\mathbf{h}^T\nabla r_t} = 0 \qquad \text{in } \Omega \tag{16}$$

where $\mathbf{h} = [h_1, h_2, h_3]^T$ is a characteristic length vector.

Boundary conditions.

$$\phi - \phi^p = 0 \quad \text{on } \Gamma_D \tag{17a}$$

$$r_\Gamma + \underline{\frac{1}{2}h_n r_t} = 0 \quad \text{on } \Gamma_N \quad , \quad \text{with } h_n = \mathbf{h}^T\mathbf{n} \tag{17b}$$

Eqs. (16) and (17b) are obtained by expressing the balance of fluxes in an arbitrary prismatic space domain of size $h_1 \times h_2 \times h_3$ within the global domain and at the Neumann boundary, respectively. The distances h_i are termed *characteristic lengths* of the FIC method. The underlined terms in Eqs. (16) and (17) introduced by the FIC technique provide the necessary stability for the numerical solution.

The characteristic lengths are expressed as a proportion of a typical grid dimension [60]. Note that, as the characteristic length vector $\mathbf{h}$ tends to zero, the FIC governing equations tend to the standard infinitesimal form; that is, $r_t \to 0$ in Ω and $r_\Gamma \to 0$ on Γ_N as $\mathbf{h} \to \mathbf{0}$. For details of the FIC method see [60].

In the semi-Lagrangian formulation, the effect of advection is neglected in the diffusion–absorption step. Consequently, vector $\mathbf{h}$ is defined to account for boundary instabilities due to absorption effects only as [33]

$$\mathbf{h} = \mathbf{h}_r = \frac{2}{r_t}\mathbf{D}_s\nabla\phi \tag{18}$$

The system of Eqs. (16)–(17) is discretized in space with the FEM and in time using an implicit Generalized Trapezoidal rule [61,62]. Detail of the matrices and vectors of the FIC-FEM formulation can be

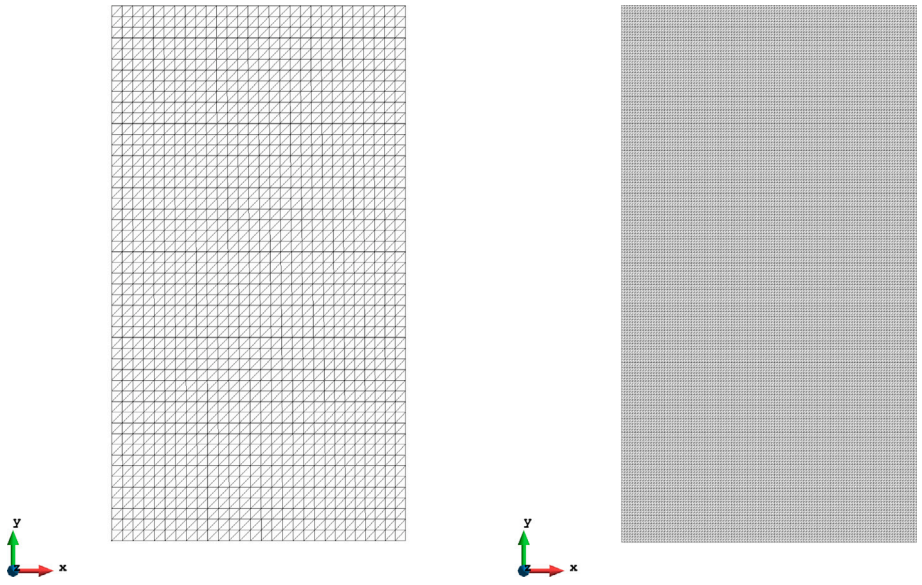

(a) Coarse mesh, l = 0.4m (b) Fine mesh, l = 0.1m

Fig. 10. 2D street canyon problem. Coarse and fine mesh in the area of study.

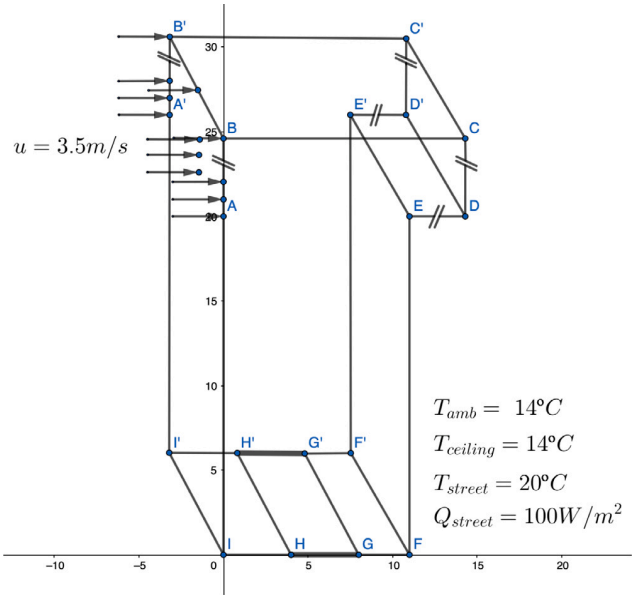

Fig. 11. 3D problem. Schematics of the 3D street canyon geometry.

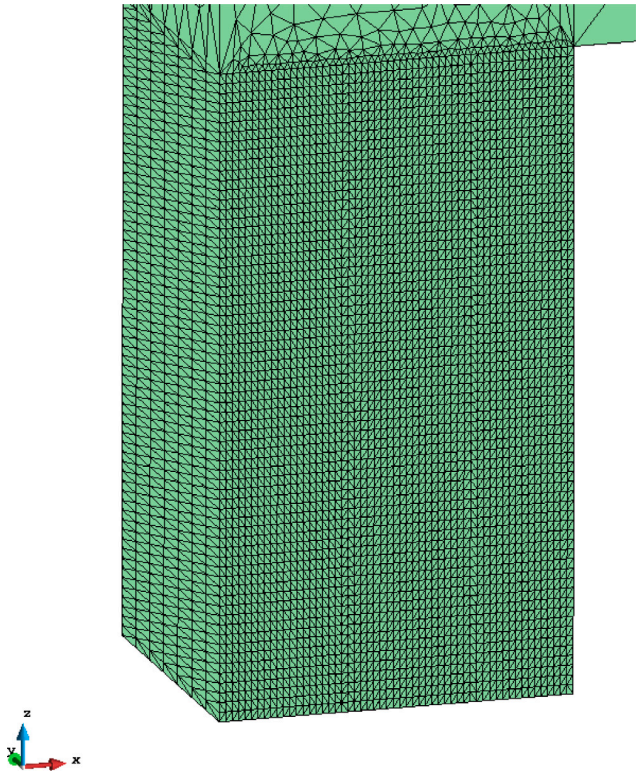

Fig. 12. 3D problem. Mesh on the street canyon geometry.

found in [38]. The solution for the nodal values at a time instant is found using an incremental strategy as

$$\mathbf{H}^n \Delta\boldsymbol{\phi} = -\mathbf{r}_t^n \tag{19}$$

where $\Delta\boldsymbol{\phi}$ is the increment of the nodal variables, $(\cdot)^n$ denotes values at time $t = t_n$ and

$$\mathbf{H}^n = \frac{1}{\Delta t}\mathbf{M} + \mathbf{K}^n + \mathbf{S} \tag{20}$$

$$\mathbf{r}_t^n := \mathbf{M}\dot{\boldsymbol{\phi}} + [\mathbf{K}^n + \mathbf{S}]\boldsymbol{\phi}^n - \mathbf{f}^n \tag{21}$$

In Eq. (21) we define $\dot{\boldsymbol{\phi}} = \frac{\boldsymbol{\phi}^n - \boldsymbol{\phi}^{n-1}}{\Delta t}$.

From the value of $\Delta\boldsymbol{\phi}$ obtained from Eq. (19) we compute the value of $\boldsymbol{\phi}^{n+1}$ as

$$\boldsymbol{\phi}^{n+1} = \boldsymbol{\phi}^n + \Delta\boldsymbol{\phi} \tag{22}$$

Details of the above matrices and vectors and of the transient solution scheme can be found in [38].

7. Results and discussion

7.1. Case study

Microclimatic changes in a street canyon occur mainly due to its geometry parameters (height-to-width ratio (H/W)) and the street orientation [7,10,63,64].

The chosen geometry in this work is a street canyon in Barcelona, Spain, specifically the *Torrent de l'Olla* street, around the number 218 (See Fig. 3). The simulation makes use of the boundary conditions from the days that Amato et al. [48] measured the BC concentration during November 2015. Measurements were taken by means of AE-51 micro-aethalometers (Aethlabs, Fig. 4), every 5 min during a period of four days. The data used for the validation was taken in the afternoon, from around 17.30h until 20.30h.

In both the 2D and 3D simulation the effect of trees has been disregarded because the experimental values were taken in a street section in which there were no trees significant for the simulation (the dense trees that can be seen in Fig. 6 are more than 5 m behind the studied section). We have not taken into account cars as it is one of the lowest traffic neighbourhood in Barcelona [65].

An ambient temperature of 14 °C has been taken, which corresponds to the average temperature of the three hour period of time in the days when the measurements were taken. The variation of temperature during that period can be seen in Fig. 5. The street temperature considered in this work is 20 °C (the average of the measured values).

Different simulations have been carried out to assess the effect of several variables on the BC concentration such as the street temperature, the mesh size and the time increment for solving the air flow and the transport equations.

Fig. 6 shows the studied two-dimensional (2D) section of the street canyon.

The height of the buildings in both sides of the canyon is 20 m and the width of the street is approximately 11 m, which gives $H/W \approx 1.82$.

A simplified 2D case has been studied first with a geometry shown in Fig. 7

where the segments $\overline{ABCD}$ represent the air domain over the buildings. This domain is chosen so it can be affected by the inwards and outwards velocity fluxes in the street canyon. It is also extended to avoid backflows on its outlets. It has an inlet velocity of 3.5 m/s parallel to the street, in the x direction. The wind direction was predominant on a South-West direction (see Figs. 3 and 8).

The wind rose of a nearby meteorological station can be seen in Fig. 9. It can be seen that the direction taken corresponds to one of the predominant directions on the wind rose. The value of this velocity is taken as the average of the wind speed in that station during the days of the measurements [49]. The segment $\overline{HG}$ of length 4 m represents the street section, which has an imposed heat source of 100 W/m^2. This value was chosen based on the calculations and experiments made in [66]. This corresponds to an average that can be found on an asphalt street during daytime and represents the captured solar heat by the asphalt. The walls have been considered to have low to no difference in temperature with the ambient air because they are mainly painted with clear colours and solar irradiation was low during the days the experimental data was taken (around 2 kWh/m^2 [49], which is among

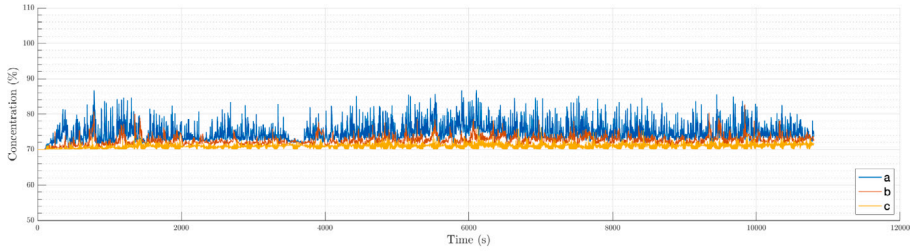

(a) Coarse mesh (l = 0.4 m)

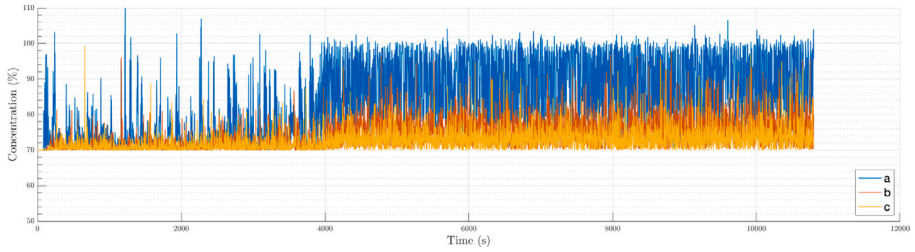

(b) Fine mesh (l = 0.1 m)

Fig. 13. 2D street canyon analysis. Measurements taken during a period of three hours for three different heights (a = 5 m, b = 15 m and c = 20 m) at 0.2 m from the wall. All analysis were carried out for a Courant number (C ≈ 1)

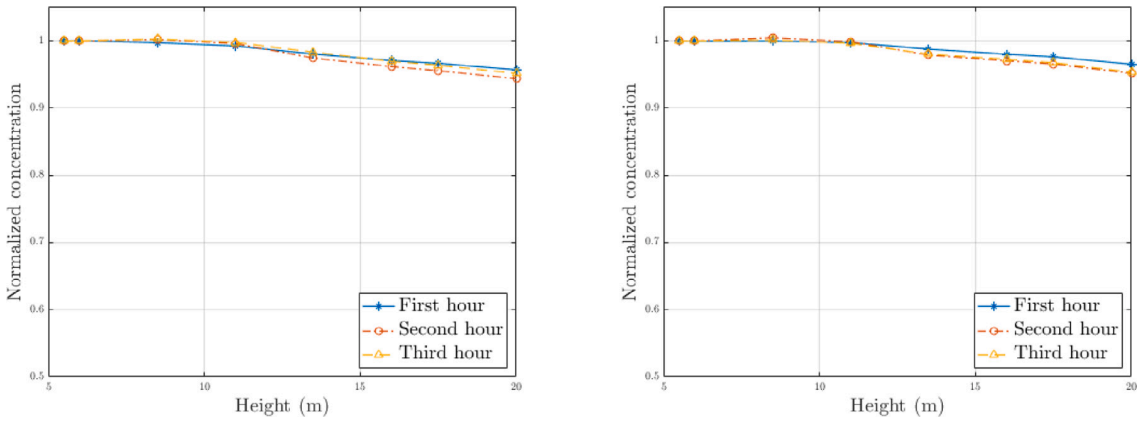

(a) 0.2 m from the wall

(b) 0.5 m from the wall

Fig. 14. 2D street canyon study. Measurements taken at two distances from the wall during three hours with a coarse mesh (l = 0.4 m) and a C ≈ 1. The ambient temperature is 14 °C and the street temperature is 20 °C.

lowest monthly values of the year [67]). Also, as the sun in November sets in Barcelona around 17:45h, there were no sun/shade walls.

The street canyon domain is discretized in two regular finite element meshes of 2.8k and 44k 3-noded triangles with two mesh sizes of l = 0.4 m and l = 0.1 m, respectively, for comparison purposes. The two meshes can be seen in Fig. 10. The mesh size effect has been assessed with several simulations for the same Courant number ($C = u\Delta t/\Delta x$), namely C ≈ 1 and C ≈ 3, taking into account that the average velocity inside the canyon is around 1 m/s. Other Courant numbers have been used to assess its effect in the same mesh.

Several simulations were run with the coarse mesh to study the effect of the street temperature and the ambient temperature on the distribution of the pollutant (Table 1). The rest of the cases were run with an ambient temperature of 14 °C and a street temperature of 20 °C.

The Dirichlet boundary conditions for the BC transport were chosen as ϕ = 100 kg/m^2 along the segment $\overline{HG}$ and ϕ = 70 kg/m^2 on the segments $\overline{ABCD}$. The ambient concentration of BC was chosen to be 70% of the concentration found in the street level, which corresponds to the measurements not affected by local sources [31].

Table 1
Temperature combinations.

Ambient temperature [°C]	Street temperature [°C]
14	14
	20
	25

A simplified three-dimensional (3D) case has been also studied with a geometry shown in Fig. 11

where the area $\overline{ABCDD'C'B'A'}$ represents the air domain over the buildings. Note that the section is the same as in Fig. 7. A depth of 10 m has been added to the previous model via an extrusion in the y direction.

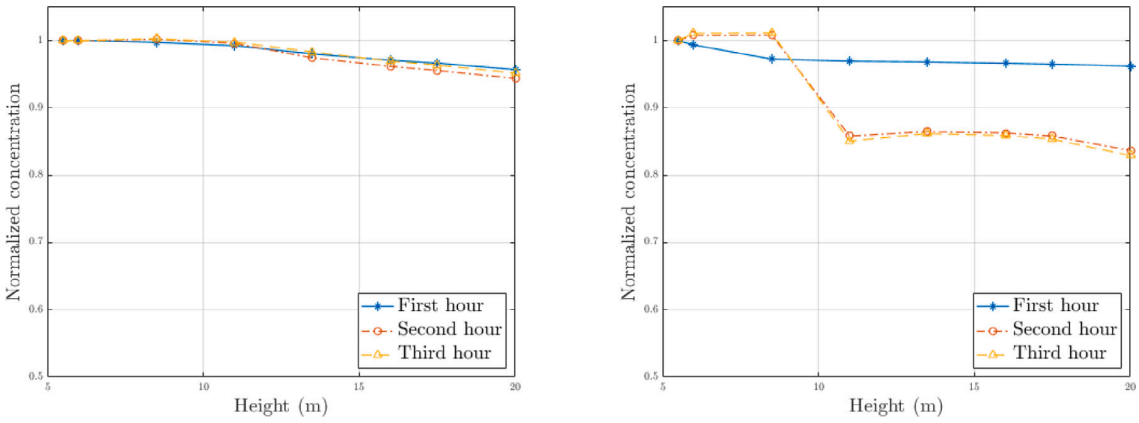

(a) $\Delta t = 0.4$ s (C $\approx$ 1.0) **(b)** $\Delta t = 0.1$ s (C $\approx$ 1.0)

Fig. 15. 2D street canyon study. Effect of the mesh size on the concentration fraction during 3 h with the same Courant numbers. The ambient temperature is 14 °C and the street temperature is 20 °C.

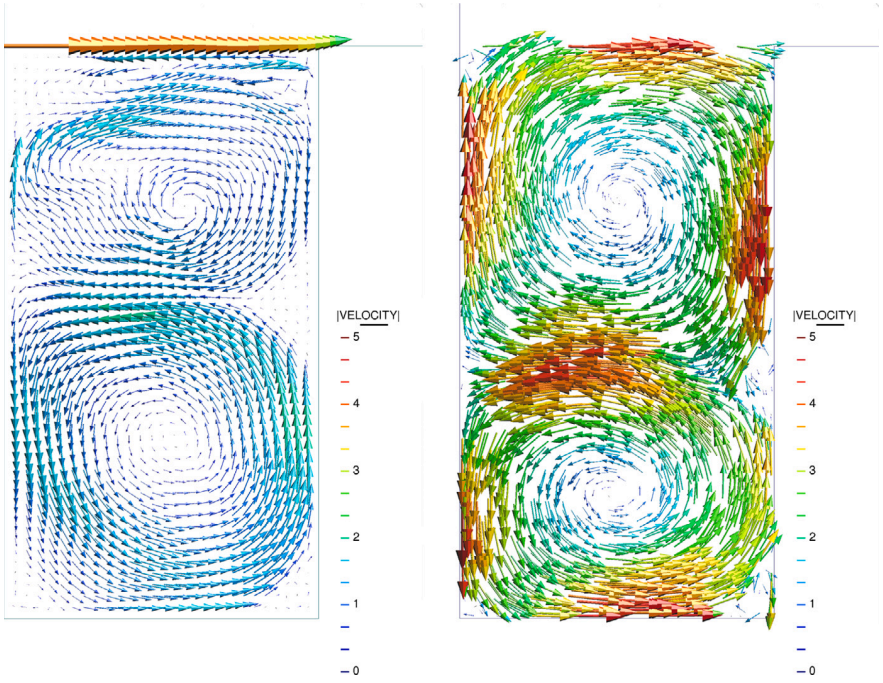

(a) Coarse mesh (l = 0.4 m) **(b)** Fine mesh (l = 0.1 m)

Fig. 16. 2D street canyon. Velocity vectors for the same Courant number (C $\approx$ 1.0) and different mesh sizes.

The 3D domain was chosen so it could be affected by the inwards and outwards velocity fluxes in the street canyon. It has an inlet velocity section of 3.5 m/s parallel to the street, in the x direction. The value of this velocity was taken, again, as the average of the wind speed in a nearby meteorological station during the days of the measurements. The area $\overline{HGG'H'}$, of length 4 m and depth 10 m, represents the street section, which has an imposed heat source of 100 W/m^2 [66]. This represents the captured solar heat by the asphalt. The walls have been considered to have low to no difference in temperature with the ambient air, because they are mainly painted with clear colours.

The Dirichlet boundary conditions chosen for the BC transport were $\phi = 100$ kg/m^2 along the street section $\overline{HGG'H'}$ and $\phi = 70$ kg/m^2 on the top section $\overline{ABCDD'C'B'A'}$. The ambient concentration of BC was chosen to be 70% of the concentration found in the street level, which corresponds to the measurements not affected by local sources [31].

The street canyon domain is discretized in a regular finite element mesh of 154k 4-noded linear tetrahedra with a mesh size of $l_x = 0.2$ m, $l_y = 1.4$ m and $l_z = 0.3$ m approximately, which gives an average Courant number close to 5 in the velocity direction, taking into account that the average velocity inside the canyon is around 1.5 m/s and the $\Delta t = 1$ s. Details of the mesh can be seen in Fig. 12.

The transient solution has been obtained with various time steps (Δt), depending on the Courant number considered in each case.

7.2. 2D results

Fig. 13 shows the time evolution of the concentration obtained at the heights 5, 15 and 20 m for a period of 3 h and 0.2 m away from the most affected wall, which is the one first reached by the pollutant

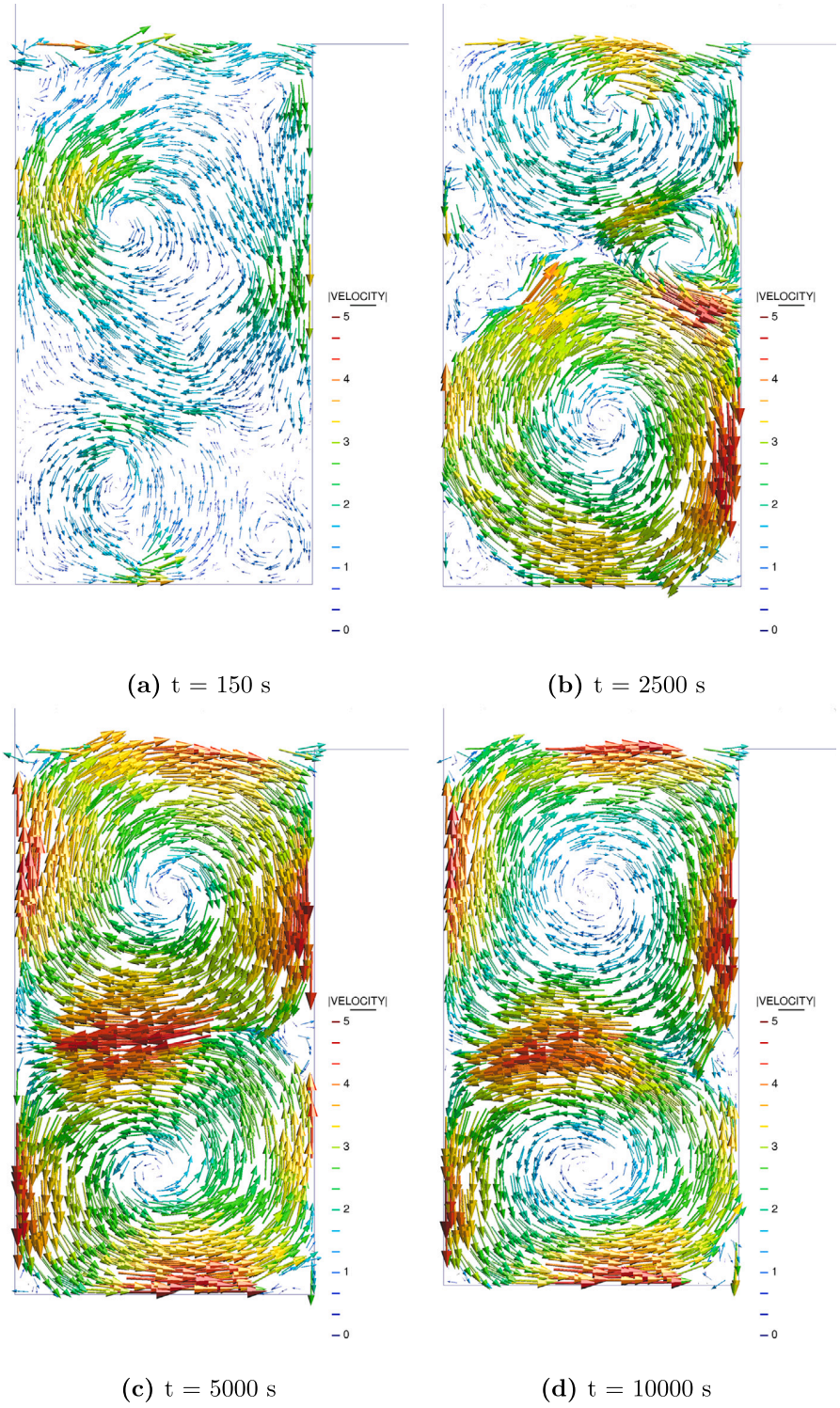

Fig. 17. 2D street canyon study. Velocity vectors at different time steps with a fine mesh and C ≈ 1.0. The ambient temperature is 14 °C and the street temperature is 20 °C.

depending on the eddies distribution. For instance, if there is a strong eddy in the lower part of the street canyon and it is rotating clockwise during the simulation, the most affected wall will be the upstream one.

The normalized concentration values shown in this section correspond to the distribution of the concentration of BC at different heights normalized with the average value of the concentration at 5.5 m. These values are averaged during the first, second and third hour in the street canyon and are taken at heights of 5.5, 6, 8.5, 11, 13.5, 16, 17.5 and 20 m and at a distance of 0.2 m from the wall, be it the downstream or the upstream one, as shown in Fig. 7.

We took these heights in order to compare the numerical results with the experimental ones reported in [48]. In the experiments, measurements of the BC concentration were taken every 5 min during a period of four days. As we use an average temperature and run three hours of simulations only, the data taken from [48] is the average in a daytime. The distance from the wall corresponds to an approximated

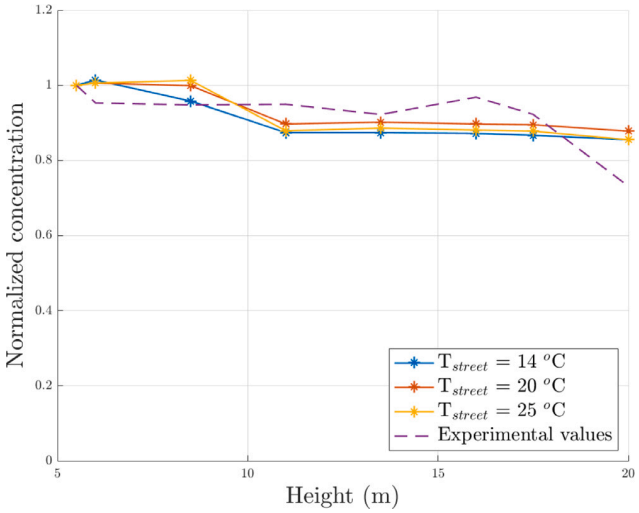

Fig. 18. Comparison of simulations with different street temperatures and an ambient temperature of 14 °C (C ≈ 1.0). Experimental results [48] are shown in a dashed line.

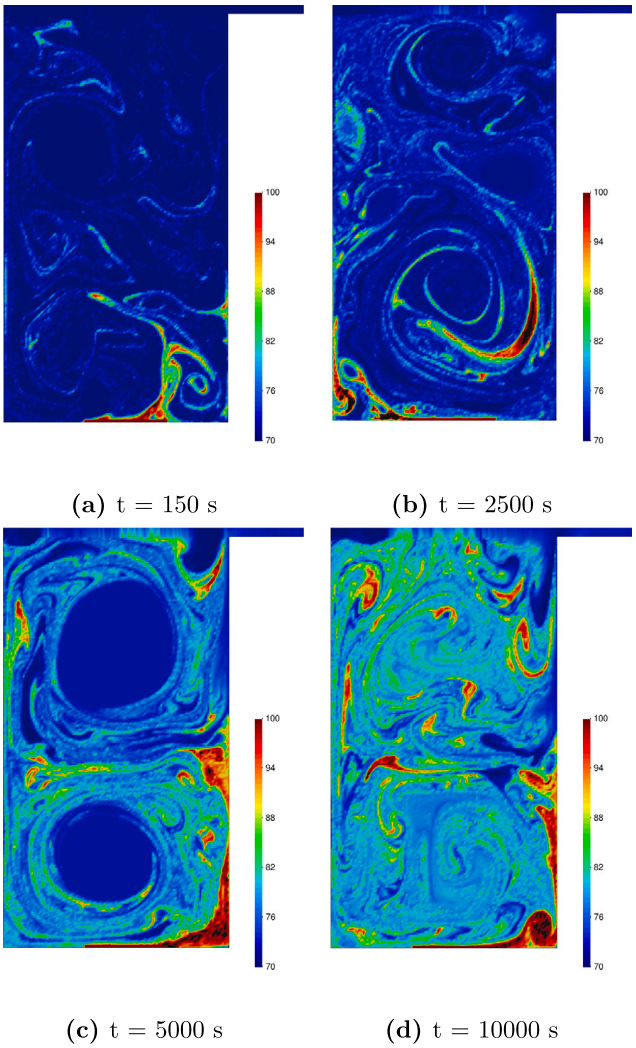

Fig. 19. 2D problem. Concentration contours of BC at different time steps with a fine mesh and a C ≈ 1.0. The ambient temperature is 14 °C and the street temperature is 20 °C.

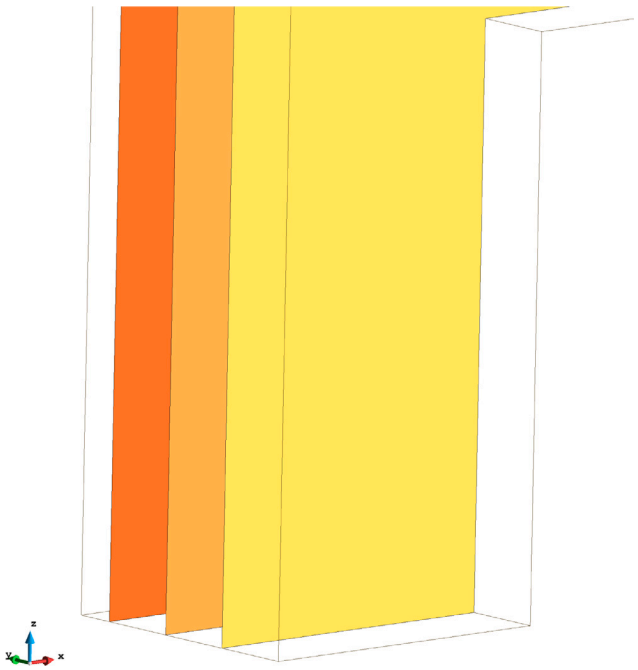

Fig. 20. 3D problem. Slices of the 3D street canyon model.

size of the BC sensor. Other simulations were run to determine whether the distance to the wall had effect on the normalized concentration curves. The computations showed that if we measure the values at short distance from the wall (between 0.2 and 0.5 m), the result has minimal differences (Fig. 14).

Fig. 15 shows the effect of the mesh size on the normalized BC concentration value during the three hours, using the same Courant number (C ≈ 1). The difference in the normalized concentration fraction in Fig. 15(b) is due to the creation of stronger eddies in the lower part of the street canyon as the fine mesh captures better the velocity gradients in the air. A smoother distribution of the velocity fields in the case of Fig. 15(a) is found. The fact that a stronger lower eddy is created prevents the pollutant from leaving it, which means that a higher normalized concentration will be found in the region from 5 to 10 m of height.

Fig. 16 shows two snapshots of the solution at the same time for the coarse and fine meshes, and the same Courant number (C ≈ 1). Although results show high similarity, it can be seen that the fine mesh results (Fig. 16(b)) capture better the high gradients in the air flow those of the coarse mesh (Fig. 16(a)).

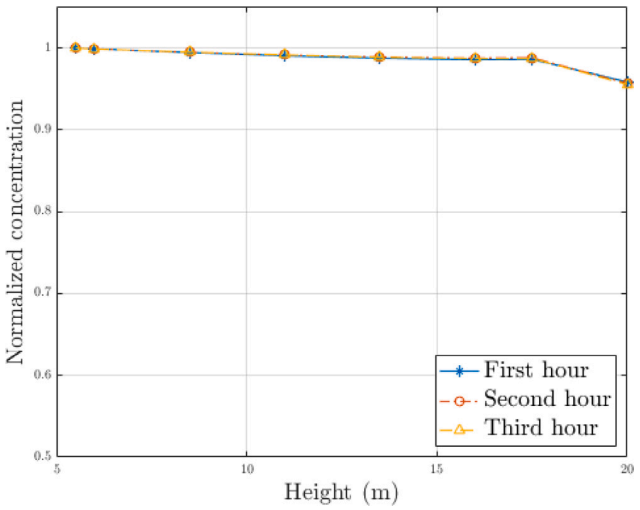

Fig. 22. 3D street canyon analysis. Concentration fraction on the 3 h with a Courant number of around 5. The ambient temperature is 14 °C and the street temperature is 20 °C.

Different simulations using the temperatures in Table 1 were carried out to assess the influence of the street temperature in the concentration distribution of BC for C ≈ 1.0.

Fig. 17 shows the eddies that appear when the ambient temperature is 14 °C and the street temperature is 20 °C using the fine mesh and a Courant number of ≈ 1.0. Note that at $t = 150$ s, when the velocity from the wind has still not influenced the lower part of the street canyon, small eddies appear due to the effect of the buoyancy induced by the difference of temperature between the street and the ambient.

Different eddies appear for cases in which street or ambient temperature vary and is one of the reasons why the BC distribution depends on the street temperature.

The normalized concentration is plotted in Fig. 18 against the height of the measurements. The numerical results obtained have been plotted together with the experimental ones obtained by Amato et al. [48].

Good correlation between numerical and experimental results is obtained.

Fig. 18 also shows that the street temperature has a slight effect on the normalized concentration values. All three configurations tend to create a strong eddy that stays during a relatively long time and increases the concentration in the lower part of the street canyon, which accumulates in the first 8–9 m and then decreases slowly until the 20 m of height. The authors' interpretation of the gap at 20 m is due to the simplifications made in the paper, most likely the one made on the geometry and the constant air speed. We believe the effects of

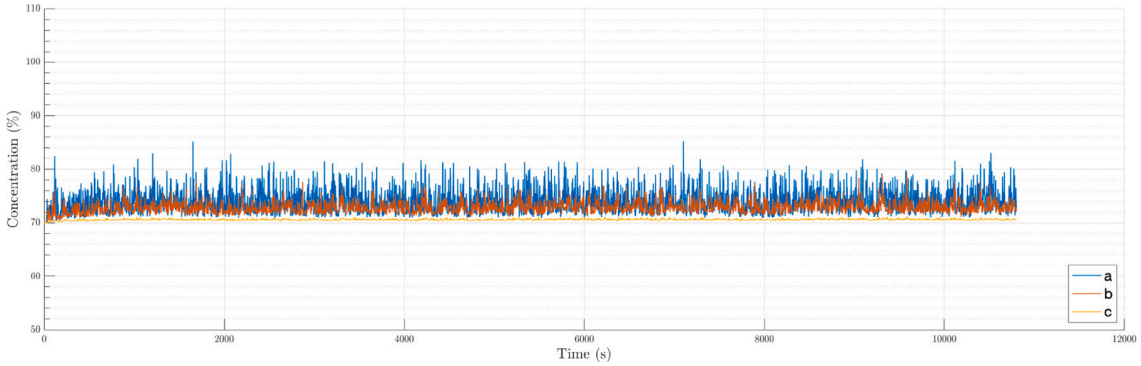

Fig. 21. 3D street canyon study. Measurements taken during a period of three hours for three different heights (a = 5 m, b = 15 m and c = 20 m) at 0.2 m from the wall. The analysis was carried out for a Courant number (C ≈ 5).

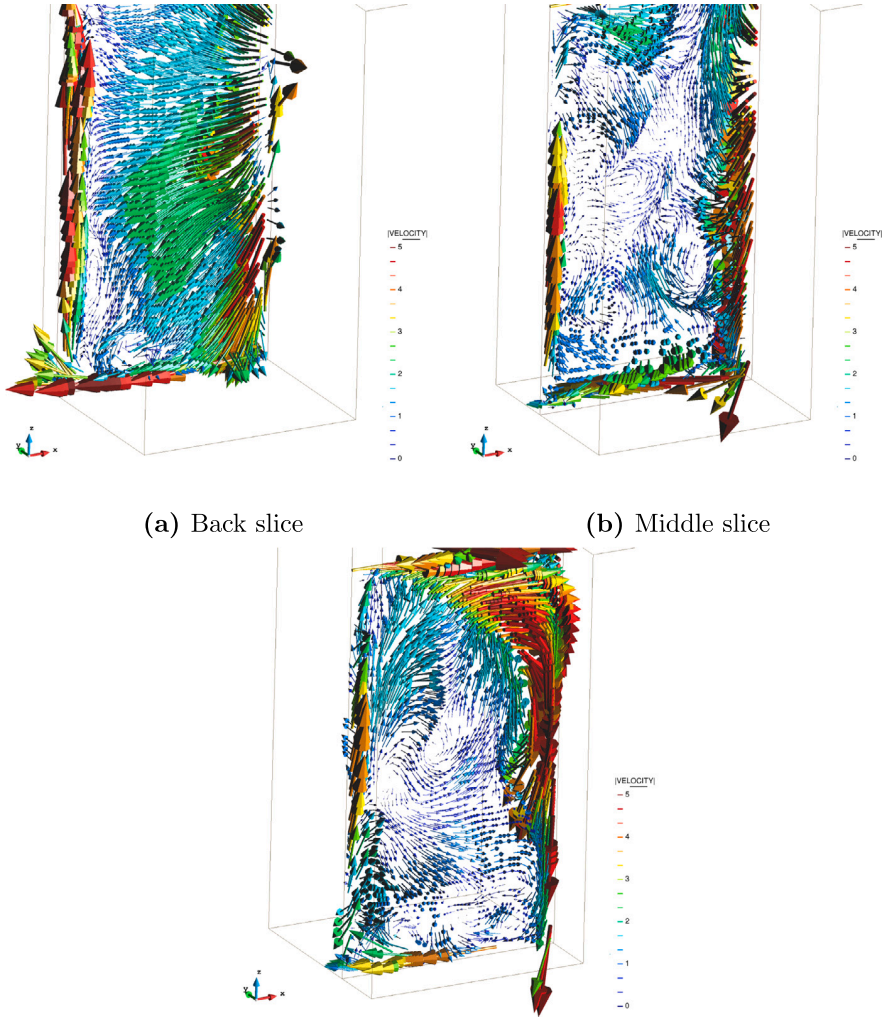

(a) Back slice (b) Middle slice

(c) Front slice

Fig. 23. 3D street canyon problem. Velocity vectors for a Courant number (C ≈ 5.0) on different slices at $t = 5000$ s. The street temperature and ambient temperature are 20 °C and 14 °C, respectively.

Table 2
Comparison of numerical and experimental values of BC concentration at different heights.

	Coarse mesh				Fine mesh			Experimental
	C = 0.5	C = 1.0	C = 2.5	C = 3.0	C = 1.0	C = 3.0	C = 5.0	
5.5 m	1.0000 0.00%	1.0000 0.00%	1.0000 0.00%	1.0000 0.00%	1.0000 0.00%	1.0000 0.00%	1.0000 0.00%	1.0000
6 m	0.9985 4.78%	0.9999 4.92%	1.0045 5.40%	1.0034 5.29%	1.0094 5.92%	0.9957 4.48%	0.9656 1.33%	0.9530
8.5 m	0.9977 5.28%	1.0024 5.77%	1.0308 8.77%	1.0326 8.97%	1.0099 6.57%	0.9892 4.38%	0.8676 −8.45%	0.9477
11 m	0.9856 3.80%	0.9969 4.99%	0.8778 −7.55%	0.8872 −6.56%	0.8545 −10.01%	0.9865 3.89%	0.8802 −7.30%	0.9495
13.5 m	0.9452 2.49%	0.9788 6.14%	0.8774 −4.85%	0.8811 −4.46%	0.8634 −6.37%	0.9895 7.30%	0.8788 −4.71%	0.9222
16 m	0.9293 −4.03%	0.9657 −0.27%	0.8764 −9.49%	0.8818 −8.94%	0.8609 −11.09%	1.0522 8.66%	0.8797 −9.15%	0.9683
17.5 m	0.9229 0.05%	0.9597 4.04%	0.8759 −5.05%	0.8825 −4.33%	0.8559 −7.22%	1.0529 14.14%	0.8771 −4.92%	0.9225
20 m	0.9063 23.90%	0.9478 29.57%	0.8456 15.60%	0.8441 15.39%	0.8330 13.88%	0.8711 19.08%	0.8171 11.71%	0.7315

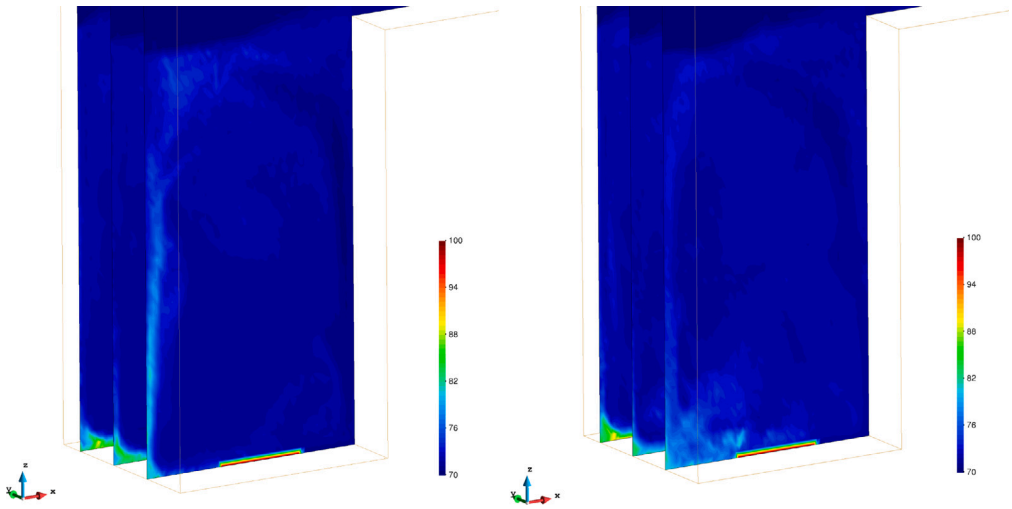

Fig. 24. 3D street canyon problem. BC concentration contours for a Courant number (C ≈ 5.0) at$t$ = 2500 s and$t$ = 5000 s. The street temperature and ambient temperature are 20 °C and 14 °C, respectively.

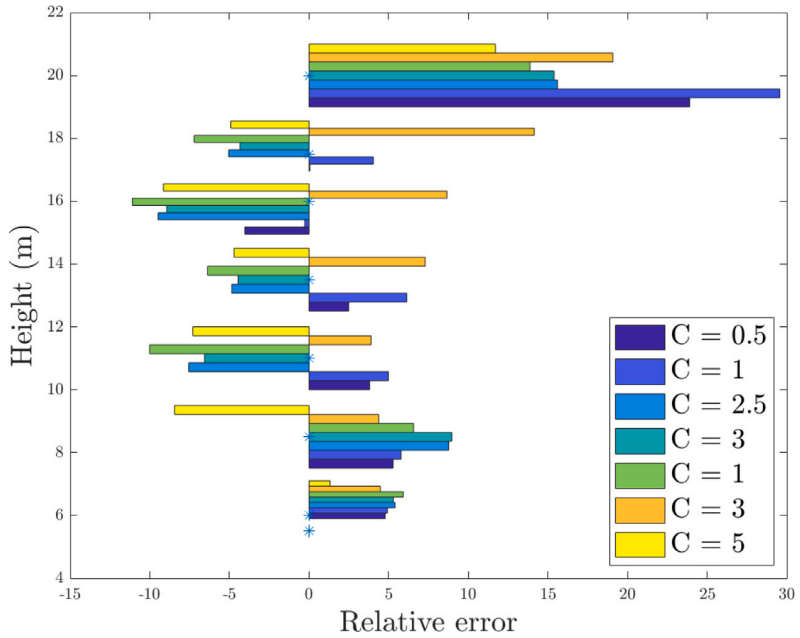

Fig. 25. Vertically distributed graph from Table 2.

such simplification are magnified at higher heights, far from the source of pollutant.

Fig. 19 shows different snapshots of BC concentration at several time steps for the case in which the street temperature is 20 °C and the ambient temperature is 14 °C.

7.3. 3D results

The 3D case we show in this paper corresponds to a 2D extrusion to demonstrate that three-dimensional phenomena are captured correctly with the proposed semi-Lagrangian formulation. The ultimate goal would be to run more elaborated simulations to get more detailed results. For this example we used the conditions which were more similar to the case study ran in Section 7.2, namely an ambient temperature of 14 °C, a street temperature of 20 °C with an imposed heat source of 100 W/m^2 and an imposed inlet velocity of 3.5 m/s.

Fig. 20 shows the three cuts chosen in the 3D domain in order to show the 3D results.

Fig. 21 shows the time evolution of the concentration obtained at the heights 5, 15 and 20 m for a period of 3 h and 0.2 m away from the most affected wall at the slice situated in the middle (Fig. 20).

Fig. 22 shows the normalized BC concentration value during the three hours, using the same Courant number (C ≈ 5).

In Fig. 23 we can see the different velocity vectors after$t$ = 5000 s. These vectors are much more chaotic than the ones shown in Fig. 17 due to the effect of the third component of the air velocity. However, a large clockwise eddy can be seen along the whole street canyon.

Snapshots of the BC concentration contours at$t$ = 2500 s and$t$ = 5000 s are shown in Fig. 24.

Table 3
MAPE of BC concentration for different computations.

	Coarse mesh				Fine mesh		
	C = 0.5	C = 1.0	C = 2.5	C = 3.0	C = 1.0	C = 3.0	C = 5.0
MAPE	5.54%	6.96%	7.09%	6.74%	7.63%	7.74%	5.94%

Table 4
Numerical and experimental values of BC concentration at different heights for the 3D problem.

	3D		Experimental
	C = 5.0	C = 10.0	
5.5 m	1.0000 0.00%	1.0000 0.00%	1.0000
6 m	0.9989 4.82%	0.9969 4.61%	0.9530
8.5 m	0.9947 4.96%	0.9906 4.53%	0.9477
11 m	0.9912 4.39%	0.9884 4.10%	0.9495
13.5 m	0.9884 7.18%	0.9880 7.14%	0.9222
16 m	0.9869 1.92%	0.9876 1.25%	0.9683
17.5 m	0.9871 7.01%	0.9880 7.11%	0.9225
20 m	0.957 30.83%	0.9763 34.70%	0.7315

Table 5
MAPE of BC concentration for the 3D problem.

	3D	
	C = 5.0	C = 10.0
MAPE	7.64%	7.87%

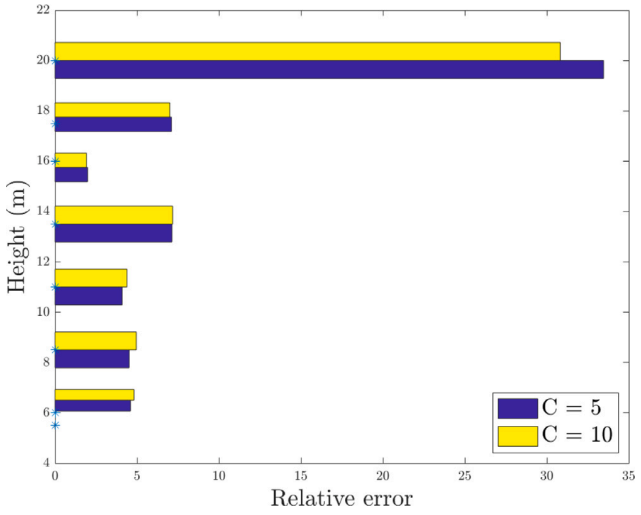

Fig. 26. Vertically distributed graph from Table 4.

7.4. Comparison of results

In this section we compare in more detail the numerical results obtained in this work with the experimental data.

Table 2 presents the different normalized BC concentration values for the studied heights obtained in the simulations as well as a column with the concentrations obtained experimentally for the 2D problem. We show the relative error for each simulation values, calculated as

$$err_i = \frac{\hat{x}_i|_{sim} - \hat{x}_i|_{exp}}{\hat{x}_i|_{exp}} \tag{23}$$

where $\hat{x}_i|_{sim}$ represents the simulated value at each point and $\hat{x}_i|_{exp}$ is the experimental value at the same height point.

Fig. 25 shows the results from Table 2 as a vertically distributed graph.

Table 3 shows the Mean Absolute Percentage Error (MAPE) of BC concentration for every simulation computed as

$$MAPE = \frac{1}{n}\sum_{i=1}^{n} |err_i| \tag{24}$$

The MAPE value for each Courant number stays within 5%–8%. These results show that, although having simplified the problem in several aspects, the semi-Lagrangian formulation presented can predict the pollutant transport with a good range of accuracy.

Table 4 presents the different normalized BC concentration values for the studied heights obtained in the 3D simulations as well as a column with the experimental concentrations. Fig. 26 shows a vertically distributed graph for the readers' ease. Table 5 shows the MAPE for the same case. The MAPE values are higher than in the 2D case, presumably due to the higher Courant number used for the 3D simulations.

8. Concluding remarks

The semi-Lagrangian finite element formulation presented has proven to be a useful tool to predict the distribution of BC in a street canyon using a short time resolution (scale of seconds). Although several simplifications were made in the problem, these have led to reasonably low differences between the calculated results and the ones obtained experimentally. In 2D, the effects of the velocity in the longitudinal direction have been neglected and in 3D, the effect of cars has not been taken into account. The authors are aware of the limitations of the simplifications that have been made but these can be partially overcome with the use of more detailed geometries. A more detailed configuration could explain, closely, how pollutants affect pedestrians.

An important feature of the coupled numerical method presented is its ability for transient predictions and the possibility of studying microscale problems in a city, not only in several points like in the experimental case here considered, but in the whole street canyon area.

We highlight the importance of choosing the proper initial and boundary conditions as small street or ambient temperature differences can yield different BC concentration distributions.

The simulation tool here proposed can also be used to reduce the impact of pollutants on pedestrians as well as to design street canyons to lessen the pollution effect in urban areas either studying the direct impact of the pollutants, or the accumulated normalized values.

Planned extensions of the method presented are the addition of obstacles on the street, such as trees, cars or even pedestrians, the modification of the wind velocity at different times using weather models, the addition of chemical reactions and adapting the street fixed concentration of BC at street level using traffic data as input, among others. Also, for longer simulations one should carry out an unsteady radiation and conduction simulation in walls which are in contact with the air, as it can introduce buoyancy effects. For a better more accurate validation, experimental data throughout the whole street canyon would be desirable.

Declaration of competing interest

The authors declare that they have no known competing financial interests or personal relationships that could have appeared to influence the work reported in this paper.

Acknowledgements

This research was partially funded by the projects PRECISE (BIA2017-83805-R) and PARAFLUIDS (PID2019-104528RB-I00) of the Natural Research Plan of the Spanish Government. The first author acknowledges the support of the FI grant provided by the Generalitat de Catalunya, Spain. The authors also acknowledge the financial support from the CERCA programme of the Generalitat de Catalunya, Spain, and from the Spanish Ministry of Economy and Competitiveness, through the "Severo Ochoa Programme for Centres of Excellence in R&D" (CEX2018-000797-S).

References

[1] Health Effects Institute, State of Global Air 2020. Special Report, Health Effects Institute, Boston, MA, 2020.
[2] World Health Organization, WHO Air Quality Guidelines for Particulate Matter, Ozone, Nitrogen Dioxide and Sulfur Dioxide: Global Update 2005: Summary of Risk Assessment (No. WHO/SDE/PHE/OEH/06.02), World Health Organization, 2005.
[3] Y. Huang, et al., Numerical investigation of the thermal effect on flow and dispersion of rooftop stack emissions with wind tunnel experimental validations, Environ. Sci. Pollut. Res. (2020) 1–19.
[4] T. Lauriks, et al., Application of improved CFD modeling for prediction and mitigation of traffic-related air pollution hotspots in a realistic urban street, Atmos. Environ. 246 (2021) 118127.
[5] J.S. Lighty, J.M. Veranth, A.F. Sarofim, Combustion aerosols: factors governing their size and composition and implications to human health, J. Air Waste Manage. Assoc. 50 (9) (2000) 1565–1618.
[6] P. Rajagopalan, N. Wong, Parametric studies on urban geometry, airflow and temperature, Int. J. Archit. Sci. 6 (3) (2005) 114–132.
[7] N. Shishegar, Street design and urban microclimate: analyzing the effects of street geometry and orientation on airflow and solar access in urban canyons, J. Clean Energy Technol. 1 (1) (2013).
[8] W.C. Cheng, C.H. Liu, D.Y. Leung, On the correlation of air and pollutant exchange for street canyons in combined wind-buoyancy-driven flow, Atmos. Environ. 43 (24) (2009) 3682–3690.
[9] J.J. Kim, J.J. Baik, Effects of inflow turbulence intensity on flow and pollutant dispersion in an urban street canyon, J. Wind Eng. Ind. Aerodyn. 91 (3) (2003) 309–329.
[10] J.F. Sini, S. Anquetin, P.G. Mestayer, Pollutant dispersion and thermal effects in urban street canyons, Atmos. Environ. 30 (15) (1996) 2659–2677.
[11] X.X. Li, C.H. Liu, D.Y. Leung, Numerical investigation of pollutant transport characteristics inside deep urban street canyons, Atmos. Environ. 43 (15) (2009) 2410–2418.
[12] Y. Tominaga, T. Stathopoulos, CFD modeling of pollution dispersion in building array: evaluation of turbulent scalar flux modeling in RANS model using LES results, J. Wind Eng. Ind. Aerodyn. 104 (2012) 484–491.
[13] T. Oke, Street design and urban canopy layer climate, Energy Build. 11 (1988) 103–113.
[14] X. Xie, Z. Huang, J. Wang, Z. Xie, The impact of solar radiation and street layout on pollutant dispersion in street canyon, Build. Environ. 40 (2) (2005) 201–212.
[15] B. Galperin, S. Sukoriansky, P.S. Anderson, On the critical richardson number in stably stratified turbulence, Atmos. Sci. Lett. 8 (3) (2007) 65–69.
[16] C.W. Miller, L.M. Hively, A review of validation studies for the Gaussian plume atmospheric dispersion model, Nucl. Saf. 28 (4) (1987) 522–531.
[17] A.J. Cimorelli, et al., AERMOD: A dispersion model for industrial source applications. Part I: General model formulation and boundary layer characterization, J. Appl. Meteorol. 44 (5) (2005) 682–693.
[18] S.G. Perry, CTDMPLUS: A dispersion model for sources near complex topography. Part i: Technical formulations, J. Appl. Meteorol. 31 (7) (1992) 633–645.
[19] D.J. Carruthers, et al., UK-ADMS: A new approach to modelling dispersion in the earth's atmospheric boundary layer, J. Wind Eng. Ind. Aerodyn. 52 (1994) 139–153.
[20] D.J. Carruthers, A.M. Mckeown, D.J. Hall, S. Porter, Validation of ADMS against wind tunnel data of dispersion from chemical warehouse fires, Atmos. Environ. 33 (12) (1999) 1937–1953.
[21] CERC ADSM-Urban, User Guide, Cambridge Environmental Research Consultant, 2006.
[22] F. Toja-Silva, C. Pregel-Hoderlein, J. Chen, On the urban geometry generalization for CFD simulation of gas dispersion from chimneys: Comparison with Gaussian plume model, J. Wind Eng. Ind. Aerodyn. 177 (2018) 1–18.
[23] Á. Leelössy, F. Molnár, F. Izsák, Á. Havasi, I. Lagzi, R. Mészáros, Dispersion modeling of air pollutants in the atmosphere: a review, Cent. Eur. J. Geosci. 6 (3) (2014) 257–278.
[24] R. Longo, et al., A multi-fidelity framework for the estimation of the turbulent Schmidt number in the simulation of atmospheric dispersion, Build. Environ. 185 (2020) 107066.
[25] J. Eichhorn, Validation of a microscale pollution dispersal model, in: Air Pollution Modeling and Its Application XI, Springer, Boston, MA, 1996, pp. 539–547.
[26] I. Bey, et al., Global modeling of tropospheric chemistry with assimilated meteorology: Model description and evaluation, J. Geophys. Res.: Atmos. 106 (D19) (2001) 23073–23095.
[27] G.A. Grell, S.E. Peckham, R. Schmitz, S.A. McKeen, G. Frost, W.C. Skamarock, B. Eder, Fully coupled online chemistry within the WRF model, Atmos. Environ. 39 (37) (2005) 6957–6975.
[28] K. Wang, Y. Zhang, C. Jang, S. Phillips, B. Wang, Modeling intercontinental air pollution transport over the trans-Pacific region in 2001 using the community multiscale air quality modeling system, J. Geophys. Res.: Atmos. 114 (D4) (2009).
[29] D.B. Ryall, Maryon R.H., Validation of the UK met office's NAME model against the ETEX dataset, Atmos. Environ. 32 (24) (1998) 4265–4276.
[30] A. Stohl, M. Hittenberger, G. Wotawa, Validation of the Lagrangian particle dispersion model FLEXPART against large-scale tracer experiment data, Atmos. Environ. 32 (24) (1998) 4245–4264.
[31] S. Vardoulakis, B.E. Fisher, K. Pericleous, N. Gonzalez-Flesca, Modelling air quality in street canyons: a review, Atmos. Environ. 37 (2) (2003) 155–182.
[32] R. Codina, Stabilized finite element approximation of transient incompressible flows using orthogonal subscales, Comput. Methods Appl. Mech. Engrg. 191 (39–40) (2002) 4295–4321.
[33] A. Puigferrat, M. Masó, I. de Pouplana, G. Casas, E. Oñate, Semi-Lagrangian formulation for the advection-diffusion-absorption equation, Comput. Methods Appl. Mech. Eng. 380 (2021) 113807.
[34] S. Idelsohn, N. Nigro, A. Limache, E. Oñate, Large time-step explicit integration method for solving problems with dominant convection, Comput. Methods Appl. Mech. Engrg. 217–220 (2012) 168–185.
[35] S. Idelsohn, E. Oñate, N. Nigro, P. Becker, J. Gimenez, Lagrangian versus Eulerian integration errors, Comput. Methods Appl. Mech. Engrg. 293 (2015) 191–206.
[36] E. Oñate, J. Miquel, P. Nadukandi, An accurate FIC-FEM formulation for the 1D advection–diffusion–reaction equation, Comput. Methods Appl. Mech. Engrg. 298 (2016) 373–406.
[37] E. Oñate, P. Nadukandi, J. Miquel, Accurate FIC-FEM formulation for the multidimensional steady-state advection–diffusion–absorption equation, Comput. Methods Appl. Mech. Engrg. 327 (2017) 352–368.
[38] A. Puigferrat, I. de Pouplana, E. Oñate, FIC–FEM Formulation for the multidimensional transient advection–diffusion–absorption equation, Comput. Methods Appl. Mech. Engrg. 365 (2020) 112984.
[39] B. Cushman-Roisin, J.M. Beckers, Introduction To Geophysical Fluid Dynamics: Physical and Numerical Aspects, Academic press, 2011.
[40] G. Flierl, R. Ferrari, 12.820 Turbulence in the Ocean and Atmosphere. Spring 2007. Massachusetts Institute of Technology: MIT OpenCourseWare https://ocw.mit.edu License: Creative Commons BY-NC-SA.
[41] S.A. Socolofsky, G.H. Jirka, Special topics in mixing and transport processes in the environment, in: Engineering–Lectures, fifth ed., Texas A & M University, 2005, pp. 1–93.
[42] B. Perot, Large Eddy Simulation using a Transport Equation for the Subgrid-Scale Stress Tensor, Dept. of Mechanical Engineering, University of Massachusetts, Amherst, 2007.
[43] Y. Tominaga, T. Stathopoulos, Numerical simulation of dispersion around an isolated cubic building: model evaluation of RANS and LES, Build. Environ. 45 (10) (2010) 2231–2239.
[44] J. Cotela Dalmau, E. Oñate, R. Rossi, Applications of Turbulence Modeling in Civil Engineering, International Centre for Numerical Methods in Engineering (CIMNE), 2016.
[45] E.A. Spiegel, G. Veronis, On the Boussinesq approximation for a compressible fluid, Astrophys. J. 131 (1960) 442.
[46] Y. Tominaga, T. Stathopoulos, CFD simulation of near-field pollutant dispersion in the urban environment: A review of current modeling techniques, Atmos. Environ. 79 (2013) 716–730.
[47] D.J. Tritton, Physical Fluid Dynamics, Springer Science & Business Media, 2012.
[48] F. Amato, N. Pérez, M. López, A. Ripoll, A. Alastuey, M. Pandolfi, et al., Vertical and horizontal fall-off of black carbon and NO2 within urban blocks, Sci. Total Environ. 686 (2019) 236–245.
[49] Servei Meteorològic de Catalunya *Generalitat de Catalunya* https://en.meteocat.gencat.cat/?lang=en.
[50] TJR. Hughes, Multiscale phenomena: Green's functions, the Dirichlet-to-Neumann formulation, subgrid scale models, bubbles and the origins of stabilized methods, Comput. Methods Appl. Mech. Engrg. (1995).
[51] R. Codina, A stabilized finite element method for generalized stationary incompressible flows, Comput. Methods Appl. Mech. Engrg. (2001).
[52] V. Gravemeier, The variational multiscale method for laminar and turbulent flow, Arch. Comput. Methods Eng. (2006).
[53] T.M. van Opstal, J. Yan, C. Coley, J.A. Evans, T. Kvamsdal, Y. Bazilevs, Isogeometric divergence-conforming variational multiscale formulation of incompressible turbulent flows, Comput. Methods Appl. Mech. Engrg. (2017).
[54] M. Cervera, M. Chiumenti, L. Benedetti, R. Codina, Mixed stabilized finite element methods in nonlinear solid mechanics. Part III: Compressible and incompressible plasticity, Comput. Methods Appl. Mech. Engrg. (2015).

[55] N. Abboud, G. Scovazzi, Elastoplasticity with linear tetrahedral elements: A variational multiscale method, Internat. J. Numer. Methods Engrg. (2018).
[56] B.G. Galerkin, Series solution of some problems of elastic equilibrium of rods and plates, Vestnik inzhenerov i tekhnikov 19 (7) (1915) 897–908.
[57] T.J.R. Hughes, L.P. Franca, G.M. Hulbert, A new finite element formulation for computational fluid dynamics: VIII. The Galerkin/least-squares method for advective-diffusive equations, Comput. Methods Appl. Mech. Engrg. (1989).
[58] T.J. Hughes, The Finite Element Method: Linear Static and Dynamic Finite Element Analysis, Courier Corporation.
[59] E. Oñate, J. Miquel, F. Zarate, Stabilized solution of the multidimensional advection-diffusion-absorption equation using linear finite elements, Comput. & Fluids 36 (2007) 92–112.
[60] E. Oñate, Derivation of stabilized equations for numerical solution of advective-diffusive transport and fluid flow problems, Comput. Methods Appl. Mech. Engrg. 151 (1998) 233–265.
[61] J. Donea, A Taylor-Galerkin method for convective transport problems, Internat. J. Numer. Methods Engrg. 20 (1984) 101–119.
[62] O.C. Zienkiewicz, R.L. Taylor, J.Z. Zhu, The Finite Element Method. The Basis, sixth ed., Elsevier, 2005.
[63] A.J. Arnfield, G.M. Mills, An analysis of the circulation characteristics and energy budget of a dry, asymmetric, east–west urban canyon. I. Circulation characteristics, Int. J. Climatol. 14 (2) (1994) 119–134.
[64] P.E. Todhunter, Microclimatic variations attributable to urban-canyon asymmetry and orientation, Phys. Geogr. 11 (2) (1990) 131–141.
[65] Statistics department *Ajuntament de Barcelona* https://www.bcn.cat/estadistica/angles/index.htm.
[66] T. Asaeda, V.T. Ca, A. Wake, A heat storage of pavement and its effect on the lower atmosphere, Atmos. Environ. 30 (3) (1996) 413–427.
[67] Access to solar irradiation maps of Spain (ADRASE) *CIEMAT* http://www.adrase.com/en/.

Chapter 5

Conclusions

The aim of this chapter is to summarize all the work done in the thesis, pointing out its innovative points and main contributions. The parallel and future lines of research that appear as a consequence of this work are given in the last section of this chapter.

The main goal of this thesis was to obtain a new stabilized numerical solving tool for complex environmental problems involving the transport of substances in fluids. The practical aim the thesis was that the tool could be used to help better understand the transport of air pollution parts of a city.

The main scientific contribution of this work has been the development of a robust and accurate numerical method for the solution of general transient advection-diffusion-absorption transport problems. Subsequently, this numerical formulation has been coupled with stabilized FEM methods for solving the fluid equations and practical problems have been successfully solved.

5.1 Achievements

We highlight below the main results obtained during the development of the thesis:

- Derivation and validation of a new stabilization procedure based on the Finite Increment Calculus (FIC) and the FEM for solving the transient transport equation in multidimensional cases.

- A second relevant result is a new semi-Lagrangian procedure for solving transient advection dominated problems, accounting for the effect of diffusion and absorption effects. The semi-Lagrangian procedure has been validated with existing numerical results.
- The third key contribution of the thesis is a new procedure to couple the FEM solution of the Navier-Stokes for a thermal incompressible fluids with the semi-Lagrangian procedure for solving advection and/or absorption dominated transport problems, accounting for other transport effects. The practical aim has been the accurate prediction of the transport of contaminants in air.
- The applicability of the semi-Lagrangian procedure developed in the thesis has been proved in the solution of several problems of air pollution transport. In particular, we have successfully modelled the transport of black carbon in a city canyon for which experimental results are available.

5.2 Lines of future work

Several simplifications were made in the thesis for solving the problem of transporting a pollutant in an urban area. This results in certain inaccuracies that can be overcome by developing more detailed models.

In this respect, extensions of the method developed in the thesis are planned in order to obtain more accurate results. These possible improvements include to add obstacles in the geometry, to take into account modifications of the initial conditions such as the wind speed at different times, the modification of the wind direction using information obtained by meteorological models, the addition of chemical reactions to be able to model a greater number of pollutants and the introduction of traffic information, among others.

Currently, work is being done in a project to simulate the transport of pollutants in large areas of cities by coupling a shallow water-type method for the transport of pollutant in air at pedestrian level with the "FluidTransport Application" for local simulations of the transport of pollution in street canyons in a specific street.

Another line of future work is to adapt the code to perform simulations in porous media

in order to broaden the range of applicability of the current formulation.

When it comes to code optimization, there is still room for cleaning the implemented procedures to make them more efficient. However, the first aspect that should be addressed is: the parallel programming.

As commented in Chapter 1, the code has been implemented in the Kratos programming framework based on C++ language. Kratos is prepared for parallel computing using OpenMP (Open Multiprocessing) and MPI (Message Passing Interface) procedures. However, certain features of the code, such as the Lagrangian advective transport, are currently designed to work only in OpenMP, but not in MPI. In order to develop a computational technology that can solve efficiently large 3D problems, the extension of the code to MPI is a priority task in the near future.

Appendix A

Academic street canyon

A.1 Introduction

This simulation aims to study the effect of heating in the lower part of the street canyon on the distribution of the wind velocity vectors as well as on the distribution of a pollutant emitted from its lower part.

The mathematical model is the one exposed in Chapter 3 of the thesis and is composed of the Navier-Stokes equations for incompressible fluids and the transport equations calculated with the semi-Lagrangian method [78]. The simulation has been carried out in the Kratos Multiphysics platform [44].

The wind speed is imposed constant over time perpendicular to the cavity, in the x direction. The geometry represents a street with a height / width (H/W) ratio of 1. Figure A.1 shows a schematic of the model used for this simulation.

This represents an idealized street canyon. The width and the height of the canyon are taken as H/W = 1. A line source of pollutant is set in the middle of the street canyon. The Dirichlet boundary conditions for the pollutant's transport are chosen as $\phi = 100$ kg/m^2 on the source point and $\phi = 0$ kg/m^2 over the top of the free flow.

The buoyancy forces have been taken into account in the simulation for the transport of temperature, since its variation makes a force gradient appear that modifies the velocity field [14, 84].

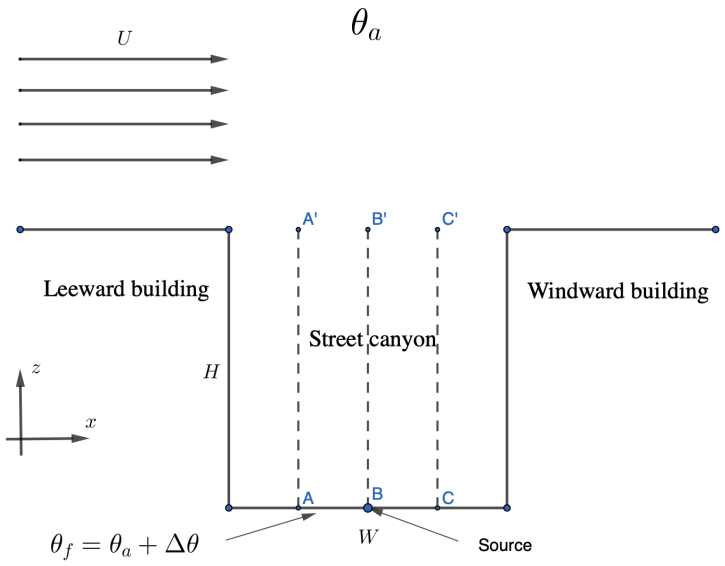

Figure A.1: Schematics of the domain used for the fluid and transport simulation in the street canyon.

The spatial domain has been discretized into 43k elements and 21k nodes. Surfaces of the buildings and the street have been defined as no-slip boundary conditions.

The Reynolds number $Re = Uh/\nu$ for this problem is $\sim$ 2000, depending on the case. The street canyon domain (H/W = 1) is discretized in a regular finite element mesh of 50x50x2 three-noded triangles. A Courant number ($C = U\Delta t/\Delta x$) of 2 has been used, taking into account that the velocity U over the street canyon domain is around 0.5 m/s. The results are compared when a steady state is reached.

Three scenarios of ground heating for the same H/W ratio have been investigated: no heating, normal heating and strong heating. The thermal effects are quantified by the bulk Richardson number (Equation (A.1)).

$$R_b = -\frac{gh}{U^2}\frac{\Delta\theta}{\theta_a} \tag{A.1}$$

The bulk Richardson numbers chosen for this study are 0, -0.05 and -0.2, respectively. The temperature at the top of the domain is set equal to the ambient temperature (θ_a) and the floor temperature is defined as $\theta_f = \theta_a + \Delta\theta$.

A.2 Results

The results obtained in the $R_b \approx -0.2$ scenario are compared with the ones obtained experimentally by Uehara et al. [91]. Figure A.2 shows the obtained normalized horizontal velocity along the vertical centerline of the street canyon compared with the experimental results. The results obtained in the simulation present a good agreement with the measurements inside the wind tunnel, which suggests that the model used is valid for practical simulations. Some differences can be found between both of them which may be due to the imposed boundary conditions (such as a different imposed velocity profile), the measurements of the experimental values (as the velocity on the floor should be 0 m/s) or uncertainties from the fluid calculating model.

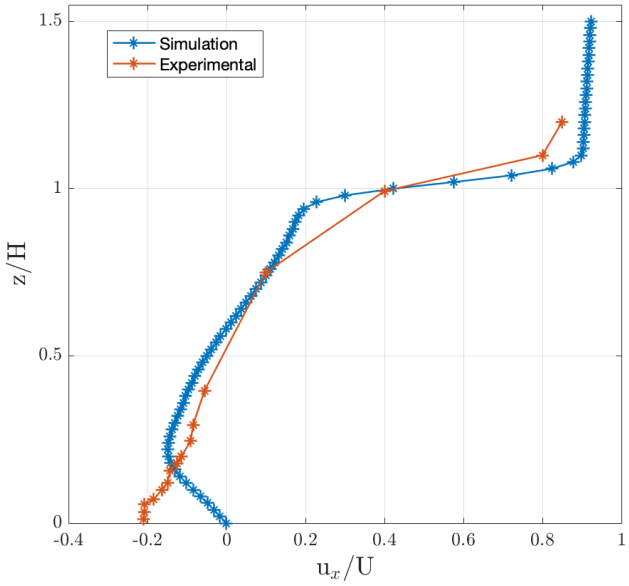

Figure A.2: Normalized horizontal velocity along the center line of the street canyon.

A.2.1 Flow study

In the three scenarios, one main vortex appears in the street canyon when it reaches an steady state. Also, other smaller vortices appear, two on the leeward wall and one on the windward wall, as seen in Figure A.3. The main streamlines can be also seen in this figure. These results agree well with the ones obtained by other authors [48, 49, 100].

Figure A.4 shows the normalized horizontal and vertical velocities. The effect of the ground heating can be seen on the different scenarios and the results show good agreement with the ones done previously by other authors [48, 49]. The ground heating affects the main eddy giving it a higher rotation. It also makes the lower windward eddy grow.

A.2.2 Pollutant dispersion

In this section the distribution of the pollutant has been calculated for the different scenarios. It can be seen that its distribution is similar in all the cases, however, the concentration distribution is slightly different with higher thermal effects, as can be seen in Figure A.5.

A higher $\Delta\theta$ incurs in a higher global energy in the street canyon, which translates into a higher transport of pollutant from the source. Therefore, it can be seen in Figure A.6d that the concentration drops faster with higher thermal effects as it is transported to the leeward wall due to a faster eddy.

Three different cuts at 0.25 W, 0.5 W and 0.75 W ($\overline{AA'}$, $\overline{BB'}$ and $\overline{CC'}$, respectively) are shown to assess the concentration of pollutant inside the street canyon and can be used for future comparison. Figure A.6 shows the values of the normalized concentration along the height of the street canyon. Figures A.6b, A.6d and A.6f show a zoom of the different cuts for a clearer understanding of the results.

A.3 Conclusion

The semi-Lagrangian finite element formulation presented in Chapter 3 has proven to be a useful tool to predict the distribution of a pollutant in a street canyon using a short time resolution (scale of seconds). This on-going study shows that the results obtained in simulations when using the semi-Lagrangian approach are accurate and can be used for practical applications. The comparison between experimental and simulated values shows a good agreement.

Buoyancy effects must be considered when predicting the distribution of pollutants in street canyons. The results obtained in this study have potential for urban planners

working on air pollution in cities as well as remodelling of these areas to lessen the pollution effect in urban areas either studying the direct impact of the pollutants.

This study has been made in parallel with the paper in Chapter 4. An important feature of the coupled numerical method presented is its ability for transient predictions and the possibility of studying microscale problems in a city, not only in several points like in the experimental case here considered, but in the whole street canyon area.

Planned extensions of the method are the addition of obstacles on the street, such as trees, cars or even pedestrians, the modification of the wind velocity at different times using weather models, the addition of chemical reactions and adapting the street fixed concentration of pollutants at street level using traffic data as input, among others. Also, for longer simulations one should carry out an unsteady radiation and conduction simulation in walls which are in contact with the air, as it can introduce buoyancy effects. For a better more accurate validation, experimental data throughout the whole street canyon would be desirable.

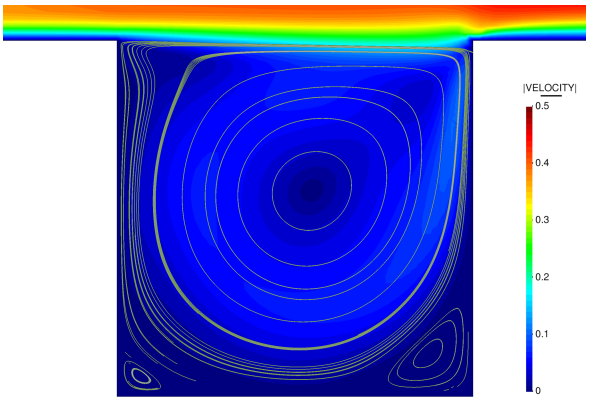

(a) No floor heating

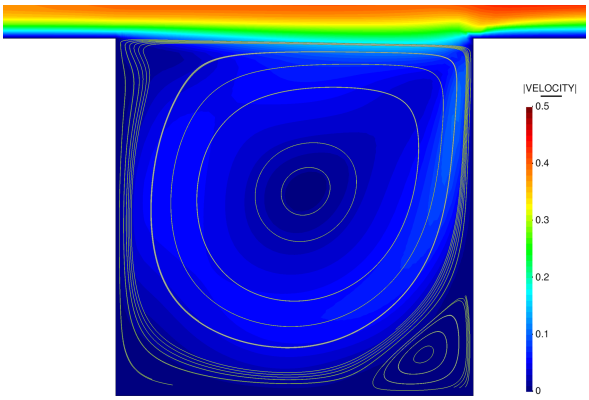

(b) Floor heating, $R_b \approx -0.05$

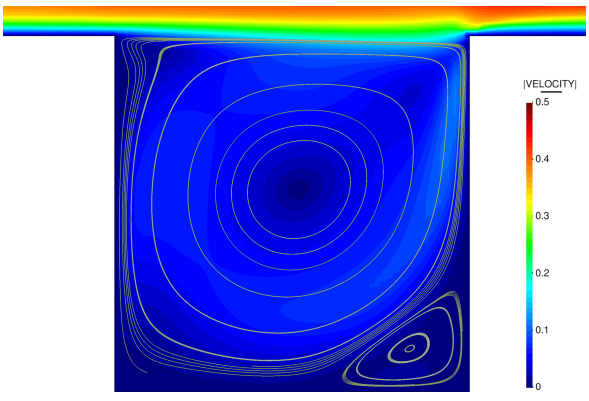

(c) Floor heating, $R_b \approx -0.2$

Figure A.3: Distribution of the eddies in the street canyon with different floor heatings when an steady state has been reached.

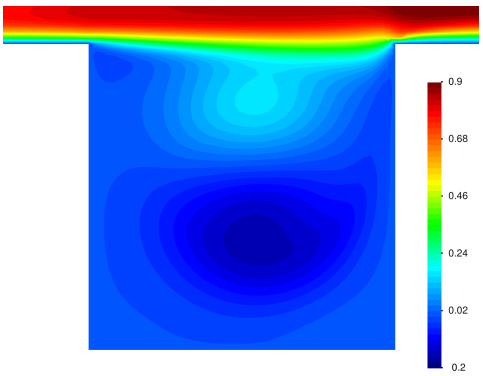

(a) Normalized x velocity, no floor heating

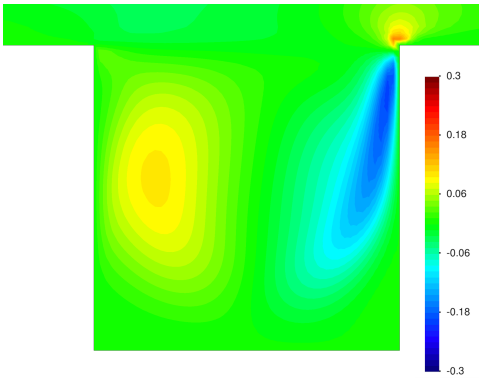

(b) Normalized z velocity, no floor heating

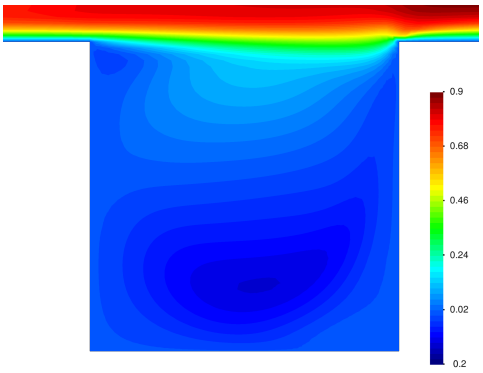

(c) Normalized x velocity, floor heating, $R_b \approx -0.05$

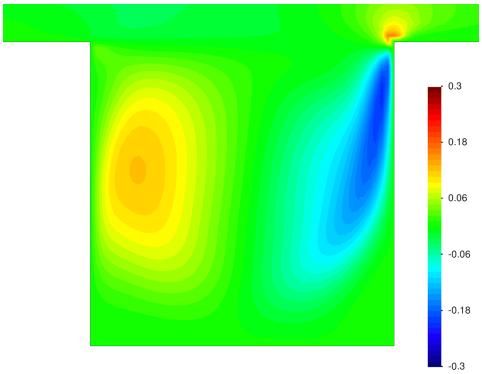

(d) Normalized z velocity, floor heating, $R_b \approx -0.05$

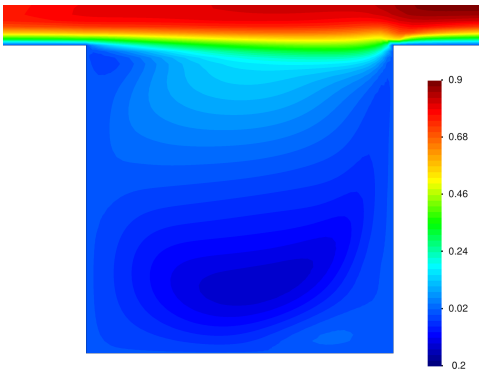

(e) Normalized x velocity, floor heating, $R_b \approx -0.2$

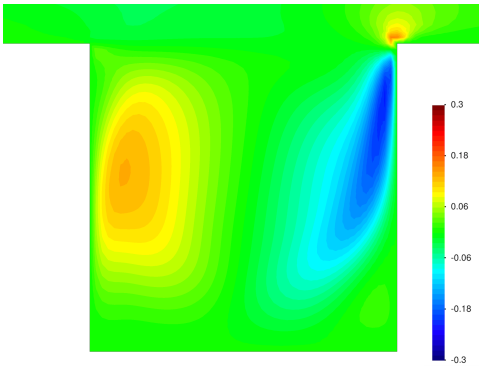

(f) Normalized z velocity, floor heating, $R_b \approx -0.2$

Figure A.4: Normalized x and z velocities in the street canyon.

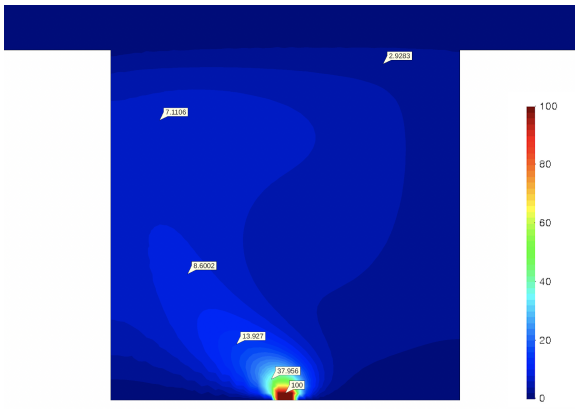

(a) No floor heating

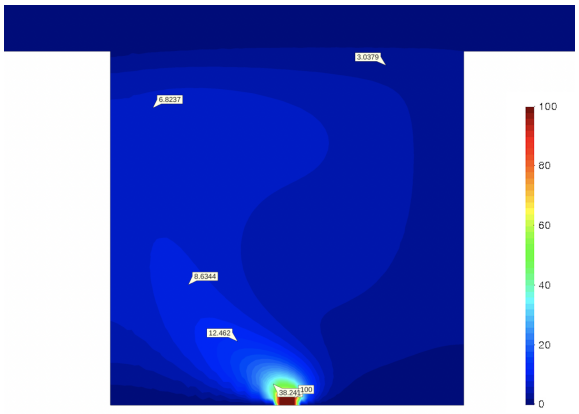

(b) Floor heating, $R_b \approx -0.05$

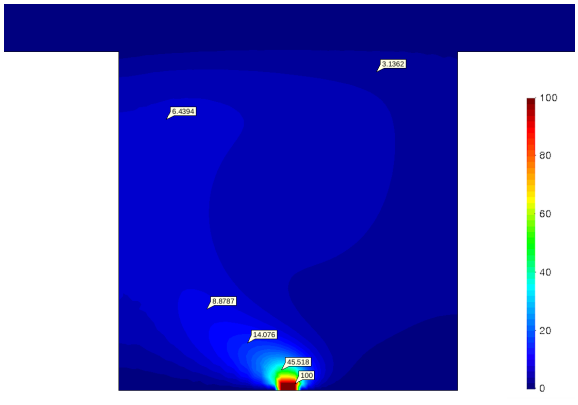

(c) Floor heating, $R_b \approx -0.2$

Figure A.5: Distribution of the pollutant in the street canyon with different floor heatings when an steady state has been reached.

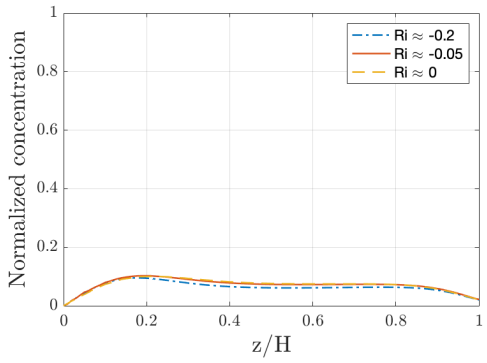

(a) $\overline{AA'}$

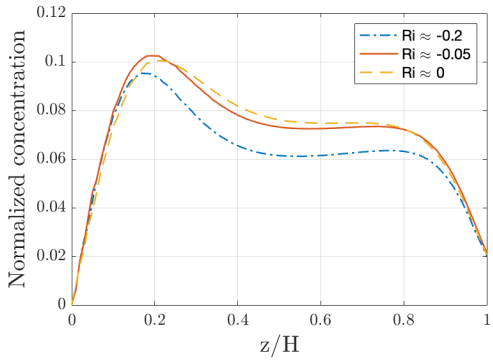

(b) $\overline{AA'}$ zoom

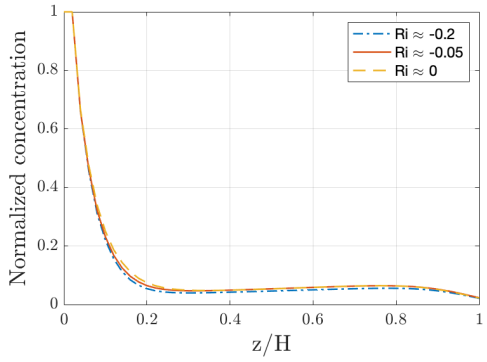

(c) $\overline{BB'}$

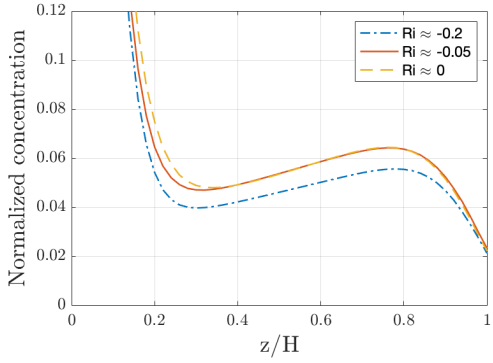

(d) $\overline{BB'}$ zoom

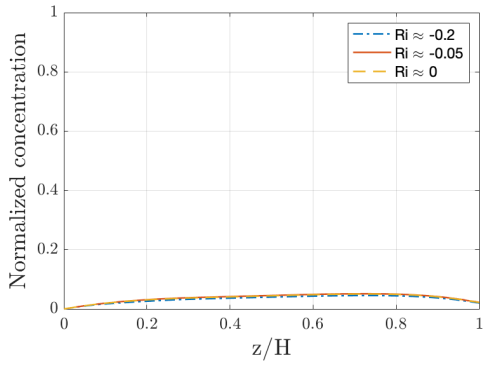

(e) $\overline{CC'}$

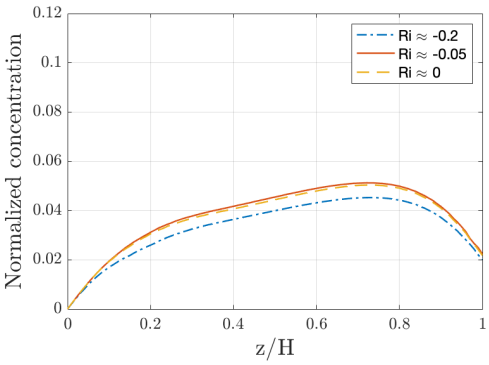

(f) $\overline{CC'}$ zoom

Figure A.6: Normalized concentration in different cuts inside the street canyon. On the right side we show a zoom for a clearer view.

Bibliography

[1] M. Al-Lawatia. An eulerian-lagrangian control volume scheme for two-dimensional unsteady advection-diffusion problems. *Numerical methods for partial differential equations*, 28(5):1481–1496, 2012.

[2] F. Amato, N. Pérez, M. López, A. Ripoll, A. Alastuey, M. Pandolfi, A. Karanasiou, A. Salmatonidis, E. Padoan, D. Frasca, et al. Vertical and horizontal fall-off of black carbon and no2 within urban blocks. *Science of the total environment*, 686:236–245, 2019.

[3] A. E. d. M. Baptista. *Solution of advection-dominated transport by Eulerian-Lagrangian methods using the backwards method of characteristics*. PhD thesis, Massachusetts Institute of Technology, 1987.

[4] I. Bey, D. J. Jacob, R. M. Yantosca, J. A. Logan, B. D. Field, A. M. Fiore, Q. Li, H. Y. Liu, L. J. Mickley, and M. G. Schultz. Global modeling of tropospheric chemistry with assimilated meteorology: Model description and evaluation. *Journal of Geophysical Research: Atmospheres*, 106(D19):23073–23095, 2001.

[5] F. Brezzi, M.-O. Bristeau, L. P. Franca, M. Mallet, and G. Rogé. A relationship between stabilized finite element methods and the galerkin method with bubble functions. *Computer methods in applied mechanics and engineering*, 96(1):117–129, 1992.

[6] F. Brezzi and A. Russo. Choosing bubbles for advection-diffusion problems. *Mathematical Models and Methods in Applied Sciences*, 4(04):571–587, 1994.

[7] A. N. Brooks and T. J. Hughes. Streamline upwind/petrov-galerkin formulations for convection dominated flows with particular emphasis on the incompressible navier-stokes equations. *Computer methods in applied mechanics and engineering*, 32(1-3):199–259, 1982.

[8] H. Burridge, D. Parker, E. Kruger, J. Partridge, and P. Linden. Conditional sampling of a high péclet number turbulent plume and the implications for entrainment. *Journal of Fluid Mechanics*, 823:26–56, 2017.

[9] R. Cady. *An adaptive multi-dimensional Eulerian-Lagrangian finite element method for simulating advection-dispersion.* PhD thesis, The University of Arizona, 1989.

[10] R. Cady and S. P. Neuman. Three-dimensional adaptive eulerian-lagrangian finite element method for advection-dispersion. In *Developments in Water Science*, volume 36, pages 183–193. Elsevier, 1988.

[11] D. Carruthers, R. Holroyd, J. Hunt, W. Weng, A. Robins, D. Apsley, D. Thompson, and F. Smith. Uk-adms: A new approach to modelling dispersion in the earth's atmospheric boundary layer. *Journal of wind engineering and industrial aerodynamics*, 52:139–153, 1994.

[12] D. Carruthers, A. Mckeown, D. Hall, and S. Porter. Validation of adms against wind tunnel data of dispersion from chemical warehouse fires. *Atmospheric Environment*, 33(12):1937–1953, 1999.

[13] CERC. *ADSM-Urban, User Guide.* Cambridge Environmental Research Consultant, 2006.

[14] W. Cheng, C.-H. Liu, and D. Y. Leung. On the correlation of air and pollutant exchange for street canyons in combined wind-buoyancy-driven flow. *Atmospheric Environment*, 43(24):3682–3690, 2009.

[15] M. Chiumenti, Q. Valverde, C. A. De Saracibar, and M. Cervera. A stabilized formulation for incompressible elasticity using linear displacement and pressure interpolations. *Computer methods in applied mechanics and engineering*, 191(46):5253–5264, 2002.

[16] A. J. Cimorelli, S. G. Perry, A. Venkatram, J. C. Weil, R. J. Paine, R. B. Wilson, R. F. Lee, W. D. Peters, and R. W. Brode. Aermod: A dispersion model for industrial source applications. part i: General model formulation and boundary layer characterization. *Journal of applied meteorology*, 44(5):682–693, 2005.

[17] R. Codina. Comparison of some finite element methods for solving the diffusion-convection-reaction equation. *Computer methods in applied mechanics and engineering*, 156(1-4):185–210, 1998.

[18] R. Codina. On stabilized finite element methods for linear systems of convection–diffusion-reaction equations. *Computer Methods in Applied Mechanics and Engineering*, 188(1-3):61–82, 2000.

[19] R. Codina. A stabilized finite element method for generalized stationary incompressible flows. *Computer Methods in Applied Mechanics and Engineering*, 190(20-21):2681–2706, 2001.

[20] J. Cotela-Dalmau, R. Rossi, and E. Oñate. A fic-based stabilized finite element formulation for turbulent flows. *Computer Methods in Applied Mechanics and Engineering*, 315:607–631, 2017.

[21] P. Dadvand, R. Rossi, and E. Oñate. An object-oriented environment for developing finite element codes for multi-disciplinary applications. *Archives of computational methods in engineering*, 17(3):253–297, 2010.

[22] J. Donea. A taylor–galerkin method for convective transport problems. *International Journal for Numerical Methods in Engineering*, 20(1):101–119, 1984.

[23] J. Douglas, Jr and T. F. Russell. Numerical methods for convection-dominated diffusion problems based on combining the method of characteristics with finite element or finite difference procedures. *SIAM Journal on Numerical Analysis*, 19(5):871–885, 1982.

[24] J. Eichhorn. Validation of a microscale pollution dispersal model. In *Air pollution modeling and its application XI*, pages 539–547. Springer, 1996.

[25] L. P. Franca and E. G. D. Do Carmo. The galerkin gradient least-squares method. *Computer Methods in Applied Mechanics and Engineering*, 74(1):41–54, 1989.

[26] L. P. Franca and F. Valentin. On an improved unusual stabilized finite element method for the advective–reactive–diffusive equation. *Computer Methods in Applied Mechanics and Engineering*, 190(13-14):1785–1800, 2000.

[27] G. A. Grell, S. E. Peckham, R. Schmitz, S. A. McKeen, G. Frost, W. C. Skamarock, and B. Eder. Fully coupled "online" chemistry within the wrf model. *Atmospheric Environment*, 39(37):6957–6975, 2005.

[28] G. A. Grell, S. E. Peckham, R. Schmitz, S. A. McKeen, G. Frost, W. C. Skamarock, and B. Eder. Fully coupled "online" chemistry within the wrf model. *Atmospheric Environment*, 39(37):6957–6975, 2005.

[29] I. Harari and T. J. Hughes. Stabilized finite element methods for steady advection–diffusion with production. *Computer Methods in Applied Mechanics and Engineering*, 115(1-2):165–191, 1994.

[30] G. Hauke and A. García-Olivares. Variational subgrid scale formulations for the advection–diffusion-reaction equation. *Computer Methods in Applied Mechanics and Engineering*, 190(51-52):6847–6865, 2001.

[31] R. W. Healy and T. F. Russell. Solution of the advection-dispersion equation in two dimensions by a finite-volume eulerian-lagrangian localized adjoint method. *Advances in Water Resources*, 21(1):11–26, 1998.

[32] HEI. State of global air 2020. Technical report, Health Effects Institute, Boston, MA, 2020.

[33] C. Hirsch. Numerical computation of internal and external flows. 1990. computational methods for inviscid and viscous flows, 1990.

[34] T. J. Hughes. A theoretical framework for petrov-galerkin methods with discontinuous weighting functions: Application to the streamline-upwind procedure. *Finite element in fluids*, 4:Chapter–3, 1982.

[35] T. J. Hughes, G. R. Feijóo, L. Mazzei, and J.-B. Quincy. The variational multiscale method - a paradigm for computational mechanics. *Computer methods in applied mechanics and engineering*, 166(1-2):3–24, 1998.

[36] T. J. Hughes, L. P. Franca, and G. M. Hulbert. A new finite element formulation for computational fluid dynamics: Viii. the galerkin/least-squares method for advective-diffusive equations. *Computer methods in applied mechanics and engineering*, 73(2):173–189, 1989.

[37] T. J. Hughes and M. Mallet. A new finite element formulation for computational fluid dynamics: Iii. the generalized streamline operator for multidimensional advective-diffusive systems. *Computer methods in applied mechanics and engineering*, 58(3):305–328, 1986.

[38] S. Idelsohn, N. Nigro, A. Larreteguy, J. M. Gimenez, and P. Ryzhakov. A pseudo-dns method for the simulation of incompressible fluid flows with instabilities at different scales. *Computational Particle Mechanics*, 7(1):19–40, 2020.

[39] S. Idelsohn, N. Nigro, A. Limache, and E. Oñate. Large time-step explicit integration method for solving problems with dominant convection. *Computer Methods in Applied Mechanics and Engineering*, 217:168–185, 2012.

[40] S. Idelsohn, E. Oñate, N. Nigro, P. Becker, and J. Gimenez. Lagrangian versus eulerian integration errors. *Computer Methods in Applied Mechanics and Engineering*, 293:191–206, 2015.

[41] F. Kikuchi and T. Ushijima. Theoretical analysis of some finite element schemes for convective diffusion equations. In *3rd International Conference on Finite Elements in Flow Problems*, volume 1, pages 82–95, 1981.

[42] J.-J. Kim and J.-J. Baik. Effects of inflow turbulence intensity on flow and pollutant dispersion in an urban street canyon. *Journal of Wind Engineering and Industrial Aerodynamics*, 91(3):309–329, 2003.

[43] J.-J. Kim and J.-J. Baik. Effects of inflow turbulence intensity on flow and pollutant dispersion in an urban street canyon. *Journal of Wind Engineering and Industrial Aerodynamics*, 91(3):309–329, 2003.

[44] Kratos multiphysics. `http://www.cimne.com/kratos/`, 2021.

[45] R. Lazarov, I. D. Mishev, and P. S. Vassilevski. Finite volume methods for convection-diffusion problems. *SIAM Journal on Numerical Analysis*, 33(1):31–55, 1996.

[46] E. Lee and K. Y. Huh. Zone conditional modeling of premixed turbulent flames at a high damköhler number. *Combustion and flame*, 138(3):211–224, 2004.

[47] Á. Leelőssy, F. Molnár, F. Izsák, Á. Havasi, I. Lagzi, and R. Mészáros. Dispersion modeling of air pollutants in the atmosphere: a review. *Central European Journal of Geosciences*, 6(3):257–278, 2014.

[48] X.-X. Li, R. E. Britter, T. Y. Koh, L. K. Norford, C.-H. Liu, D. Entekhabi, and D. Y. Leung. Large-eddy simulation of flow and pollutant transport in urban street canyons with ground heating. *Boundary-layer meteorology*, 137(2):187–204, 2010.

[49] X.-X. Li, R. E. Britter, L. K. Norford, T.-Y. Koh, and D. Entekhabi. Flow and pollutant transport in urban street canyons of different aspect ratios with ground heating: large-eddy simulation. *Boundary-layer meteorology*, 142(2):289–304, 2012.

[50] X.-X. Li, C.-H. Liu, and D. Y. Leung. Numerical investigation of pollutant transport characteristics inside deep urban street canyons. *Atmospheric Environment*, 43(15):2410–2418, 2009.

[51] X.-X. Li, C.-H. Liu, and D. Y. Leung. Numerical investigation of pollutant transport characteristics inside deep urban street canyons. *Atmospheric Environment*, 43(15):2410–2418, 2009.

[52] R. Löhner, K. Morgan, and O. C. Zienkiewicz. The solution of non-linear hyperbolic equation systems by the finite element method. *International Journal for Numerical Methods in Fluids*, 4(11):1043–1063, 1984.

[53] R. Longo, A. Bellemans, M. Derudi, and A. Parente. A multi-fidelity framework for the estimation of the turbulent schmidt number in the simulation of atmospheric dispersion. *Building and Environment*, 185:107066, 2020.

[54] C. Miller and L. Hively. A review of validation studies for the gaussian plume atmospheric dispersion model. *Nuclear Safety*, 28(4):522–531, 1987.

[55] P. Nadukandi, E. Oñate, and J. Garcia. A high-resolution petrov–galerkin method for the 1d convection–diffusion–reaction problem. *Computer methods in applied mechanics and engineering*, 199(9-12):525–546, 2010.

[56] P. Nadukandi, E. Oñate, and J. García. A high-resolution petrov–galerkin method for the convection–diffusion–reaction problem. part ii – a multidimensional extension. *Computer methods in applied mechanics and engineering*, 213:327–352, 2012.

[57] H. Natarajan and G. B. Jacobs. An explicit semi-lagrangian, spectral method for solution of lagrangian transport equations in eulerian-lagrangian formulations. *Computers & Fluids*, 207:104526, 2020.

[58] S. P. Neuman and S. Sorek. Eulerian-lagrangian methods for advection-dispersion. In *Finite elements in water resources*, pages 849–876. Springer, 1982.

[59] T. R. Oke. Street design and urban canopy layer climate. *Energy and buildings*, 11(1-3):103–113, 1988.

[60] B. Oliveira, J. C. Afonso, and S. Zlotnik. A lagrangian–eulerian finite element algorithm for advection–diffusion–reaction problems with phase change. *Computer Methods in Applied Mechanics and Engineering*, 300:375–401, 2016.

[61] E. Oñate. Derivation of stabilized equations for numerical solution of advective-diffusive transport and fluid flow problems. *Computer methods in applied mechanics and engineering*, 151(1-2):233–265, 1998.

[62] E. Oñate. A stabilized finite element method for incompressible viscous flows using a finite increment calculus formulation. *Computer methods in applied mechanics and engineering*, 182(3-4):355–370, 2000.

[63] E. Oñate, A. Franci, and J. M. Carbonell. Lagrangian formulation for finite element analysis of quasi-incompressible fluids with reduced mass losses. *International Journal for Numerical Methods in Fluids*, 74(10):699–731, 2014.

[64] E. Oñate, S. R. Idelsohn, and C. A. Felippa. Consistent pressure laplacian stabilization for incompressible continua via higher-order finite calculus. *International journal for numerical methods in engineering*, 87(1-5):171–195, 2011.

[65] E. Oñate and M. Manzan. A general procedure for deriving stabilized space–time finite element methods for advective–diffusive problems. *International Journal for Numerical Methods in Fluids*, 31(1):203–221, 1999.

[66] E. Oñate and M. Manzan. Stabilization techniques for finite element analysis of convection-diffusion problems. *Developments in Heat Transfer*, 7:71–118, 2000.

[67] E. Oñate, J. Miquel, and G. Hauke. Stabilized formulation for the advection–diffusion–absorption equation using finite calculus and linear finite elements. *Computer Methods in Applied Mechanics and Engineering*, 195(33-36):3926–3946, 2006.

[68] E. Oñate, J. Miquel, and P. Nadukandi. An accurate fic–fem formulation for the 1d advection–diffusion–reaction equation. *Computer Methods in Applied Mechanics and Engineering*, 298:373–406, 2016.

[69] E. Oñate, J. Miquel, and F. Zárate. Stabilized solution of the multidimensional advection–diffusion–absorption equation using linear finite elements. *Computers & fluids*, 36(1):92–112, 2007.

[70] E. Oñate, P. Nadukandi, and J. Miquel. Accurate fic–fem formulation for the multidimensional steady-state advection–diffusion–absorption equation. *Computer Methods in Applied Mechanics and Engineering*, 327:352–368, 2017.

[71] E. Oñate, J. Rojek, R. L. Taylor, and O. C. Zienkiewicz. Finite calculus formulation for incompressible solids using linear triangles and tetrahedra. *International Journal for Numerical Methods in Engineering*, 59(11):1473–1500, 2004.

[72] E. Onate, R. L. Taylor, O. C. Zienkiewicz, and J. Rojek. A residual correction method based on finite calculus. *Engineering Computations*, 2003.

[73] E. Oñate, F. Zárate, and S. R. Idelsohn. Finite element formulation for convective–diffusive problems with sharp gradients using finite calculus. *Computer methods in applied mechanics and engineering*, 195(13-16):1793–1825, 2006.

[74] S. Patankar. Numerical heat transfer and fluid flow, series in computational methods in mechanics and thermal sciences,(1980).

[75] S. G. Perry. Ctdmplus: A dispersion model for sources near complex topography. part i: Technical formulations. *Journal of Applied Meteorology and Climatology*, 31(7):633–645, 1992.

[76] J. Principe and R. Codina. On the stabilization parameter in the subgrid scale approximation of scalar convection–diffusion–reaction equations on distorted meshes. *Computer methods in applied mechanics and engineering*, 199(21-22):1386–1402, 2010.

[77] A. Puigferrat, I. de Pouplana, and E. Oñate. Fic–fem formulation for the multidimensional transient advection–diffusion–absorption equation. *Computer Methods in Applied Mechanics and Engineering*, 365:112984, 2020.

[78] A. Puigferrat, M. Masó, I. De-Pouplana, G. Casas, and E. Oñate. Semi-lagrangian formulation for the advection–diffusion–absorption equation. *Computer Methods in Applied Mechanics and Engineering*, 380:113807, 2021.

[79] L. F. Rossi. A comparative study of lagrangian methods using axisymmetric and deforming blobs. *SIAM Journal on Scientific Computing*, 27(4):1168–1180, 2006.

[80] F. Ruan and D. McLaughlin. An investigation of eulerian-lagrangian methods for solving heterogeneous advection-dominated transport problems. *Water Resources Research*, 35(8):2359–2373, 1999.

[81] D. Ryall and R. Maryon. Validation of the uk met. office's name model against the etex dataset. *Atmospheric Environment*, 32(24):4265–4276, 1998.

[82] D. Ryall and R. Maryon. Validation of the uk met. office's name model against the etex dataset. *Atmospheric Environment*, 32(24):4265–4276, 1998.

[83] R. Sevilla, S. Fernández-Méndez, and A. Huerta. Comparison of high-order curved finite elements. *International Journal for Numerical Methods in Engineering*, 87(8):719–734, 2011.

[84] E. A. Spiegel and G. Veronis. On the boussinesq approximation for a compressible fluid. *The Astrophysical Journal*, 131:442, 1960.

[85] A. Stohl, M. Hittenberger, and G. Wotawa. Validation of the lagrangian particle dispersion model flexpart against large-scale tracer experiment data. *Atmospheric Environment*, 32(24):4245–4264, 1998.

[86] A. Stohl, M. Hittenberger, and G. Wotawa. Validation of the lagrangian particle dispersion model flexpart against large-scale tracer experiment data. *Atmospheric Environment*, 32(24):4245–4264, 1998.

[87] B. D. Storey, B. Zaltzman, and I. Rubinstein. Bulk electroconvective instability at high péclet numbers. *Physical Review E*, 76(4):041501, 2007.

[88] M. Tavelli and W. Boscheri. A high-order parallel eulerian-lagrangian algorithm for advection-diffusion problems on unstructured meshes. *International Journal for Numerical Methods in Fluids*, 91(7):332–347, 2019.

[89] F. Toja-Silva, C. Pregel-Hoderlein, and J. Chen. On the urban geometry generalization for cfd simulation of gas dispersion from chimneys: Comparison with gaussian plume model. *Journal of Wind Engineering and Industrial Aerodynamics*, 177:1–18, 2018.

[90] Y. Tominaga and T. Stathopoulos. Cfd modeling of pollution dispersion in building array: evaluation of turbulent scalar flux modeling in rans model using les results. *Journal of Wind Engineering and Industrial Aerodynamics*, 104:484–491, 2012.

[91] K. Uehara, S. Murakami, S. Oikawa, and S. Wakamatsu. Wind tunnel experiments on how thermal stratification affects flow in and above urban street canyons. *Atmospheric Environment*, 34(10):1553–1562, 2000.

[92] J.-W. van de Meent, I. Tuval, and R. E. Goldstein. Nature's microfluidic transporter: rotational cytoplasmic streaming at high péclet numbers. *Physical Review Letters*, 101(17):178102, 2008.

[93] S. Vardoulakis, B. E. Fisher, K. Pericleous, and N. Gonzalez-Flesca. Modelling air quality in street canyons: a review. *Atmospheric environment*, 37(2):155–182, 2003.

[94] H. Wang, R. E. Ewing, G. Qin, S. L. Lyons, M. Al-Lawatia, and S. Man. A family of eulerian–lagrangian localized adjoint methods for multi-dimensional advection-reaction equations. *Journal of Computational Physics*, 152(1):120–163, 1999.

[95] K. Wang. A uniform optimal-order estimate for an eulerian-lagrangian discontinuous galerkin method for transient advection–diffusion equations. *Numerical Methods for Partial Differential Equations: An International Journal*, 25(1):87–109, 2009.

[96] K. Wang and H. Wang. A uniform estimate for the mmoc for two-dimensional advection-diffusion equations. *Numerical Methods for Partial Differential Equations*, 26(5):1054–1069, 2010.

[97] K. Wang, H. Wang, and M. Al-Lawatia. An eulerian-lagrangian discontinuous galerkin method for transient advection-diffusion equations. *Numerical Methods for Partial Differential Equations: An International Journal*, 23(6):1343–1367, 2007.

[98] K. Wang, Y. Zhang, C. Jang, S. Phillips, and B. Wang. Modeling intercontinental air pollution transport over the trans-pacific region in 2001 using the community multiscale air quality modeling system. *Journal of Geophysical Research: Atmospheres*, 114(D4), 2009.

[99] K. Wang, Y. Zhang, C. Jang, S. Phillips, and B. Wang. Modeling intercontinental air pollution transport over the trans-pacific region in 2001 using the community multiscale air quality modeling system. *Journal of Geophysical Research: Atmospheres*, 114(D4), 2009.

[100] P. Wang, D. Zhao, W. Wang, H. Mu, G. Cai, and C. Liao. Thermal effect on pollutant dispersion in an urban street canyon. *International Journal of Environmental Research*, 5(3):813–820, 2011.

[101] WHO. Who air quality guidelines for particulate matter, ozone, nitrogen dioxide and sulfur dioxide: global update 2005: summary of risk assessment. Technical Report WHO/SDE/PHE/OEH/06.02, World Health Organization, 2005.

[102] X. Xie, Z. Huang, J. Wang, and Z. Xie. The impact of solar radiation and street layout on pollutant dispersion in street canyon. *Building and Environment*, 40(2):201–212, 2005.

[103] D. Young, C. Fan, C. Tsai, C. Chen, and K. Murugesan. *Eulerian-Lagrangian method of fundamental solutions for multi-dimensional advection-diffusion equation*. PhD thesis, National Taiwan University, Taipei, 10617, Taiwan, 2006.

[104] D. Young, Y. Wang, and T. Eldho. Solution of the advection–diffusion equation using the eulerian–lagrangian boundary element method. *Engineering analysis with boundary elements*, 24(6):449–457, 2000.

[105] O. C. Zienkiewicz and R. Codina. A general algorithm for compressible and incompressible flow – part i. the split, characteristic-based scheme. *International Journal for Numerical Methods in Fluids*, 20(8-9):869–885, 1995.

[106] O. C. Zienkiewicz and R. L. Taylor. *The finite element method*, volume 3. Butterworth-Heinemann, Oxford, 2000.